Université d'Ottawa · University of Ottawa

Université d'Ottawa · University of Ottawa

FACULTÉ DES ÉTUDES SUPÉRIEURES ET POSTDOCTORALES

FACULTY OF GRADUATE AND POSTDOCTORAL STUDIES

Shawn BEUG

AUTEUR DE LA THÈSE - AUTHOR OF THESIS

M. Sc. (Cellular and Molecular Medicine)

GRADE - DEGREE

Department of Cellular and Molecular Medicine

FACULTÉ, ÉCOLE, DÉPARTEMENT - FACULTY, SCHOOL, DEPARTMENT

TITRE DE LA THÈSE - TITLE OF THE THESIS

The Role of Growth Arrest-Specific 6 in Notophthalamus viridescens Forelimb Regeneration

C. Tsilfidis

DIRECTEUR DE LA THÈSE - THESIS SUPERVISOR

CO-DIRECTEUR DE LA THÈSE - THESIS CO-SUPERVISOR

EXAMINATEURS DE LA THÈSE - THESIS EXAMINERS

M. Ekker

D. Picketts

J-M. De Koninck, Ph D

LE DOYEN DE LA FACULTÉ DES ÉTUDES SUPÉRIEURES ET POSTDOCTORALES

DEAN OF THE FACULTY OF GRADUATE AND POSTODORAL STUDIES

The Role of *Growth Arrest-Specific 6* in *Notophthalmus viridescens* Forelimb Regeneration

by

Shawn Beug

A Thesis Submitted as a Partial Fulfillment of the Degree of Master of Science Program in Cellular and Molecular Medicine

University of Ottawa
Ottawa, ON.
April 22, 2004

Your file Votre référence
ISBN: 0-494-01418-0
Our file Notre référence
ISBN: 0-494-01418-0

ABSTRACT

Red-spotted newts are capable of regenerating diverse structures and organs, including limb, tail and retina. The epimorphic regenerative response is a complex process that involves dedifferentiation, cellular proliferation and transdifferentiation. Although receptor tyrosine kinases (RTKs) and their ligands are important for normal cellular physiology, no studies have as of yet attempted to isolate and characterize any of these receptors and their ligands during newt forelimb regeneration. I isolated a newt homologue of growth arrest-specific 6 (NvGas6), a RTK ligand involved in multiple functions during ontogeny and normal physiological processes, and its expression was characterized in a polyclonal blastema cell line (B1H1) and during limb regeneration. NvGas6 encodes for a 671 amino acid polypeptide that shares 64% identity (78% similarity) with mammalian Gas6. In B1H1 cells, *NvGas6* is upregulated during myogenesis and is downregulated during cell cycle reentry. Upon amputation, *NvGas6* expression increases, peaking during maximal blastemal cell proliferation and declines during redifferentiation. *NvGas6* transcripts were colocalized to distal mesenchymal cells during dedifferentiation and proliferation, and were found in areas of redifferentiation. Although the *in vitro* and *in vivo* results seem paradoxical, studies by others have shown that Gas6 can have diverse roles in cell survival, proliferation and differentiation, it is possible that *NvGas6* is involved in cell survival *in vitro* and cellular proliferation *in vivo*. However, taken together, these results suggest that NvGas6 may be primarily involved in mediating cell survival and migration during regeneration.

TABLE OF CONTENTS

LIST OF TABLES

LIST OF FIGURES

LIST OF ABBREVIATIONS

°C	degrees celsius
AEC	apical epidermal cap
BLAST	basic local alignment search tool
bp	base pair
cDNA	complementary DNA
cm	centimeter
dd	deionized distilled
DEPC	dimethylpyrocarbonate
ECM	extracellular matrix
EGF	epidermal growth factor
EtOH	ethanol
FBS	foetal bovine serum
g	relative centrifugal force
GAPDH	glyceraldehyde-6-phosphatase
Gas6	growth arrest-specific 6
gm	gram
GLA	γ-carboxyglutamic acid
GLU	glutamic acid
GnRH	gonadotropin-releasing hormone
H_2O	water
LamG	laminin-G
μg	microgram
μL	microliter
μM	micromolar
min	minute
mg	milligram
mL	milliliter
MMP	matrix metalloproteinase
ng	nanogram
nm	nanometer
nM	nanomolarity
Nv	Notophthalmus viridescens
O/N	overnight
PA	post-amputation
PCR	polymerase chain reaction
qPCR	quantitative PCR
RACE	rapid amplification of the cDNA ends
rpm	revolutions per minute
RT	room temperature
RTK	receptor tyrosine kinase
RT-qPCR	reverse transcriptase quantitative PCR
sec	second
C_T	threshold cycle
U	unit
WE	wound epithelium
w/v	weight/volume

ACKNOWLEDGMENTS

Thank you to my supervisor Cathy for taking a chance on me so long ago. I am grateful that you went through this thick thesis without feeling the urge to throw it at my head!

I thank my committee members Drs. Marc Ekker and Valerie Wallace, and external examiner Dr. David Picketts for their invaluable comments, which provided me additional insight into my project.

I am also grateful for the welcoming environment of the Tsilfidis lab, in particular Candice Sy, Adam Baker and Sandy Vascotto who made me realize that one can have fun outside the lab. I also send a shout out to Craig Cameron for his continuing friendship and as a workout partner.

Thank you to my parents, who have supported me throughout this degree both financially and emotionally.

Most of all, thank you to the person who has suffered the most in the pursuit of this degree, Rachelle McGregor. I appreciate you allowing me to get away with a weekend or two there so that I can work on the weekends! Most importantly, I appreciate the emotional support through thick and thin over the past few years.

CHAPTER 1. INTRODUCTION

1.1 Introduction to Regeneration

All eukaryotes are capable of some form of regeneration, from simple wound closure in some organisms to complete replacement of entire appendages in others. At the most basic level, regenerative capability involves wound closure and tissue repair. Following tissue damage, the wound is sealed by migration of either differentiated or undifferentiated cells that oftentimes results in formation of scar tissue. Tissue regeneration is the replacement of lost cells and associated extracellular matrix (ECM) by remaining cells, resulting in the formation of a tissue/matrix that protects the wound from further insult. A slightly more complex form of regeneration is liver hyperplasia, which is accomplished by proliferation and organization of existing liver tissues (Diehl 2002). Remarkable properties of the liver hyperplasia include retention of cellular identity and function and ability to completely replace lost liver tissue (Diehl 2002). Even more complex is muscle regeneration that uses a reserve cell population of undifferentiated myoblasts called satellite cells. Upon muscle injury, regeneration is accomplished by proliferation, migration and fusion of satellite cells in order to repair or repopulate muscle tissue (Goldring et al. 2002). Next in the complexity ladder is regeneration of an entire head or foot that is observed in the cnidarian *Hydra*, by a process termed morphallaxis. The morphallactic response involves the repositioning and repatterning of existing undifferentiated cells that involves negligible growth (Bode 2003). As *Hydra* reproduces by budding, it is believed that the ability to regenerate is linked to asexual reproduction.

While the ability to regenerate whole bodily sections is extraordinary, the most complex form of regeneration occurs within the lissamphibians by epimorphic regeneration. In contrast to morphallaxis, epimorphic regeneration involves both growth and repatterning. Most urodeles and several anurans are capable of complete limb regeneration (Scadding

1981). Limb regeneration proceeds by the localized recruitment of differentiated cells, the dedifferentiation and proliferation of these cells and their redifferentiation into the structures of the missing appendage. The result is a complete regenerate that is indistinguishable from the original.

1.2 Epimorphic Regeneration – Overview

Epimorphic limb regeneration can be separated into 4 major phases: wound healing, dedifferentiation, blastema formation and redifferentiation (Figure 1 and 2; Iten and Bryant 1973). The complex cellular and molecular network that culminates into a perfect regenerate begins with injury or amputation. This signals rapid migration of epithelial cells to cover the wound surface and develop a transient structure called the wound epithelium (WE) which subsequently thickens and is called the apical epidermal cap (AEC). Within 3 days postamputation (PA), dedifferentiation of the distalmost mesodermal stump tissue begins, whereby differentiated cells lose their specialized character and revert to an embryonic-like cell state. Dedifferentiated cells become progenitor cells that converge to form a mesenchymal zone of cells called a blastema. Blastemal cells proliferate until they reach a critical mass and then undergo redifferentiation and morphogenesis to form the regenerate. The process of *Notophthalmus viridescens* forelimb regeneration is completed within 2 months, resulting in a limb that is morphologically and histologically indistinguishable from the original. The major events that transpire during regeneration are outlined in more detail below.

1.2.1 Wound Healing

Following the loss of a limb, wound healing begins with the formation of a thrombus and this is followed by the lateral migration of basal epithelial cells with

Figure 1. *Notophthalmus viridescens* epimorphic regeneration response. The epimorphic regenerative process can be divided into 4 main phases: wound healing, dedifferentiation, blastema formation and redifferentiation. Wound healing is initiated with migration of epithelial cells to cover the wound stump (Day 0-5). Wound covering is followed by onset of dedifferentiation of distalmost stump tissues, which proliferate to form a blastema. Prolonged proliferation results in transformation of the blastema from a bulbous mass (Day 21) into a cone-like shape (Day 25) and eventually a flattened palette (Day 28). Formation of a palette is indicative of redifferentiation and ontogenesis. Subsequently, the palette develops into rudimentary digital projections (Day 32) and continues until regeneration is complete (Day 72). Figure from Brockes (1997).

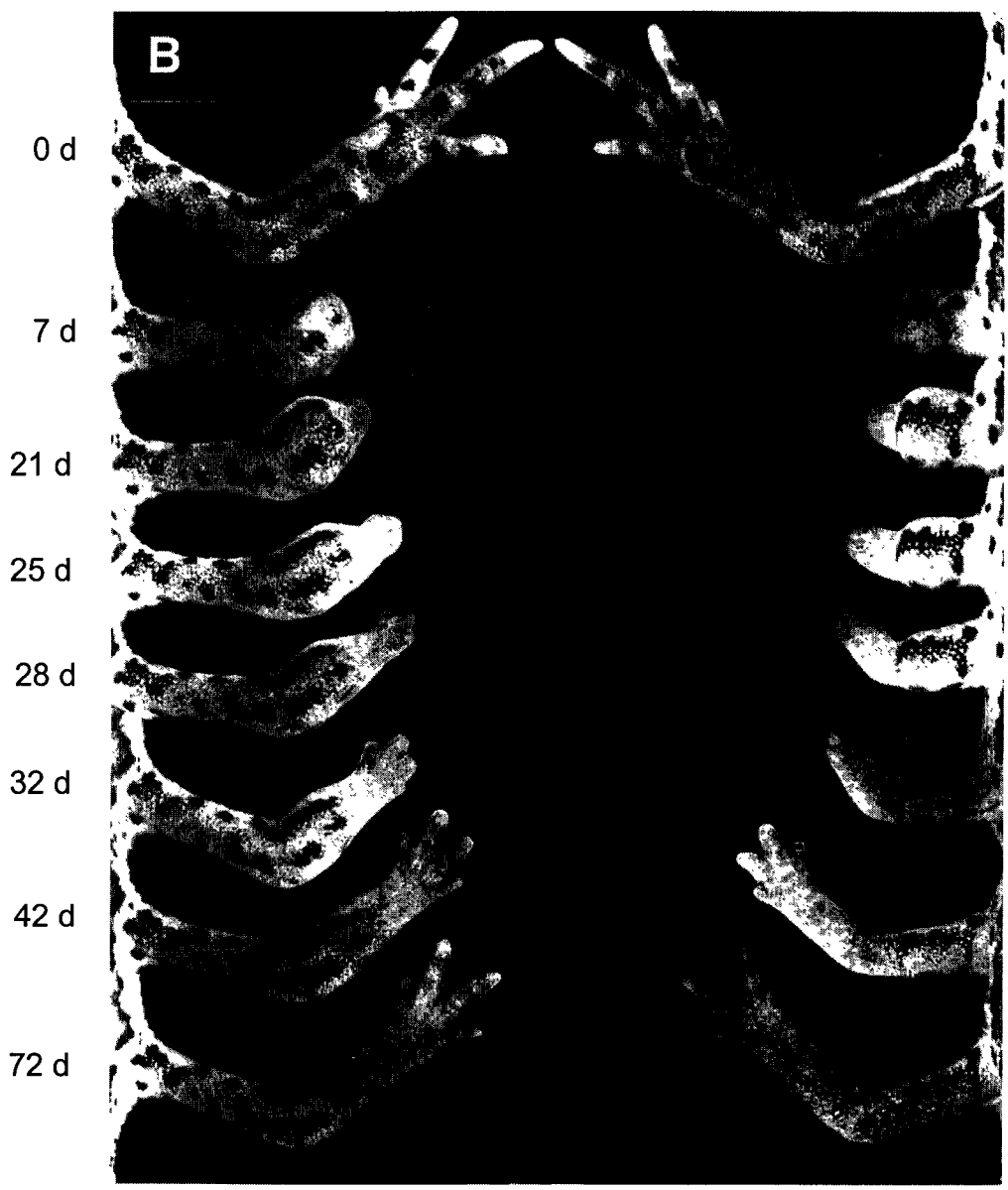
B
0 d
7 d
21 d
25 d
28 d
32 d
42 d
72 d

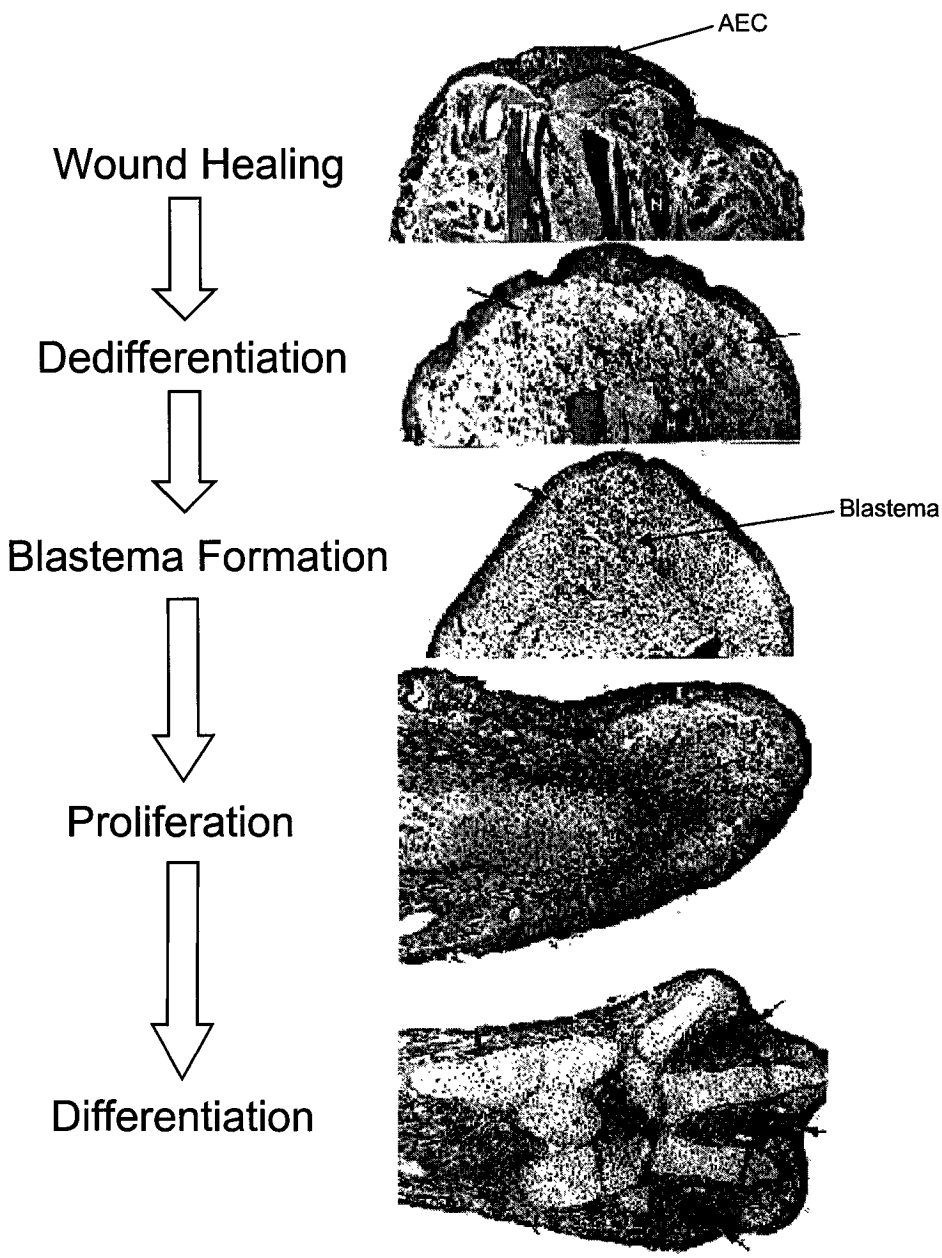
Wound Healing
Dedifferentiation
Blastema Formation
Proliferation
Differentiation
AEC
Blastema

Figure 2. Histological analysis of *Notophthalmus viridescens* forelimb regeneration. Wound healing proceeds by the lateral migration of epithelial cells to cover the wound stump and subsequently thicken to form an apical epidermal cap (AEC). Mesodermal cells beneath the AEC dedifferentiate to yield undifferentiated, multipotent cells that proliferate and apically migrate to form a mesenchymal mound of cells called a blastema. Blastemal cells proliferate and subsequently transdifferentiate into different cell types that construct the regenerate. Adapted from Iten and Bryant (1973).

pseudopodium-like activity to cover the wound stump (Iten and Bryant 1973; Repesh and Oberpriller 1978). This WE protects the underlying structures from the environment, and is necessary for the occurrence and continuation of regeneration (Mescher 1976; Dunis and Namenwirth 1977; Tassava and Garling 1979; Altizer et al. 2002). Within 3 days PA, the WE thickens into 5-7 cell layers as a result of epithelial cell proliferation (Hay and Fischman 1961), and this structure is now referred to as the AEC. With injury, cellular debris accumulates between the WE and distalmost mesodermal tissues. This leads to invasion by granulocytes and subsequent infiltration by monocytes and macrophages to clear up the cellular debris (Greenhalgh 1998). With the formation of the AEC and the removal of cellular debris as a result of the inflammatory response, the groundwork has been laid for setting the next stage, dedifferentiation.

1.2.2 Dedifferentiation

Central to amphibian regeneration is the process of dedifferentiation, whereby fully differentiated cells lose their specialized cytoplasmic characteristics, revert to an embryonic-like state and reenter the cell cycle. These undifferentiated cells proliferate and migrate distally to yield a population of mesenchymal blastema cells. The events that permit dedifferentiation involve prior restructuring of the ECM, enzymatic action that cleaves or breaks cell-cell and cell-matrix contact, loss of the differentiated state, reentry into the cell cycle and proliferation to yield apparent multipotent cells. Some of the factors involved in this process are discussed below.

Iten and Bryant (1973) classified days 6-11 PA as the dedifferentiation stage. The amputated surface has a swollen and translucent appearance, appearing blister-like (Figure 2; Iten and Bryant 1973). The AEC further thickens to 8-15 cell layers by 11 days PA (Iten and Bryant 1973). Neovascularization is evident at this stage, with capillaries reaching the AER (Rageh et al. 2002). Innervation also begins around this stage, as fine axonal fibres

reach the AER; however, dedifferentiation is nerve-independent, as denervation does not inhibit dedifferentiation (Brockes 1987). On the other hand, removal of the AEC does inhibit dedifferentiation (Stocum and Dearlove 1972), suggesting that dedifferentiating signals originate from the AEC.

Two main hypotheses exist for the origin of blastemal cells: reserve cells and dedifferentiation. The reserve cell hypothesis arose when it was discovered that deboned regenerating limbs gave rise to a perfect regenerate (reviewed in Liversage 1991). It was postulated that the blastema was formed by the presence of undifferentiated reserve cells, possibly satellite cells or pluripotent stem cells. Schrag and Cameron (1983) demonstrated that mononucleate myogenic cells, most likely satellite cells in origin fused to form mature myofibrils. These authors concluded that newt muscle regeneration does not depend on dedifferentiation. There are problems with the reserve cell hypothesis; cell availability and cell cycle kinetics do not provide a sufficient quantity of cells to form a blastema. For example, Brockes and Kumar (2002) estimated that the 4 day blastema contains approximately 900 cells. Since the doubling time of blastemal cells is between 36-48 hours (Hay and Fischman 1961; Lo et al. 1993), this would require a large number of available reserve cells. Secondly, a corollary of this hypothesis purports that reserve cells are incapable of transdifferentiation, so reserve cells would have to be found in all cell types.

Presently, there is consensus that dedifferentiation of the distal stump tissues yields the source of blastema cells. The dedifferentiation hypothesis was proposed in the early 1930s. Supporting evidence for the dedifferentiation hypothesis came from classic x-irradiation experiments (as reviewed in Wallace 1981), demonstrating that blastemal cells arise from local mesodermal tissues immediately proximal to the amputated site. In the 1950's, histological studies showed cells budding from myofibres and their apparent subsequent location in the blastema (Hay 1959). More recently, this view was reinforced by

cellular and molecular studies. Lo et al. (1993) and Kumar et al. (2000) injected labelled multinucleate myotubes underneath the WE and observed scattered labelled mononucleate cells. In both studies, the number of mononucleate cells increased as regeneration progressed, indicating that the labelled cells proliferated. Additionally, during the differentiation stages, labelled cells were found in muscle and cartilage tissues, demonstrating the transdifferentiation potential of dedifferentiated myotubes (Lo et al. 1993). The authors concluded that the environment is able to destabilize the differentiated state and promote dedifferentiation and subsequent cell proliferation. Although dedifferentiation has been showed to yield the bulk of progenitor cells for the blastema, the full regenerate probably results from a combination of both dedifferentiation and reserve cells.

The breakdown of the ECM is critical for the initiation of dedifferentiation. A number of ECM factors and proteases (e.g., matrix metalloproteinases (MMPs), fibronectin, laminin, collagen and tenascin) have been implicated but the details of these studies are beyond the scope of this thesis. The dedifferentiating factor has yet to be identified, but studies by Tanaka and colleagues (Tanaka et al. 1997; Tanaka and Brockes 1998; Tanaka et al. 1999) suggest that thrombin may be involved. Thrombin is an essential zymogen in the coagulation cascade, responsible for formation of a thrombus by cleaving fibrinogen into fibrin (Dahlback 2000). Elevated levels of thrombin have been localized to the distalmost mesenchymal stump tissues (Tanaka and Brockes 1998), and treatment of cultured newt myotubes with thrombin in the presence of fetal bovine serum (FBS) promotes cell cycle reentry (Tanaka and Brockes 1998; Tanaka et al. 1999). Thrombin alone does not promote cell cycle reentry, suggesting that it works on a downstream target present in the FBS.

Although all regenerative stages are important for regeneration, it has been postulated that the ability to dedifferentiate separates animals with advanced regenerative ability from those with limited capabilities.

1.2.3 Blastema Formation and Proliferation

The blastema is a mesenchymal growth zone that contains the progenitor cells for the regenerate. Formation of the self-organizing blastema occurs by the proliferation of dedifferentiated cells and their accumulation under the AEC. Blastemal cells begin to accumulate during the early dedifferentiation stage, but the blastema structure is not visible until the early bud stage (12-17 days PA, Iten and Bryant 1973; Rageh et al. 2002). At the same time as blastemal cells are accumulating, other events are progressing in the regenerate. Reinnervation and revascularization of the blastema supplies growth factors necessary for proliferation. ECM remodelling is required for both reinnervation and revascularization, and allows the proliferating cells to migrate. In the early and medium bud stages (14-20 days PA), the AEC is thick only at the apex (4-9 cell layers) and tapers at the edges; dedifferentiation of the stump tissues continues and there is aggregation of blastemal cells at the centre of the blastema that is normally associated with the end of a nerve fibre (Iten and Bryant 1973). Dedifferentiation peaks around 15 days PA and ceases by the end of the medium bud stage (Iten and Bryant 1973). Blastema cell proliferation peaks between 17-21 days PA (Iten and Bryant 1973) and by the end of the late bud stage the blastema is composed of 1-1.5 x 10^5 cells (Liversage 1991). Other characteristics of the late bud stage are the appearance of chondrogenesis in the proximal region of the blastema, scattered dermal melanophores in the dermis, and melanocytes and melanin granules in the epidermis. Thus, blastema cell proliferation, dedifferentiation and differentiation are occurring simultaneously in different regions of the regenerating forelimb.

Source of Cells

Although it has been demonstrated that the distalmost mesodermal stump tissues dedifferentiate to yield the blastema cells (Chapter 1.2.2), the composition and percentage of dedifferentiated cells is a matter of debate. Grafted labelled cartilage into a blastema resulted in labelled nuclei in the blastema vicinity, demonstrating that cartilage was able to dedifferentiate and transdifferentiate into cartilage and connective tissues (Steen 1968). Likewise, when Lo et al. (1993) and Kumar et al. (2000) injected labelled cultured myotubes into the regenerating limb, they observed labelled mononucleate cells in the blastema and later in myofibres and chondrocytes. These results indicate that these two tissue types do contribute towards formation of the blastema. Mescher (1996) estimated that almost half of the blastemal cell population is derived from fibroblasts of dermal, muscle, nerve and blood vessel origin, while the other half is mainly composed of cells of osteoclast and muscle origin.

Nerve Dependency

Blastema cell proliferation is a nerve-dependent process that depends on growth factors secreted from nerves and blood vessels (Scadding 1984). If denervation is performed at the time of amputation, dedifferentiation occurs but proliferation of the dedifferentiated cells does not occur (Tassava et al. 1983). Rather, the dedifferentiated cells undergo apoptosis and are engulfed by macrophages (Mescher et al. 2000). Denervation of moderate and early bud stage blastemas result in inhibition of regeneration and stumping (Tassava et al. 1983; Rageh et al. 2002). Finally, if denervation is accomplished when the blastema has reached its 'critical mass' and redifferentiation begins, an incomplete regenerate will develop with a proximodistal truncation (Tassava et al. 1983). In search for the neurotrophic factor, several mitogens have been proposed. Several lines of evidence have implicated FGFs and associated receptors in amphibian regeneration. *FGF-8* and *-10* are expressed in

the AEC and in the distal blastema zone (Han et al. 2001), and expression at these areas increases with formation of the blastema (Christensen et al. 2001). Additionally, *FGFR1*, which is a receptor for FGF-1, -2 and -4, is expressed in blastemal cells (Poulin et al. 1993), and both FGF-1 and FGF-2 can substitute for the AEC in promoting blastema cell proliferation (Albert et al. 1987; Dungan et al. 2002). As well, FGFs modulate *Msx-1* expression (Poss et al. 2000), which is highest during maximal blastemal cell proliferation (Simon et al. 1995). Another mitogenic candidate is the *Dlx3* gene, a homeobox orthologue of *Drosophila distal-less* which is strongly expressed in the AEC; *Dlx3* expression peaks at the late bud stage and is downregulated by denervation (Beauchemin and Savard 1992; Mullen et al. 1996). Dlx3 interacts with Msx-1, thus influencing *Msx-1* expression (Bryan and Morasso 2000). Although each mitogen may modulate blastemal cell proliferation, it is unlikely that there is a single neurotrophic factor; rather, they all act in concert.

It is unlikely that nerves alone provide the necessary growth factors for the proliferating blastemal cells (Han et al. 2001), and it is possible that nerves affect the AEC, which in turn affects blastema formation and outgrowth (Christensen et al. 2001). While urodeles lack an apical ectodermal ridge (AER) during limb ontogeny (Hanken 1986), the AEC has similar outgrowth-promoting properties as the AER, and may be functionally homologous (Christensen and Tassava 2000). Removal of the AEC during blastemal cell proliferation results in an incomplete proximodistal pattern whereby distal structures are lacking, as the signals for cell cycling are lacking (Stocum and Dearlove 1972). Additionally, if the centrally-located AEC is radially moved several degrees from the original location, regeneration proceeds from the new location, resulting in a limb that protrudes from an angle relative to proximal structures (Thornton 1960). As such, both nerves and AEC are necessary for blastema cell proliferation.

In summary, several major events occur during the blastema stage: continued reorganization of the ECM, accumulation and proliferation of blastemal cells, and innervation and revascularization that affects the rate of proliferation of blastemal cells. Once a 'critical mass' of these undifferentiated blastemal cells has accumulated between the AEC and distal stump tissues, differentiation and morphogenesis proceeds.

1.2.4 Redifferentiation

During this stage, extensive changes occur within the ECM facilitating continuation of neovascularization and blastemal cell migration. In addition, signals that stimulate differentiation are expressed. Differentiation is initiated in the late bud stage, with the appearance of newly-formed chondrocytes at the base of the regenerate (Iten and Bryant 1973). There is an extensive capillary network (Iten and Bryant 1973; Rageh et al. 2002) and further differentiation of the dermis, including melanophores and melanin (Iten and Bryant 1973). The late bud stage proceeds into the palette stage (22-28 days PA), denoted by the presence of epidermal pigmentation at the stump, further chondrogenesis that is immediately proximal to the blastema and myogenesis around the developing cartilage (Iten and Bryant 1973). Digital projections that are separated by avascular interdigital zones at the stump are first seen in the early digit stage (24-33 days PA). At the same time, a basement membrane is formed beneath the AEC (Neufeld and Day 1996), and various dermal glands appear (Iten and Bryant 1973). By the medium digit stage (30-40 days PA), the remaining blastemal cells are restricted to the distal regions of the autopodium and skeletal elements are beginning to fuse (Iten and Bryant 1973). The late digit stage (34 days PA and beyond) is marked by extensive elongation of the digits, full differentiation and ossification (Iten and Bryant 1973; Stock et al. 2003).

ECM changes begin to decline as differentiation progresses. Transcript levels of MMPs slowly taper but are still present in areas of differentiation (Miyazaki et al. 1996;

Kato et al. 2003), suggesting that localized ECM remodelling is warranted. *CollagenXII* is not expressed in chondrocytes, but expression is localized to the perichondrium, suggesting that colXII has a role in establishing a matrix for chondrogenesis. *Tenascin* expression is localized to areas with differentiation and growth (Onda et al. 1991), while *laminin* expression is confined to areas of myogenesis (Gulati et al. 1983) and fibronectin is localized to areas of condensing cartilage, between differentiating myoblasts and blood vessels (Repesh et al. 1982; Nace and Tassava 1995). Thus, these molecules likely mediate differentiation by altering migration and cell-cell interactions, and the distribution of these molecules coincide with the formation of the basement membrane. Neufeld and Day (1996) postulate that the basement membrane acts as a barrier between the AEC and blastema, depriving the proliferating blastemal cells of growth factors. Thus, the formation of the basement membrane may be responsible for the observation that dermogenesis occurs before chondrogenesis and myogenesis. Coincident with the condensing cartilage is the process of ossification (Iten and Bryant 1973; Gonzales et al. 2001; Stock et al. 2003). This obviously results in further changes in the ECM, as osteoclast fusion and calcium mineralization further alters the bone and surrounding matrix.

Transdifferentiation

Blastemal cells are capable of transdifferentiation; that is, they do not necessarily revert to their original state, but can redifferentiate into another cell type. Multipotency was first demonstrated by Steen (1968). He grafted labelled cartilage into a regenerating limb and observed labelled chondrocytes and a few labelled connective tissues. More recently, a myogenic-chondrogenic transdifferentiation was observed. Lo et al. (1993) and Kumar et al. (2000) implanted labelled cultured myotubes into a blastema and observed mostly labelled myogenic cells with scattered labelled chondrocytes. However, the transdifferentiation phenomenon remained a question due to intensity of cell labelling, accuracy of cell

localization and low numbers of detected transdifferentiated cells. To overcome these limitations, Echeverri and Tanaka (2002) transfected individual ependymal cells with green fluorescent protein driven by a promoter that is specific to ependymal cells of the mature spinal cord. The authors were able to observe real-time cell division, migration and differentiation into neurons, glia, neural crest derivatives, melanocytes and muscle. This is the first direct evidence for ectodermal-mesodermal transdifferentiation in regeneration. However, it is currently unknown if mesenchymal blastema cells are capable of transdifferentiating into ectodermal lineages.

Overall, the redifferentiation stage involves changes in growth signals, changes within the ECM and selective expression of differentiation signals. Blastemal cells cease proliferating, begin to migrate and differentiate into their various tissue types. The result of the differentiation stage is the formation of a regenerate that is histologically, morphologically and functionally indistinguishable from the original.

1.3 Growth Arrest Specific 6 (Gas6)

1.3.1 Receptor Tyrosine Kinase Signal Transduction

All cellular function depends on signalling pathways governing diverse functions such as metabolism, growth, migration, differentiation and apoptosis. These complex signalling networks are heavily influenced by secreted growth factors that diffuse freely in the extracellular environment and transmit their effects by binding to transmembrane receptors. A large portion of growth factors are high affinity ligands for the family of receptor tyrosine kinases (RTK), which mediate their function via intrinsic phosphorylation events (Fedi et al. 2000). As such, tyrosine kinase signal transduction is defined as a process whereby an extracellular signal is transmitted across the plasma membrane and into the nucleus, thus altering gene expression.

RTK activity is initiated upon ligand binding, leading to autophosphorylation of tyrosyl residues and the subsequent phosphorylation of diverse downstream molecules. Activation is normally mediated by extracellular high-affinity receptor homo- or heterodimerization, that result in conformational changes of the receptor (Hubbard and Till 2000). The conformational changes lead to autophosphorylation of specific juxtamembrane and cytoplasmic tyrosine residues, further altering the structure and increasing its intrinsic catalytic activity (Hubbard and Till 2000). As a consequence of autophosphorylation, docking sites for intracellular signalling molecules that recognize phosphotyrosine are generated (Hubbard and Till 2000). Specific modules possess specific motifs, mediating protein-protein interactions that involve downstream enzymatic cascades and second messenger production that eventually mediate transcription factor expression.

As RTKs are important regulators for signal-transduction networks, they are subjected to tight regulation. As a result, mutations or other genetic alterations oftentimes contribute towards development and malignancy of cancer, and many RTKs have been identified as oncogenes (Blume-Jensen and Hunter 2001). For example, several *Axl* (from the Greek word 'anexelekto' or uncontrolled) family members are overexpressed in numerous cancer cell lines and are associated with malignancies (Taylor et al. 1995; Nemoto et al. 1997; Chen et al. 1999; Meric et al. 2002; Wu et al. 2002). Axl members are associated with migration, proliferation, apoptosis and cellular adhesion, all of which is important in carcinogenesis (Goruppi et al. 1996; Li et al. 1996; Avanzi et al. 1997; Bellosta et al. 1997; Goruppi et al. 1997; Nakano et al. 1997; Fridell et al. 1998; Allen et al. 1999; Goruppi et al. 1999; Melaragno et al. 1999; Demarchi et al. 2001; Yanagita et al. 2001; Allen et al. 2002; D'Arcangelo et al. 2002; Lee et al. 2002; Yagami et al. 2002). These events are important during dedifferentiation and blastema formation, suggesting a role for Axl members in regeneration.

1.3.2 Gas6

1.3.2.1 Structure

The common ligand for the Axl family members is the product of the *growth arrest-specific 6* (*Gas6*) gene (Stitt et al. 1995; Varnum et al. 1995; Li et al. 1996; Nakano et al. 1996; McCloskey et al. 1997). Gas6 is a 75 kDa secreted vitamin K-dependent ligand, characterized by posttranslational γ-carboxylation of glutamic (GLU) residues that results in conversion of GLU residues to γ-carboxyglutamic acid (GLA) residues (Manfioletti et al. 1993) and mediates binding to phospholipid membranes. Mammalian Gas6 is composed of a GLA domain followed by tandem repeats of epidermal-like growth factor (EGF) modules and laminin G-like (LamG) domains (Figure 3). Gas6 exerts its effects by binding to 3 known RTKs, Axl, Sky (c-sea related protein kinase for tyrosine) and Mer, which accounts for Gas6's numerous physiological functions.

The GLA domain is a ~ 40 amino acid long module that is associated with proteins involved in wound healing (Sato et al. 1998), ECM (Booth 1997; Shanahan et al. 1998; Saxena et al. 2001), coagulation (Dahlback 2000), cell adhesion (Avanzi et al. 1998), migration (Fridell et al. 1998) and signal transduction (Kulman et al. 1997; Kulman et al. 2001). Carboxylation is believed to result in Ca^{2+} binding with the GLA residues, resulting in a conformational change that mediates interaction of the protein with the negatively-charged plasma membrane (Berkner 2000). In the case of Gas6, it is believed that the complete GLA domain 'fixes' the protein conformation such that Gas6 is in its active form, while the propeptide (GLU) form or the absence of Ca^{2+} leaves Gas6 in its inactive form (Nakano et al. 1997; Tanabe et al. 1997). Although Gas6 can exert its physiological effects without the GLA domain, the presence of both GLA and Ca^{2+} is required for maximal activity (Mark et al. 1996; Nakano et al. 1997; Hall et al. 2002).

Figure 3. Mammalian Gas6 domains. Gas6 is comprised of an amino terminus γ-carboxyglutamic acid (GLA) domain followed by epidermal growth factor-like (EGF_CA) domains and laminin G-like (LamG) domains situated near the carboxy terminus.

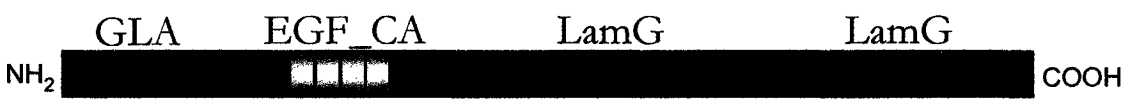
GLA
EGF_CA
LamG
LamG
NH2
COOH

Following the GLA domain are 4 EGF-like repeats (Manfioletti et al. 1993). EGF-like modules are involved in protein-protein interactions and are present in a large number of ECM and membrane-bound proteins, being involved in diverse functions such as coagulation, fibrinolysis, cell adhesion, growth and differentiation (Rao et al. 1995; Stenflo et al. 2000). EGF-Ca^{2+} binding is essential for protein activity and is thought to be important for orienting neighbouring domains in a manner which is required for maximal physiological function (Nakano et al. 1997; Stenflo et al. 2000). Using a deletion strategy, Mark et al. (1996) concluded that while the EGF domain is not necessary for ligand binding, this module in conjunction with the GLA domain is likely indispensable for modulating Gas6 activity *in vivo*.

The carboxy-terminal region of Gas6 is homologous to the steroid hormone-binding globulin (SHBG) protein and contain tandem globular domains (Manfioletti et al. 1993). The LamG domains consist of ~190 amino acid residues and are found in a diverse array of proteins that range in function from signal transduction, adhesion, migration and differentiation (Timpl et al. 2000; Rudenko et al. 2001). These include ECM proteins, cell surface receptors and hormone-binding proteins. The LamG domains are required for RTK binding and proper folding of the molecule (Mark et al. 1996; Goruppi et al. 1997; Tanabe et al. 1997; Sasaki et al. 2002). As well, Ca^{2+} binding in the LG domain is indispensable for maintaining the proper structure conformation (Sasaki et al. 2002).

Gas6 is similar to the negative coregulator of the coagulation cascade, protein S (Manfioletti et al. 1993). Protein S is a vitamin K-dependent protein that serves as a cofactor for activated protein C (Dahlback 2000). Gas6 and protein S share the same structural motifs (42% amino acid identity), both encoding for a GLA domain, EGF-like domain and LamG domain (Manfioletti et al. 1993). However, a key difference is the absence of a thrombin-sensitive cleavage site in Gas6, which is replaced by a loop structure

(Manfioletti et al. 1993). Protein S binds to the RTKs *in vitro*, but its ability to bind and exert a physiological function *in vivo* is unknown (Stitt et al. 1995; Nagata et al. 1996; Wimmel et al. 1999).

1.3.2.2 Gas6 Receptors

Gas6 exerts its effects by acting as a ligand for members of the Axl family, which includes Axl (also named Ark, Tyro7, Ufo), Sky (also named Tyro3, Brt, Dtk, Etk, Rse, Tif, Rek) and Mer (also named Eyk, MERTK, Nyk, Tyro12). These RTKs are characterized by 2 ligand-binding immunoglobulin domains and 2 fibronectin type III repeats, followed by a single-pass transmembrane domain and a cytoplasmic protein tyrosine kinase domain (Robinson et al. 2000). The extracellular domains are responsible for mediating signalling via either direct cell-cell contact or soluble ligands. Gas6 binds and activates all 3 RTKs with differing affinities ((Axl > Sky >> Mer) Stitt et al. 1995; Varnum et al. 1995; Nagata et al. 1996). With differing affinities and expression, Gas6 exerts its multiple physiological functions in a wide variety of tissues.

The Axl family is important for normal cellular function. Mice that are deficient for all 3 RTKs (i.e., $Axl^{-/-}$, $Sky^{-/-}$, $Mer^{-/-}$) surprisingly are not embryonic lethal, but these mice demonstrate somewhat severe abnormalities in the vision, reproductive, nervous, immune and vascular systems (Lu et al. 1999; Lu and Lemke 2001). The triple knockout mice exhibit photoreceptor degeneration, leading to blindness, male infertility due to germ cell apoptosis, increased apoptosis in numerous tissue types, susceptibility to seizures and paralysis, and brain neuronal loss (Lu et al. 1999; Lu and Lemke 2001). The most obvious observation occurs within the immune system; splenomegaly and lymphadenopathy that eventually lead to establishment of invasive lymphocytes throughout the body (Lu and Lemke 2001). With the occurrence of apoptosis and lymphocyte invasion, autoimmune

diseases develop throughout the body (Lu et al. 1999; Lu and Lemke 2001; Scott et al. 2001).

Axl has been implicated in a number of events. *Axl*$^{-/-}$ mice show similar defects as the triple RTK knockout, although the gross anomatical defects are not as marked (Lu et al. 1999). Ectopic *Axl* expression is associated with tumours (O'Bryan et al. 1991) and cancer cell lines (Tanaka et al. 1998; Ito et al. 1999; Jacob et al. 1999; Berclaz et al. 2001; Ito et al. 2002). Axl promotes survival in several cell lines, such as protecting endothelial cells from apoptosis via Gas6 interaction (Healy et al. 2001; D'Arcangelo et al. 2002). Similarly, increased Axl production is associated with injury of vascular smooth muscle cells, possibly mediating migration and proliferation (Melaragno et al. 1998; Yin et al. 2000). It has been speculated that Axl may be activated following cell-cell contact, mediating cellular aggregation (Crosier and Crosier 1997). As well, Axl-Gas6 interaction has a role in differentiation, inhibiting osteogenic differentiation of vascular-derived pericytes (Collett et al. 2003). A unique aspect of Axl is cleavage of the extracellular domain to generate a soluble Axl form, possibly inhibiting Gas6 from interacting with the RTKs or binding to Axl itself (Costa et al. 1996).

Mer has similar functions as Axl, with a few notable exceptions. For example, *Mer*$^{-/-}$ mice are blind as a result of postnatal photoreceptor degeneration (Camenisch et al. 1999; Scott et al. 2001; Cohen et al. 2002). Interestingly, mutations in the *Mer* gene cause the development of retinitis pigmentosa (D'Cruz et al. 2000; Gal et al. 2000; Vollrath et al. 2001). Additionally, *Mer*$^{-/-}$ mice demonstrate delayed clearance of apoptotic cells, splenomegaly and are inclined to autoimmunity (Scott et al. 2001; Cohen et al. 2002). As well as a deficient nervous system whereby adults exhibit neural degeneration leading to seizures and partial limb paralysis (Lu et al. 1999). Mer appears to play a role in engulfment and removal of apoptotic cells, as well as maintenance of tissue homeostasis. In addition,

Mer likely has a role in survival, as *Mer* is overexpressed in many cancer cell lines (Graham et al. 1994; Dirks et al. 1999; Guttridge et al. 2002; Wu et al. 2002), blocks apoptosis (Georgescu et al. 1999; Guttridge et al. 2002) and promotes cytoskeletal alterations (Guttridge et al. 2002).

Like the other 2 RTK family members, Sky is involved in developmental pathways. *Xenopus Sky* expression is marked in the early developmental stages, and becomes limited to the nervous system and in rudiments of the sensory organs at the tadpole stage (Kishi et al. 2002). In a chimeric EGFR-Sky study, Kishi et al. (2002) proposed that Sky is directly involved with growth, differentiation and migration by mediating cell-cell interactions. As well, *Sky* and *Axl* are expressed in totipotent embryonic stem cells, and in differentiating stem cells (Crosier et al. 1996), demonstrating a possible role in modulating survival and differentiation.

1.3.2.3 Gas6 Signal Transduction

Gas6 was initially isolated as one of many genes whose expression increased in serum-starved N1H 3T3 fibroblasts, and its expression was negatively regulated upon growth induction (Schneider et al. 1988; Manfioletti et al. 1993). With its high similarity to Protein S, it was believed that it could have a role in the coagulation cascade or in the regulation of a protease pathway (Manfioletti et al. 1993). However, since then, Gas6 has been demonstrated to have multiple effects through its associated RTKs in a cell- and tissue-specific manner. As Gas6 is a ligand for the Axl RTK family, stimulation of each receptor results in activation of more than one signalling pathway in cells that express multiple receptors.

Mitogenic Pathway

Gas6 exerts its mitogenic effects through interaction with Axl and Sky. Most studies that have implicated Gas6 as a mitogen have been done on serum-starved subconfluent

N1H3T3 cells (Goruppi et al. 1996; Goruppi et al. 1997), other murine cell lines (McCloskey et al. 1994; Varnum et al. 1995) and human Schwann cells (Li et al. 1996). Interestingly, Gas/Axl has no mitogenic effects on haematopoietic tissues, aortic smooth muscle cells or human lung cancer cell lines (Avanzi et al. 1997; Fridell et al. 1998; Wimmel et al. 1999; Wimmel et al. 2001). However, it must be mentioned that most proliferation studies were performed in murine cells, with either endogenous Axl or mixed species Axl constructs and using recombinant human Gas6, and that not all 3T3 cell lines express Gas6. Therefore, the weak proliferation effect may be not be recapitulated *in vivo*.

Despite the fact that Gas6/Axl-mediated proliferation is weak at best, the molecular mechanism has been partially elucidated (Figure 4). In 3T3 cells, activation of Axl via Gas6 requires PI3K activation, leading to phosphorylation of downstream targets Akt and S6K (Goruppi et al. 1997). Although the cytoplasmic region of Axl lacks a Src-binding consensus, Src is required for activation of this cascade (Goruppi et al. 1997). As well, inhibition of glycogen synthase 3 induces upregulation of cytosolic beta-catenin, which is correlated with subsequent TCF/Lef transcription activation in mammary cells (Goruppi et al. 2001). As such, Gas6/Axl may have a role in mammary tumour formation. Also required for mitogenesis is the activation of Ras GTPase in both 3T3 and mammary cells, which lead to activation of the MEK/Erk signalling cascade (Goruppi et al. 1999; Goruppi et al. 2001). Finally, Gas6-induced mesangial cell proliferation through Axl phosphorylation results in phosphorylation of the transcription factor STAT3, leading to translocation to the nucleus and activation of STAT3-dependent transcription (Yanagita et al. 2001). However, the mechanisms behind this effect are unknown.

Of particular interest is the observation that Gas6 appears to act synergistally with thrombin to increase cellular proliferation rates in vascular smooth muscle cells, possibly

Figure 4. This map identifies the signalling pathways regulated by the Axl family of tyrosine kinase receptors and its known ligand, Gas6. Proliferation requires the activation of either STAT3 transcription factors, the PI3K pathway leading to TCF/Lef transcription and/or activation of the Ras GTPases. PI3K stimulation is necessary for survival, as all downstream links include prevention of apoptosis by inhibition of the proapoptotic gene *Bcl-x_L* and activation of JNK kinases. Although the p38 MAPK pathway is involved in survival activities, it is also involved in cytoskeletal rearrangements. Lastly, activation of the Rac GTPase also results in changes in GnRH transcription, likely affecting migration. Although I have attempted to define links that are experimentally established, a caution must be noted as these links are based on studies with different cell lines. For example, the pathway leading to GnRH transcription only occurs in GnRH cells. Dotted lines indicate a link that has been suggested, but not directly proven. See main body of thesis for references. Pentagon shapes represent different classes of GTPases. Parallelograms represent kinases (blue: serine/threonine; green: lipid; grey: dual). Grey rectangles represent adaptors/regulators and yellow rectangles represent various regulators.

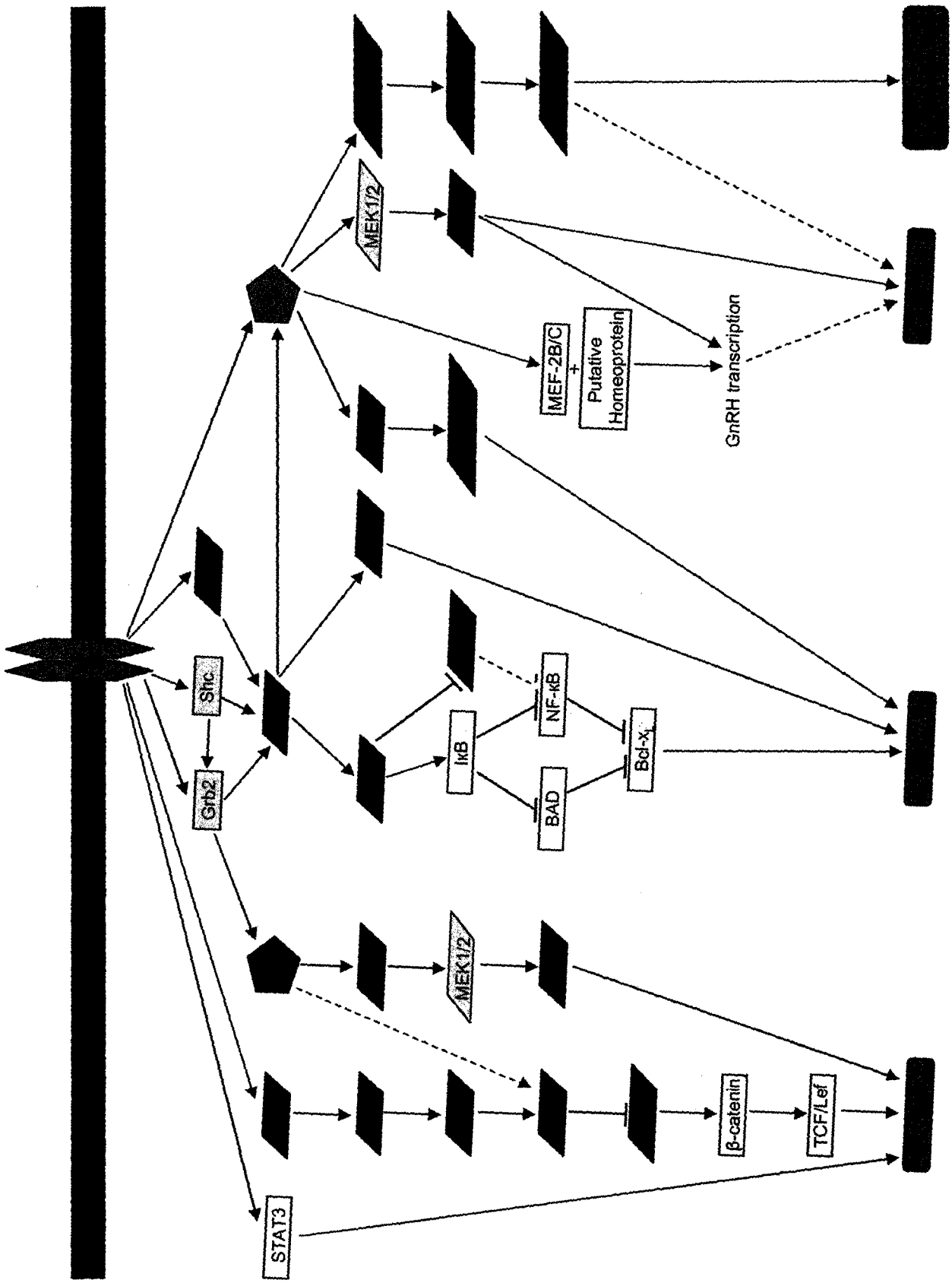
Shc
Grb2
MEK1/2
MEK1/2
STAT3
IκB
NF-κB
BAD
Bcl-X
MEF-2B/C
+
Putative
Homeoprotein
GnRH transcription
β-catenin
TCF/Lef

through interaction with Axl (Nakano et al. 1995; Nakano et al. 1997; Melaragno et al. 1998). Interestingly, this thrombin-mediated potentiation of cell cycle reentry and proliferation is not mediated through secondary growth factors, but is dependent on the presence of endogenous Gas6 (Nakano et al. 1995; Nakano et al. 1997). However, Gas6 alone is insufficient to drive cellular proliferation (Nakano et al. 1995). It remains to be seen if this relationship is directly related and is cell-type specific.

Survival Pathway

While Gas6/Axl has a weak mitogenic effect on endothelial cells, Gas6 can also mediate survival by preventing or halting apoptosis, and this activity is separate from its proliferative activities (Nakano et al. 1996; McCloskey et al. 1997; Avanzi et al. 1998; O'Donnell et al. 1999; Chan et al. 2000; Healy et al. 2001; D'Arcangelo et al. 2002; Shankar et al. 2003). For example, addition of Gas6 prevents serum-starved vascular smooth muscle cells from apoptosis and Gas6 depletion leads to apoptosis; however, it is not a per se survival factor since inhibition of Gas6 did not induce cell death during proliferation (Nakano et al. 1996). In another study, Axl was shown to be constitutively phosphorylated in growth arrested pulmonary endothelial cells, and addition of Gas6 resulted in higher *Axl* expression with fewer apoptotic cells (Healy et al. 2001). Furthermore, Gas6 exerts other activities in endothelial cells. *Axl* is expressed in capillaries, larger arterioles and veins, and in vascular smooth muscle cells, which suggests that Gas6/Axl signalling is responsible for cellular adhesion during angiogenesis (McCloskey et al. 1997; O'Donnell et al. 1999).

The protective effect is not restricted to cells of endothelial origin, but a cohort of cell types that produce Gas6 and Axl have prosurvival effects. In 3T3 cells, the protective effect depends on Axl/Sky → Akt signalling, which leads to inactivation of the Bcl-2 proapoptotic family member BAD and an increase in nuclear NFκB binding activity with subsequent induction of antiapoptotic genes such as *bcl-*x_L (Figure 4, Bellosta et al. 1997;

Goruppi et al. 1997; Goruppi et al. 1999; Lan et al. 2000; Demarchi et al. 2001). Also indispensable for the survival response in 3T3 cells is the activation of the Rho GTPase family members Rho and Rac, which leads to downregulation of p38 MAPK (Goruppi et al. 1999). However, the Gas6/Axl → Akt prosurvival mechanism is not unique to 3T3 cells; Axl receptor activation induces downstream signalling of PI3K in oligodendrocytes, gonadotropin-releasing hormone (GnRH) neurons, ovarian cancer cells and leukemia cell lines (Allen et al. 1999; Georgescu et al. 1999; Lee et al. 1999; Lee et al. 2002; Shankar et al. 2003). While Gas6 is able to promote survival in GnRH neurons, PI3K signalling is insufficient to protect cortical neurons from apoptosis (Yagami et al. 2002), demonstrating cell-specific pathways for Gas6-RTK survival activities. Overall, this survival activity is thought to be indispensable for maintaining tissue homeostasis during development and wound healing.

Cell Migration and Cytoskeletal Rearrangement

Interaction of Gas6 with Axl is linked to cell-cell and cell-matrix interactions. The Gas6-Axl system promotes cellular aggregation (Bellosta et al. 1995; McCloskey et al. 1997); however, it appears that such effects are lineage-specific. This may be related to the extracellular domain of Axl, which could possibly be involved in multiple ligand- and protein-protein interactions (O'Bryan et al. 1991). Gas6 is involved in promoting cellular adhesion; both Gas6 and Axl are produced in lung cancer cell lines that grow in adherent conditions, but are absent in cell lines that grow in suspension conditions (Wimmel et al. 2001). However, ectopic Axl or Gas6 stimulation is insufficient to induce cell adhesion of suspension cell lines, but *Axl* is expressed upon induction into cell adherent conditions (Wimmel et al. 2001). The authors postulate that the adherent mechanism induces *Axl* expression. An alternative explanation is offered by Fridell et al. (1998) in their studies with

vascular smooth muscle cells where they purport that Gas6 acts as a chemoattractant, inducing migration and adhesion.

The involvement of Axl signalling in signalling and chemotaxis is further shown in GnRH neurons, where *Axl* is differentially expressed in migratory versus nonmigratory neurons (Fang et al. 1998). Gas6 stimulates cellular alterations, such as membrane ruffling, lamellipodial extension and cheomotaxis via activation of the Rac GTPase → p38 MAPK pathway, and promotes cellular migration through the Erk pathway (Figure 4, Allen et al. 2000; Allen et al. 2002; Allen et al. 2002).

1.3.3 Gas6-Urodelean Regeneration Link

Since tyrosine kinase receptor signal transduction events are essential for normal cellular and molecular functions, it follows naturally that ligands which bind to specific RTKs would play an important role during regeneration as well. While the role of Gas6 during regeneration is unknown, published reports of its diverse roles during cellular physiology and ontogeny suggests that Gas6 may be involved during the regenerative process. Gas6 may play a role in cellular migration during wound healing and in regulating the survival of surrounding cells. Later in the regenerative process, Gas6 may stimulate and maintain blastemal cell proliferation and survival. During the final phases of regeneration, Gas6 may be involved in cell migration and adhesion during the differentiation stage of regeneration.

1.4 Statement of Hypothesis and Objectives

Although the cellular aspects of newt regeneration have been well researched for the past century, molecular studies remain in their infancy compared to other animal models. As one of the ultimate goals of regenerative research is to apply knowledge in regenerative ability to other systems, elucidating the molecular framework is the next step in using this

information. Therefore, my overall objective is to identify at least one regulatory factor that is intimately involved in urodelean forelimb regeneration. My individual goals are to clone a novel gene, elucidate the temporal and spatial expression profiles during the different regenerative stages, and to propose a role for the gene. For the above reasons, I have chosen to isolate and characterize the newt orthologue of *Gas6*.

2. MATERIALS AND METHODS

2.1 Animal Care and Tissue Collection

Adult red-spotted newts, *Notophthalmus viridescens*, were purchased from Charles D. Sullivan Co. (TN), maintained in large tubs in running dechlorinated H_2O at 21°C, and fed blackworms (*Lumbriculus variegatus*) 2-3 times a week. Operations were performed on newts anesthetised with MS222 (Appendix II, Section I.). Initial amputations were made proximal to the elbow and the tissues were trimmed to yield a flat amputation plane. Newts were placed in a recovery tank of dechlorinated H_2O until they regained consciousness and then housed with the general population as above. To collect regenerative tissues, newts were re-anesthetised and re-amputated midway through the humerus. Upon amputation, tissues were immediately flash frozen in either liquid N_2 or with 1 mL Trizol (Invitrogen) and stored at -70°C.

2.2 B1H1 Cell Culture

B1H1 cells were a kind gift from J. Brockes (University College London, London, UK). B1H1 cells were maintained on gelatin-coated plates (0.75%) in 10% FBS A.MEM at 28°C in 2% CO_2. Media was changed 2-3 times weekly. B1H1 cells were subcultured when cells approached 70-80% confluency. Cells were washed with A.PBS, detached with 0.1% trypsin-EDTA/A.PBS by incubating at RT for 2-4 min, resuspended in 10% FBS A.MEM, aliquoted into gelatin-coated plates and resupplemented with 10% FBS A.MEM.

Myogenesis was induced when cells reached 80-100% confluency and began to align. The cells were washed with A.PBS and placed in 0.5% FBS A.MEM. The media was replaced every 48 hours for 4-8 days. Myotube cell cycle reentry was induced by washing cells with A.PBS and resupplementing the media with 10% FBS A.MEM. The media was

changed every 48 hours for 4 days. All solutions and their compositions are listed in Appendix II, Section I.

To thaw a B1H1 liquid N_2 stock, the cells were thawed at 37°C, added to 4 mL of room temperature (RT) 10% FBS A.MEM, centrifuged for 5 min at 1000 x g, resuspended in 10% FBS A.MEM and plated onto a 0.75% gelatin-coated plate. To freeze down cells, the media was changed on day 1, then on day 2 cells were pelleted as above, resuspended in 10% FBS A.MEM with 10% DMSO, frozen at -70°C overnight (O/N) and the next day transferred to a N_2 tank.

2.3 Generation of Full-Length cDNA

2.3.1 Generation of B1H1 RACE cDNA Library

B1H1 cells were harvested at 80-100% confluency. The cells were washed with A.PBS, scraped off the plate in A.PBS, pelleted for 5 min at 1000 x g and flash frozen in 1 mL Trizol (Invitrogen) in liquid N_2. Total RNA extraction was performed as described in Appendix II, Section A and poly(A) mRNA was isolated using oligo(dT) beads (see Appendix II, Section C). Briefly, 150 μg of total RNA was DNaseI-treated (Sigma) as per the manufacturer's instructions, added to an equal volume of 40 mM Tris-HCl (pH 7.6), 1 M NaCl, 2 mM EDTA and 0.2% SDS, and added to cellulose oligo(dT) beads (Amersham). The solution was mixed by inversion for 5 min at room temperature (RT). The poly(A)-oligo(dT) mixture was washed 5 times with 250 μL of 20 mM Tris-HCl (pH 7.6), 0.1 M NaCl, 1 mM EDTA and 0.1 % SDS, and eluted by mixing at RT for 5 min in 250 μL of 10 mM Tris-HCl (pH 7.6), 1 mM EDTA and 0.1% SDS. Poly(A) RNA was precipitated with 0.1 volumes 3 M NaOAc (pH 5.2) and 2.5 volumes of cold 100% EtOH and incubated at -70°C for 90 min, centrifuged at max speed for 15 min at 4°C, washed with 70% EtOH and resuspended in 6 μL DEPC-treated H_2O. After determining the concentration by A_{260} spectrometry, poly(A) RNA was electrophoresed on a 1.2% agarose gel to assess its

integrity. Generation of the Marathon™ RACE library, including formation of double stranded cDNA and addition of adaptors, was per the manufacturer's instructions (Clontech).

2.3.2 Isolation of the 5' and 3' Ends of *SR4*

A 321 bp cDNA template, named SR4, was previously identified during a screen for dedifferentiation-specific genes. Primers were designed for SR4 using the PrimerSelect software (DNAStar) with the default conditions, except for specification of primers that were 23-38 nucleotides long with a melting tempterature (Tm) ≥65°C. NvFXF1 and NvFXR1 correspond to 125..146 nt and 241..261 nt of the SR4 template, respectively (Figure 8). The 50 µL PCR reaction included an overlay with mineral oil, 1X PCR Buffer, 200 µM dNTP, 1.5 mM $MgCl_2$, 2.5 U *Taq* DNA polymerase (Invitrogen), and 200 nM of NvFXF1 or NvFXR1 and AP1 (Table 1). PCR was performed using a final dilution of 1:50 of RACE library template on a Perkin-Elmer DNA Thermal Cycler 480 under the following parameters: initial denaturation at 94°C for 60 sec, 30 cycles of 94°C for 30 sec and 68°C for 4 min, with a final extension of 72°C for 10 min. The PCR products were electrophoresed on a 1.25% agarose gel and viewed with ethidium bromide.

To verify that the expanded SR4 template was amplified during the RACE procedure, a 1:20 dilution of the RACE PCR products was subjected to PCR with NvFXF1 and NvFXR1 primers. The 25 µL PCR reaction consisted of 1X PCR buffer, 1.5 mM $MgCl_2$, 200 µM dNTP, 400 nM each of NvFXF1 and NvFXR1, and 1.2 U *Taq* DNA Polymerase (Invitrogen). The PCR parameters included an initial denaturation at 95°C for 120 sec, 30 cycles of 95°C for 50 sec, 62.5°C for 30 sec, 72°C for 30 sec, and a final extension at 72°C for 10 min in an Eppendorf Mastercycler Gradient Thermocycler. The resulting PCR products were analyzed on a 1.6% ethidium bromide-stained agarose gel.

TABLE 1. Primers used in this thesis and their respective sequences, length and melting temperature (T_m). AP1 and AP2 sequences are from the Marathon RACE Library Kit (Clontech). T_m was determined from http://oligos.qiagen.com/oligos/toolkit.php.

Primer Sequence	**Sequence (5′ → 3′)**	**Length**	**T_m**
NvFXF1	CGCGCTGCTCTTTGTCCTGCTA	22	66.4
NvFXF2	CGCAGACCCCGCGCAAGGCACTAT	24	71.4
NvGas6_F2	GAAAGTAAATGCTTGCTTCCCGGTCGCT	28	67.5
NvGas6_F3	GCAAAGACTGCGTGCGGGCAACG	23	69.9
SeqGas6_F1	GGGTCGCCATACGCAAGGAATC	22	66.4
SeqGas6_F2	CACCTGCCACTGTGACGGAAGA	22	66.4
SeqGas6_F3	ATAGCGGGGCAGAGTGAAGTAAAC	24	64.6
Gas6_RT_F1	TGCCCCTGTCACTATCGCTCATCG	24	68.0
NvGas6_R2	GTGAAACGGGAAGCGGAGTTTGGTAA	26	66.2
SeqGas6_R1	CATGATAGAATGCGGTGACTGG	22	62.7
SeqGas6_R2	TTACGAAGAGTGCCAAAGAGTGAT	24	61.2
NvFXR1	GGTGGCCCTGCTTGGTCTCCT	21	68.4
NvFXR2	CAATAGTGCCTTGCGCGGGGTCTGC	25	71.1
Gas6_RT_R1	TGCCCCGCTATACCATCCACAGTC	24	68.0
NvGAPDH_F	TGTGGCGTGACGGCAGAGGTG	21	68.4
NvGAPDH_R	TCCAAGCGGCAGGTCAGGTCAAC	23	68.1
Nvβ-Actin_For	CCACTGCTGCTTCTTCATCCTCTC	24	66.3
Nvβ-Actin_Rev	GGGCACCTGAACCGCTCATTG	21	66.5
AP1	CCATCCTAATACGACTCACTATAGGGC	27	66.1
AP2	ACTCACTATAGGGCTCGAGCGGC	23	68.1
M13F	GTAAAACGACGGCCAGT	17	57.2
M13R	CAGGAAACAGCTATGAC	17	54.8

In order to identify PCR products that were specific to the expanded SR4 cDNA, nested PCR was carried out internal to the original primers used above. Nested RACE PCR was carried out with a final dilution of 1:10 of RACE PCR products under the same conditions as first round of RACE PCR, with nested primers NvFXF2, NvFXR2 and AP2 (Table 1). The cycling parameters included a touchdown step: 94°C for 1 min, 5 cycles of 94°C for 30 sec and 72°C for 4 min, 5 cycles of 94°C for 30 sec and 70°C for 4 min, 10 cycles of 94°C for 20 sec and 68°C for 4 min, and a final extension of 72°C for 10 min on an Perkin-Elmer DNA Rhermal Cycler 480. The PCR products were analyzed on a 1.1% ethidium bromide-stained agarose gel.

The 5' and 3' RACE PCR products were gel extracted using the QIAquick gel extraction kit (Qiagen) with the following modifications: elution buffer (5 mM Tris, pH 8.25) was prewarmed to 65°C, half of the recommended elution buffer volume was used and the eluant was passed through the column twice to yield a higher concentration. The gel extracted PCR products was A-tailed with 1X PCR Buffer, 1.5 mM dATP, 200 μM dATP, 5 U *Taq* polymerase (Invitrogen) and 7.5 μL PCR product at 70°C for 25 min in a 10 μL reaction. Next, 3 μL of the A-tailed products were ligated with the pGEM-T Easy Vector (Promega) at 4°C O/N. 3 μL of the ligated products were heat shock transformed into competent DH5α *Escherichia coli* and plated onto LB-ampicillin plates O/N at 37°C. Isolated colonies were replica plated and subjected to a PCR screening protocol to identify colonies with inserts. A single colony was inoculated into a 25 μL PCR reaction and PCR was carried out with the following parameters: 95°C for 2 min, 31 cycles of 94°C for 60 sec, 62°C for 90 sec and 72°C for 90 sec, and a final extension at 72°C for 10 min on an Eppendorf Mastercycler Gradient Thermocycler. The PCR solution consisted of 1X PCR Buffer, 1.5 mM $MgCl_2$, 200 μM dNTP, 50 ng of M13F and M13R primers (Table 1), and 1.25 U *Taq* DNA polymerase (Invitrogen). The products were visualized on a 1.3% agarose

gel stained with ethidium bromide. Colonies that represented the 5' and 3' RACE PCR products were inoculated into LB supplemented with ampicillin and grown O/N at 37°C with shaking. Plasmid DNA was isolated with the GenElute Plasmid Miniprep Kit (Sigma). The plasmids were sequenced by either CMRSInc or U of O Biotechnology Research Institute using the M13 sequencing primers.

2.3.3 Generation of *SR4* Full-Length cDNA

In order to confirm the SR4 contig, a PCR was undertaken to amplify the complete cDNA. Primers were constructed using the PrimerSelect software (DNAStar), using the default conditions, except that primers were restricted to the first 250 bp of both 5' and 3' ends. The 50 µL PCR conditions consisted of 1X PCR Buffer, 200 µM dNTP, 1.5 mM $MgCl_2$, 200 nM of NvGas6_F3 and NvGas6_R2 primers (Table 1; Figure 8) and 2.5 U *Taq* DNA polymerase, using 1:10 final dilution of the B1H1 RACE library. PCR was performed on an Eppendorf Mastercycler Gradient Thermocycler with the following parameters: 95°C for 2 min, 30 cycles of 94°C for 60 sec, 64°C for 60 sec and 72°C for 5 min, with a final extension of 72°C for 10 min. The PCR products were analyzed on a 1.1% agarose gel stained with ethidium bromide.

As the PCR procedure above did not result in a single band of the expected size, a PCR was undertaken to confirm that the SR4 template was amplified. 1 µL of the PCR products was subjected to PCR with the NvFXF1 and NvFXR1 primers, under the same parameters as Chapter 2.3.2.

In order to 'clean up' the PCR smear obtained above and to identify specific PCR fragments, a nested PCR was carried out. Nested PCR was performed using 2.5 µL of the original PCR products with NvGas6_F2 and NvGas6_R2 (Table 1; Figure 8) using the same cycling conditions as above, with the exception of an extension time of 3 min. The PCR products were visualized on a 1% ethidium bromide-stained agarose gel and a band of ~2.7

kb was gel extracted with the QIAquick Gel Extraction Kit (Qiagen) as above. The extracted product was subjected to the subcloning, screening and miniprep procedures mentioned in Chapter 2.3.2. This process was repeated with 2 independent PCR reactions, including one utilizing a proofreading enzyme (*Pfu* DNA Polymerase) from both B1H1 and 15 day regenerate RACE cDNA libraries to yield a consensus sequence. The *Pfu* PCR conditions were the same as above, except for extension time of 6 min, 2 mM $MgCl_2$ and 300 nM of each primer.

2.4 Real-Time Reverse Transcriptase Quantitative (RT-q)PCR

2.4.1 Primer Efficiency Analysis

Primers were synthesized with PrimerSelect (DNAStar) with the default parameters for an amplicon size of 75 to 175 bp. Total RNA was extracted from confluent B1H1 cells as described in Chapter 2.3.1. After verification of integrity and quantity with 1.2% agarose gel electrophoresis, first strand was generated from DNaseI-treated 2 µg total RNA primed with both 500 ng oligo(dT) and random hexamers (Promega) in a 30 µL standard reverse transcriptase reaction (Appendix II, Section B2). Real-time quantitative PCR (qPCR) was carried out on an iCycler iQ real-time thermocycler (Bio-Rad) using 33.3, 16.7, 3.33, 1.67, 0.333, 0.167, and 0.066 ng cDNA as template. A 25 µL PCR reaction was set up with the following conditions: 1X PCR Buffer, 2 mM $MgCl_2$, 200 µM dNTP, 0.9 U *Taq* DNA Polymerase (Invitrogen), 3:125,000 X SYBR I Green Dye (Molecular Probes), 8 nM Flourescein Calibration Dye (Bio-Rad), and 200 nM primers (NvGas6_RT_F1 and NvGas6_RT_F2, NvGAPDH_F, NvGAPDH_R, NvβActin_For and NvβActin_Rev; Table 1; Figure 8). The reaction was carried out under the following parameters: 95°C for 3 min, and 40 cycles of 94°C for 25 sec, 63°C for 25 sec and 83°C for 15 sec. This was followed by a 10 min extension at 72°C with a melt curve analysis under the following conditions: 95°C for 60 sec, 55°C for 60 sec and 80 cycles of 0.5°C increments every 10 sec. Each

reaction was performed in triplicate and 5 µL from each replicate was run on a 2.5% agarose gel. An efficiency plot of ΔC_T and log input total RNA was constructed, with the slope calculated (Appendix II, Section D).

2.4.2 B1H1 RT-qPCR Analysis

B1H1 cells were propagated and sampled under the following cell conditions: subconfluent, confluent, 4 day myotubes, 8 day myotubes and myotubes with serum resupplemented. Total RNA was extracted and verified for integrity and quantity using 1.2% agarose gel electrophoresis. First strand of each B1H1 sample was generated as previously described. Real-time RT-qPCR was carried out as above in an iCycler iQ real-time thermocycler (Bio-Rad) using 1 µL first strand as template in a 25 µL reaction. Each reaction was performed in triplicate and 5 µL of each replicate was visualized using 2.5% agarose gel electrophoresis. $\Delta\Delta C_T$ values were calculated relative to subconfluent B1H1 cells as described in Appendix II, Section D.

2.4.3 Regeneration RT-qPCR Analysis

Intact limbs, and 24 h, 5d, 7d, 15d, 21d PA and palette regenerating limbs were harvested and total RNA was extracted as per Appendix II, Section A. First strand, RT-qPCR and analysis were carried out as above.

2.5 Southern Blot Analysis

The following experiments were done to identify which portion of the NvGas6 cDNA was ideal for *in* situ hybridization analysis. Probing of the digested cDNA with newt genomic DNA was used to identify single copy (i.e., nonrepetitive) regions within the cDNA. Approximately 1 µg plasmid corresponding to the 3' ~2.5 kb RACE PCR product was incubated O/N with 5 U HindIII and SpeI, ApaI and SmaI, EcoRV and PstI, EcoRV and StyI, PstI and StyI, PvuII and XmnI, and HincII. The digests were stopped by

incubating the samples at 65°C for 15 min, and an aliquot was analyzed on a 1.3% ethidium-bromide gel to verify completeness of the restriction digest. In order to generate equimolar amounts of fragments, the amount of digested plasmid was calculated to load equal amounts onto the gel. The digested products were run on a 1.3% ethidium bromide-stained agarose gel, equimolar amounts verified by gel densitometry (ChemiDoc Gel Documentation System software, Bio-Rad) and transferred via upward capillary transfer under alkaline conditions onto a S&S Nytran Supercharge membrane (Appendix II, Section F).

Radioactive probe (^{32}P-dCTP) was generated from 50 ng of *N. viridescens* genomic DNA (prepared as per Appendix II, Section E) using the Rediprime II System (Amersham) as per the manufacturer's instructions. Following the 1 hour incubation at 37°C, the probe was topped to 100 µL with 5 µL 0.2 M EDTA and 45 µL TE buffer and the probe was purified by passing through a Microspin 3S-400 HR column (Amersham). The probe was boiled for 10 min, placed on ice and added to the hybridization solution (see below). A 5 µL aliquot was counted on a Beckman LS6000SC scintillator to determine the efficiency of the labelling reaction.

The membrane was prehybridized in a solution of 5X SSC, 5X Denhardt's, 1% SDS and 0.1 mg/mL sheared salmon sperm at 68°C for 45 min. Following this, the prehybridization solution was drained and fresh solution added along with the denatured probe. The blot was hybridized O/N at 68°C with shaking. The blot was subsequently washed twice with 2X SSC/0.1% SDS for 5 min each at RT, twice with 0.2 X SSC/0.1% SDS at RT for 5 min each, and twice with 0.2 X SSC/0.1% SDS at 42°C for 15 min each, with a final rinse in 2X SSC. The blot was exposed to Kodak Biomax MS autoradiography film for 2 days at -70°C and developed.

2.6 Sectioned In situ Hybridization

2.6.1. Tissue Fixation and Handling

In order to identify the sites of *NvGas6* expression in limb regeneration, sectioned *in situ* hybridization was performed on limb regenerates. Regenerating limbs were re-amputated at the following time points: 1, 7, 15 and 21 days, and at the palette stage. Tissues were fixed in 4% paraformaldehyde/1X PBS O/N at 4°C and equilibrated in 30% sucrose/1X PBS O/N. Subsequently, the tissues were transferred to a 50:50 mixture of 30% sucrose/1X PBS and OCT, orientated and frozen with liquid nitrogen or at -70°C. The embedded limbs were stored at -70°C until sectioning. Samples were sectioned at 16 μm in a Shandon cryostat, dried at RT for 1 hour, and stored desiccated at -70°C until use.

2.6.2 DIG-Labelled RNA Probe Generation

The region of the cDNA (as determined to be single copy by the southern blotting technique) utilised for a RNA probe was amplified by RT-PCR in a 25 μL PCR reaction consisting of 1X PCR buffer, 1.5 mM $MgCl_2$, 200 μM dNTP, 400 nM each of SeqGas6F2 and SeqGas6R2 (Table1; Figure 8), and 1.25 U *Taq* Polymerase (Invitrogen). The PCR parameters included an initial denaturation at 95°C for 120 sec, 29 cycles of 94°C for 60 sec, 63°C for 60 sec, 72°C for 90 sec, and a final extension at 72°C for 10 min on an Eppendorf Mastercycler Gradient Thermocycler. Following verification of a single amplicon of ~960 bp by 1.3% agarose gel electrophoresis, the PCR product was directly cloned into pGEM-T Easy Vector, transformed into DH5α *E. coli*, grown O/N under ampicillin selection and screened as described in Chapter 2.3.3. The colony that corresponded to the appropriate size was grown up in 5 mL LB media under ampicillin selection O/N at 37°C and the plasmid purified by a standard alkaline lysis protocol (Appendix II, Section G) and passed through a QIAprep spin column following the manufacturer's instructions (Qiagen). The plasmid was submitted for sequencing for

verification of the amplicon. Approximately 10 μg was linearized by SpeI and NcoI restriction enzymes to generate the antisense and sense probes for *NvGas6*, respectively. The digest was stopped, purified by phenol-chloroform-isoamyl alcohol extraction, and 11-digoxygenin UTP labelled RNA probe was generated as per the manufacturer's instructions (Roche).

2.6.3 *In Situ* Hybridization

The *in situ* hybridization analysis was based on a detailed protocol kindly provided by V. Wallace (OHRI, Ottawa, Canada) and is outlined in Appendix II, Section H. Briefly, slides were incubated with a solution containing 1X Salt, 50% deionised formamide, 10% dextran sulfate, 1 mg/mL yeast tRNA, 1X Denhardt's and a predetermined optimal probe dilution O/N at 65°C. The optimal probe dilution was determined by trying various dilutions and determining the dilution that gave the strongest, specific signal with minimal background staining. The next day, the slides were washed three times with a solution of 1X SSC, 50% formamide and 0.1% Tween-20 at 65°C (wash 1 = 15 min, washes 2 and 3 = 30 min each). Following this, the slides were equilibrated twice in 1X MABT for 30 min each at RT, and blocked for 2 hours at RT with a solution of 20% heat-inactivated sheep serum, 2% blocking reagent (Roche) and 1X MABT. The blocking solution was aspirated and the slides were incubated with anti-DIG antibody (Roche) diluted 1:1500 in the above blocking solution for 10 hr at 4°C.

The slides were washed with 1X MABT 4 times for 20 min each with rocking at RT, and equilibrated in 10% PVA, 100 mM NaCl, 100 mM Tris-HCl pH 9.3, 50 mM $MgCl_2$ and 0.1% Tween-20 for 10 min at RT with rocking. Following this, the slides were stained with the above solution with 0.45 mg/mL NBT (4-nitroblue tetrazolium chloride) and 0.175 mg/mL BCIP (x-phosphate/5-bromo-4-chloro-3-indolyl-phosphate) for approximately 18

hours. Development was terminated by washing 3 times with 1X PBS, and the sections were counterstained with Eosin Y (Appendix II, Section H) and mounted in Permount.

2.7 Statistical Analysis

All statistical analysis, including randomized ANOVA and paired Student T-tests were performed using the computer program RT (Manly 1997).

3. RESULTS

3.1 Identification of SR4

A 321 bp cDNA fragment (SR4) was isolated and kindly provided by S.Vascotto (OHRI, Ottawa, Canada). Initial translated basic local alignment search tool (BLASTX; http://www.ncbi.nlm.nih.gov/BLAST/) analysis using the default parameters with complexity filter switched off identified SR4 as the newt homologue of either mammalian Gas6, protein S or coagulation factor X (Figure 5). The region of similarity localized the fragment towards the 5′ end of the cDNA. However, no definite conclusions could be made concerning the identity of SR4 because the fragment exhibited strong homology to a conserved domain, the vitamin-k dependent GLA domain (Figure 6). Since this domain is found in many proteins, performing a cDNA library screen to isolate the full-length cDNA would likely result in numerous false positives. Thus, generation of the full-length cDNA was undertaken by a PCR-based strategy called rapid amplification of cDNA ends (RACE).

3.2 Isolation of Full-Length SR4 cDNA

3.2.1 Isolation of the 5′ End

The initial 5′ RACE reaction resulted in multiple bands with a slight background smear (Figure 7a). An aliquot of the RACE PCR products that was subjected to PCR using SR4-specific primers confirmed that the correct fragment was amplified during the RACE programme (data not shown). Since distinct bands were not amplified with the initial RACE reaction, a 1:10 dilution of the RACE product was used in nested RACE PCR, yielding amplicons ranging from approximately 500 bp to 100 bp (Figure 7b). Two gel-extracted clones from an area of between 300-500 bp were selected for sequencing and aligned with SR4 using the SeqMan software (DNAStar) to generate a 654 bp contig (Figure 8). There is an in-frame potential methionine (MET) start codon at 240 bp, which is immediately

Figure 5. Identity of SR4 based on a BLASTX search. The BLASTX search situated SR4 at the amino terminus of mammalian Gas6, protein S or coagulation factor X. The BLASTX search was performed with the default parameters with complexity filter switched off.

```
gi|9506715|ref|NP_062394.1| growth arrest specific 6 [Mus musculus]
Length = 673

 Score = 97.8 bits (242), Expect = 4e-20
 Identities = 50/71 (70%), Positives = 60/71 (84%)
 Frame = +3

Query: 108 AALLGAALLFVLLAADPAQGTIVLPAKEASQFLRSRQRRANQIFEETKQGHLERECVEER 287
           AA LG ALL +LLA++ +  T++L A+EA+QFLR RQRRA Q+FEE KQGHLERECVEE
Sbjct: 8   AAALGTALLLLLLASESSH-TVLLRAREAAQFLRPRQRRAYQVFEEAKQGHLERECVEEV 66

Query: 288 CSREEAREVFE 320
           CS+EEAREVFE
Sbjct: 67  CSKEEAREVFE 77

gi|16923942|ref|NP_476441.1| growth arrest specific 6 [Rattus norvegicus]
Length = 674

 Score = 96.3 bits (238), Expect = 1e-19
 Identities = 49/70 (70%), Positives = 59/70 (84%)
 Frame = +3

Query: 111 ALLGAALLFVLLAADPAQGTIVLPAKEASQFLRSRQRRANQIFEETKQGHLERECVEERC 290
           A LG ALL +LLA++ +  T++L A+EA+QFLR RQRRA Q+FEE KQGHLERECVEE C
Sbjct: 9   AALGTALLLLLLASESSH-TVLLRAREAAQFLRPRQRRAYQVFEEAKQGHLERECVEEVC 67

Query: 291 SREEAREVFE 320
           S+EEAREVFE
Sbjct: 68  SKEEAREVFE 77

gi|30841318|gb|AAO41859.1| growth arrest-specific 6 [Homo sapiens]
Length = 85

 Score = 95.5 bits (236), Expect = 2e-19
 Identities = 51/78 (65%), Positives = 56/78 (71%)
 Frame = +3

Query: 87  PSTMQAAAALLGAALLFVLLAADPAQGTIVLPAKEASQFLRSRQRRANQIFEETKQGHLE 266
           PS     AAL  A  L +LL A       +LPA+EA+QFLR RQRRA Q+FEE KQGHLE
Sbjct: 3   PSLSPGPAALRRAPQLLLLLLAAECALAALLPAREATQFLRPRQRRAFQVFEEAKQGHLE 62

Query: 267 RECVEERCSREEAREVFE 320
           RECVEE CSREEAREVFE
Sbjct: 63  RECVEELCSREEAREVFE 80

gi|31418736|gb|AAH53117.1| Unknown (protein for MGC:63860) [Danio rerio]
Length = 648

 Score = 77.4 bits (189), Expect = 5e-14
 Identities = 36/50 (72%), Positives = 45/50 (90%)
 Frame = +3

Query: 171 IVLPAKEASQFLRSRQRRANQIFEETKQGHLERECVEERCSREEAREVFE 320
           + + +++A QFLR R RRANQ+FEETKQGHLERECVEE+C++EEAREVFE
Sbjct: 21  VSVSSRQAHQFLR-RTRRANQVFEETKQGHLERECVEEKCTKEEAREVFE 69
```

```
gi|131086|sp|P07225|PRTS_HUMAN Vitamin K-dependent protein S precursor
Length = 676

 Score = 70.1 bits (170), Expect = 8e-12
 Identities = 38/65 (58%), Positives = 46/65 (70%)
 Frame = +3

Query: 126 ALLFVLLAADPAQGTIVLPAKEASQFLRSRQRRANQIFEETKQGHLERECVEERCSREEA 305
           ALL  LL   P      L  ++ASQ L  R+RRAN + EETKQG+LEREC+EE C++EEA
Sbjct: 10  ALLACLLLVLPVSEANFLSKQQASQVL-VRKRRANSLLEETKQGNLERECIEELCNKEEA 68

Query: 306 REVFE 320
           REVFE
Sbjct: 69  REVFE 73

gi|2144492|pir||EXCH coagulation factor Xa (EC 3.4.21.6) precursor - chicken
Length = 475

 Score = 67.8 bits (164), Expect = 4e-11
 Identities = 37/73 (50%), Positives = 48/73 (65%), Gaps = 4/73 (5%)
 Frame = +3

Query: 114 LLGAALLFVLLAADP----AQGTIVLPAKEASQFLRSRQRRANQIFEETKQGHLERECVE 281
           + G  LL +L AA P    A+G + +  + A +FL  R +RAN   EE KQG++EREC E
Sbjct: 1   MAGRLLLLLLCAALPDELRAEGGVFIKKESADKFLE-RTKRANSFLEEMKQGNIERECNE 59

Query: 282 ERCSREEAREVFE 320
           ERCS+EEARE FE
Sbjct: 60  ERCSKEEAREAFE 72


gi|8393340|ref|NP_058839.1| coagulation factor X [Rattus norvegicus]
Length = 482

 Score = 66.2 bits (160), Expect = 1e-10
 Identities = 36/65 (55%), Positives = 45/65 (69%)
 Frame = +3

Query: 126 ALLFVLLAADPAQGTIVLPAKEASQFLRSRQRRANQIFEETKQGHLERECVEERCSREEA 305
           +LL+V+LA+    G  V   +E +  +  R RRAN  FEE K+G+LERECVEE CS EEA
Sbjct: 8   SLLYVVLASLLLPGRSVFINRERANNVLQRIRRANSFFEEIKKGNLERECVEEICSFEEA 67

Query: 306 REVFE 320
           REVFE
Sbjct: 68  REVFE 72

gi|20893239|ref|XP_148185.1|  protein S (alpha) [Mus musculus]
Length = 675

 Score = 66.2 bits (160), Expect = 1e-10
 Identities = 36/64 (56%), Positives = 44/64 (68%)
 Frame = +3

Query: 129 LLFVLLAADPAQGTIVLPAKEASQFLRSRQRRANQIFEETKQGHLERECVEERCSREEAR 308
           LL  L    P   T  L  + ASQ L  R+RRAN +FEET +G+LEREC+EE C++EEAR
Sbjct: 11  LLACLALVIPVSETNFLSKERASQVL-VRKRRANTLFEETMKGNLERECIEELCNKEEAR 69

Query: 309 EVFE 320
           EVFE
Sbjct: 70  EVFE 73
```

Figure 6. Identification of a conserved domain on the SR4 fragment. The SR4 sequence was translated into an amino acid sequence in the +3 frame and the domain-mapping search identified a part of a module containing γ-carboxyglutamate (GLA) residues. The conserved domain search was performed with the default parameters with complexity filter switched off.

gnl|CDD|61, smart00069, GLA, Domain containing Gla (gamma-carboxyglutamate) residues. A hyaluronan-binding domain found in proteins associated with the extracellular matrix, cell adhesion and cell migration.

```
              CD-Length = 65 residues, only  80.0% aligned
              Score = 51.8 bits (124), Expect = 1e-08

Query:  55    GTIVLPAKEASQFLRSRQRRANQIFEETKQGHLERECVEERCSREEAREVFE  106
Sbjct:  1     GSVFLSRQEANKVLRRQRRANAFLLEELRPGNLERECQEEICSLEEAREVFE  52
```

gnl|CDD|7683, pfam00594, gla, Vitamin K-dependent carboxylation/gamma-carboxyglutamic (GLA) domain. This domain is responsible for the high-affinity binding of calcium ions. This domain contains post-translational modifications of many glutamate residues by Vitamin K-dependent carboxylation to form gamma-carboxyglutamate (Gla).

```
              CD-Length = 42 residues, only  66.7% aligned
              Score = 39.8 bits (93), Expect = 5e-05

Query:  79    FEETKQGHLERECVEERCSREEAREVFE  106
Sbjct:  1     LEELRPGNLERECLEEVCELEEACEIFA  28
```

Figure 7. Results of the 5′ and 3′ RACE PCR, and generation of the complete NvGas6 cDNA. a) Initial RACE PCR of the 5′ and 3′ ends resulted in multiple bands with a slight background smear. b) 3′ and 5′ nested RACE PCR. Using an aliquot of the initial RACE PCR products resulted in a range of transcripts sizes. c) The band corresponding to the intact NvGas6 cDNA is shown here.

a) Initial RACE

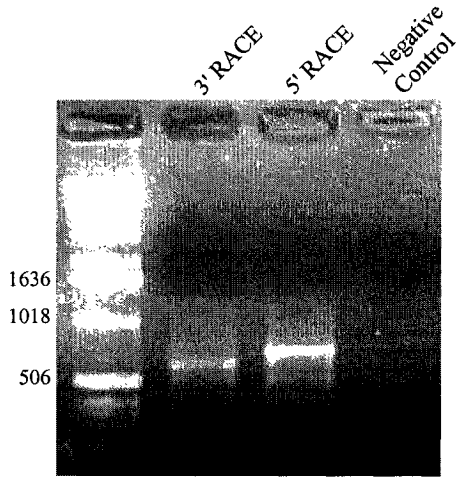

b) Nested RACE

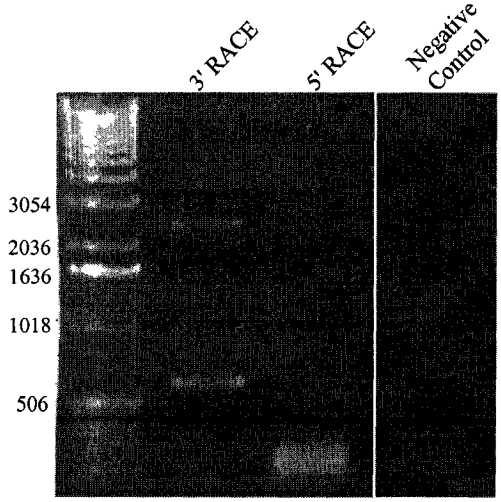

c) Complete cDNA

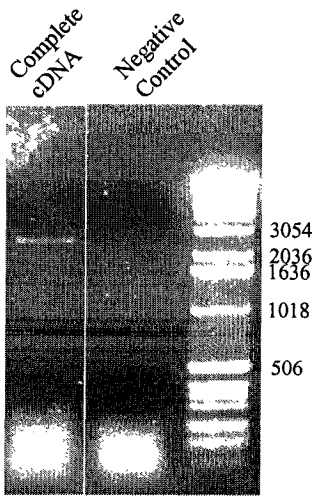

Figure 8. A "to scale" schematic of assembly of the SR4 full-length contig, with locations of primers and sizes of the RACE amplicons.

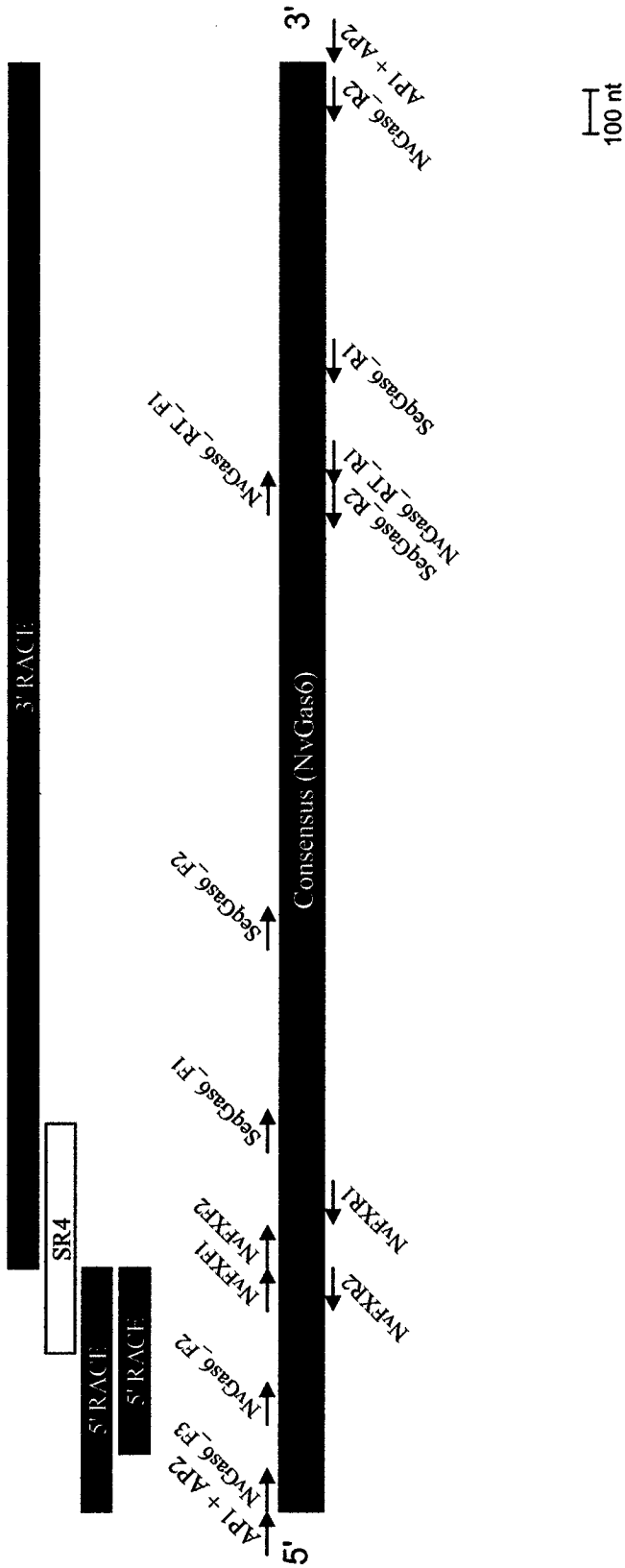
3'
5'
100 nt
API + AP2
NvGas6_R2
SeqGas6_R1
NvGas6_RT_F1
NvGas6_RT_R1
SeqGas6_R2
Consensus (NvGas6)
SeqGas6_F2
SeqGas6_F1
NvFXR1
NvFXF2
NvFXF1
NvFXR2
NvGas6_F2
NvGas6_F3
API + AP2
3' RACE
SR4
5' RACE
5' RACE

Figure 9. The complete SR4 nucleotide sequence. Identified in this 2,895 kb sequence are stop codons (red), potential MET translation start sites (green), transcription termination signal and poly(A) tail (blue).

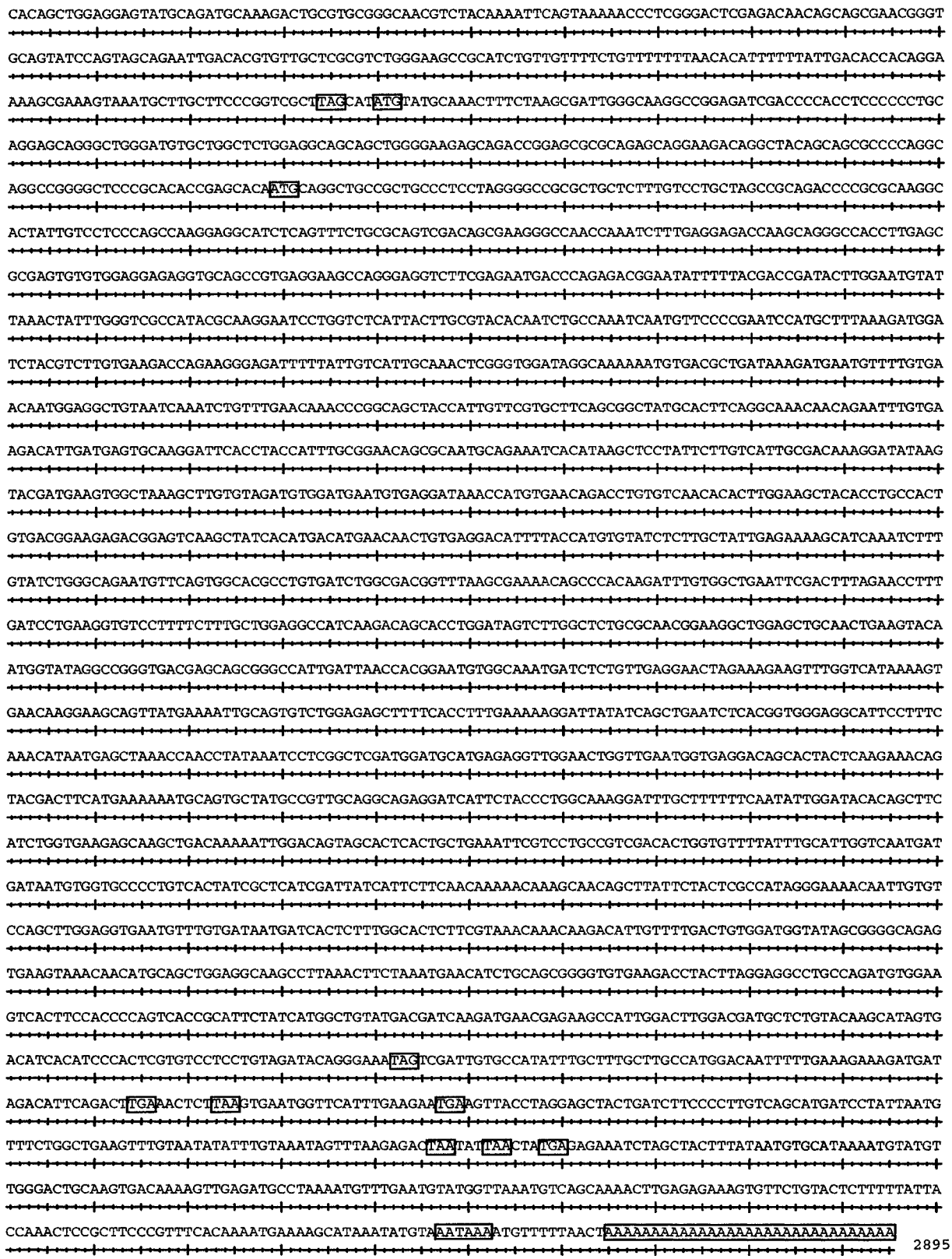
CACAGCTGGAGGAGTATGCAGATGCAAAGACTGCGTGCGGGCAACGTCTACAAAATTCAGTAAAAACCCTCGGGACTCGAGACAACAGCAGCGAACGGGT
100
GCAGTATCCAGTAGCAGAATTGACACGTGTTGCTCGCGTCTGGGAAGCCGCATCTGTTGTTTTCTGTTTTTTTAACACATTTTTTATTGACACCACAGGA
200
AAAGCGAAAGTAAATGCTTGCTTCCCGGTCGCTTAGCATATGTATGCAAACTTTCTAAGCGATTGGGCAAGGCCGGAGATCGACCCCACCTCCCCCCTGC
300
AGGAGCAGGGCTGGGATGTGCTGGCTCTGGAGGCAGCAGCTGGGGAAGAGCAGACCGGAGCGCGCAGAGCAGGAAGACAGGCTACAGCAGCGCCCCAGGC
400
AGGCCGGGGCTCCCGCACACCGAGCACAATGCAGGCTGCCGCTGCCCTCCTAGGGGCCGCGCTGCTCTTTGTCCTGCTAGCCGCAGACCCCGCGCAAGGC
500
ACTATTGTCCTCCCAGCCAAGGAGGCATCTCAGTTTCTGCGCAGTCGACAGCGAAGGGCCAACCAAATCTTTGAGGAGACCAAGCAGGGCCACCTTGAGC
600
GCGAGTGTGTGGAGGAGAGGTGCAGCCGTGAGGAAGCCAGGGAGGTCTTCGAGAATGACCCAGAGACGGAATATTTTTACGACCGATACTTGGAATGTAT
700
TAAACTATTTGGGTCGCCATACGCAAGGAATCCTGGTCTCATTACTTGCGTACACAATCTGCCAAATCAATGTTCCCCGAATCCATGCTTTAAAGATGGA
800
TCTACGTCTTGTGAAGACCAGAAGGGAGATTTTTATTGTCATTGCAAACTCGGGTGGATAGGCAAAAAATGTGACGCTGATAAAGATGAATGTTTTGTGA
900
ACAATGGAGGCTGTAATCAAATCTGTTTGAACAAACCCGGCAGCTACCATTGTTCGTGCTTCAGCGGCTATGCACTTCAGGCAAACAACAGAATTTGTGA
1000
AGACATTGATGAGTGCAAGGATTCACCTACCATTTGCGGAACAGCGCAATGCAGAAATCACATAAGCTCCTATTCTTGTCATTGCGACAAAGGATATAAG
1100
TACGATGAAGTGGCTAAAGCTTGTGTAGATGTGGATGAATGTGAGGATAAACCATGTGAACAGACCTGTGTCAACACACTTGGAAGCTACACCTGCCACT
1200
GTGACGGAAGAGACGGAGTCAAGCTATCACATGACATGAACAACTGTGAGGACATTTTACCATGTGTATCTCTTGCTATTGAGAAAAGCATCAAATCTTT
1300
GTATCTGGGCAGAATGTTCAGTGGCACGCCTGTGATCTGGCGACGGTTTAAGCGAAAACAGCCCACAAGATTTGTGGCTGAATTCGACTTTAGAACCTTT
1400
GATCCTGAAGGTGTCCTTTTCTTTGCTGGAGGCCATCAAGACAGCACCTGGATAGTCTTGGCTCTGCGCAACGGAAGGCTGGAGCTGCAACTGAAGTACA
1500
ATGGTATAGGCCGGGTGACGAGCAGCGGGCCATTGATTAACCACGGAATGTGGCAAATGATCTCTGTTGAGGAACTAGAAAGAAGTTTGGTCATAAAAGT
1600
GAACAAGGAAGCAGTTATGAAAATTGCAGTGTCTGGAGAGCTTTTCACCTTTGAAAAAGGATTATATCAGCTGAATCTCACGGTGGGAGGCATTCCTTTC
1700
AAACATAATGAGCTAAACCAACCTATAAATCCTCGGCTCGATGGATGCATGAGAGGTTGGAACTGGTTGAATGGTGAGGACAGCACTACTCAAGAAACAG
1800
TACGACTTCATGAAAAAATGCAGTGCTATGCCGTTGCAGGCAGAGGATCATTCTACCCTGGCAAAGGATTTGCTTTTTTCAATATTGGATACACAGCTTC
1900
ATCTGGTGAAGAGCAAGCTGACAAAAATTGGACAGTAGCACTCACTGCTGAAATTCGTCCTGCCGTCGACACTGGTGTTTTATTTGCATTGGTCAATGAT
2000
GATAATGTGGTGCCCCTGTCACTATCGCTCATCGATTATCATTCTTCAACAAAAACAAAGCAACAGCTTATTCTACTCGCCATAGGGAAAACAATTGTGT
2100
CCAGCTTGGAGGTGAATGTTTGTGATAATGATCACTCTTTGGCACTCTTCGTAAACAAACAAGACATTGTTTTGACTGTGGATGGTATAGCGGGGCAGAG
2200
TGAAGTAAACAACATGCAGCTGGAGGCAAGCCTTAAACTTCTAAATGAACATCTGCAGCGGGGTGTGAAGACCTACTTAGGAGGCCTGCCAGATGTGGAA
2300
GTCACTTCCACCCCAGTCACCGCATTCTATCATGGCTGTATGACGATCAAGATGAACGAGAAGCCATTGGACTTGGACGATGCTCTGTACAAGCATAGTG
2400
ACATCACATCCCACTCGTGTCCTCCTGTAGATACAGGGAAATAGTCGATTGTGCCATATTTGCTTTGCTTGCCATGGACAATTTTTGAAAGAAAGATGAT
2500
AGACATTCAGACTTGAAACTCTTAAGTGAATGGTTCATTTGAAGAATGAAGTTACCTAGGAGCTACTGATCTTCCCCTTGTCAGCATGATCCTATTAATG
2600
TTTCTGGCTGAAGTTTGTAATATATTTGTAAATAGTTTAAGAGACTAATATTAACTATGAGAGAAATCTAGCTACTTTATAATGTGCATAAAATGTATGT
2700
TGGGACTGCAAGTGACAAAAGTTGAGATGCCTAAAATGTTTGAATGTATGGTTAAATGTCAGCAAAACTTGAGAGAAAGTGTTCTGTACTCTTTTTATTA
2800
CCAAACTCCGCTTCCCGTTTCACAAAATGAAAAGCATAAATATGTAAATAAAATGTTTTTAACTAAAAAAAAAAAAAAAAAAAAAAAAAAAAA
2895

downstream of a stop codon. However, both BLASTX analysis (Chapter 3.3) and a weak similarity to the mammalian Kozak sequence (ACCATGG, Kozak 1999) place the putative MET translational start site at 429 bp from the 5′ end of the contig (Figure 9).

3.2.2 Isolation of the 3′ End

As the 3′ RACE PCR products demonstrated a smear ranging from 1 kb to 100 bp (Figure 7a), an aliquot of the products was subjected to PCR using primers NvFXF1 and NvFXR1, and this verified that the SR4 template was amplified during RACE (data not shown). An aliquot of the RACE PCR products was subjected to nested RACE PCR. The largest band (~ 2.4 kb; Figure 7b) was gel extracted and submitted for sequencing. The sequencing process yielded approximately 500 bp high-quality sequence on each end of the clone but was was unable to elucidate the ~1.4 kb of the middle sequence. Primer walking was initiated with Seq_Gas6F1, Seq_Gas6F2, SeqGas6R1 and Seq_Gas6R2 (Table 1; Figure 8; primers were designed using PrimerSelect (DNAStar) using the default parameters) to bridge the gap. The resulting 2.9 kb contig includes the 5′ UTR, complete coding sequence and the 3′ UTR, including the transcriptional termination signal (AATAAA) and poly(A) tail (Figure 9).

3.2.3 Generation of Complete cDNA

With the 5′ and 3′ ends of extended SR4 elucidated, generation of the full-length cDNA as a method of validating the assembled contig was possible by PCR. Since a primary PCR experiment resulted in no observable bands corresponding to a ~2.7 kb amplicon, an aliquot of the PCR products was used to verify that SR4 was amplified. With the presence of the SR4 amplicon (data not shown), nested PCR was performed on the original PCR products and a band corresponding to the expected size of ~2.6 kb was observed (Figure 7c). The amplicon was gel extracted and sequencing with Seq_Gas6F1,

Seq_Gas6F2, Seq_Gas6F3, SeqGas6R1 and Seq_Gas6R2 primers (Table 1; Figure 8) confirmed that the assembled contig was real.

3.3 SR4 Contig Homology Analysis

To identify potential similarity between the SR4 contig and known genes in other species, bioinformatic searches were performed utilizing BLASTX, ORF finder, and conserved domain search tools.

There are several BLAST algorithms that differ in strengths and weaknesses. A straightforward nucleotide BLAST (BLASTN) search compares a nucleotide query with DNA databases. This algorithm is the simplest and quickest method of finding relationships. However, there exists differing codon usage among species (Xia 1996), and there is no categorized list concerning caudates that can facilitate stronger relationships. As such, performing straight untranslated DNA searches is unlikely to reveal positive meaningful relationships, unless the region being analyzed is highly conserved at the nucleotide level through genera. Therefore, to maximize sensitivity when querying unknown sequences, translated searches in all 6 possible reading frames (i.e., BLASTX) with the low complexity filter switched off were performed. Using the default parameters, BLASTX analysis identified the SR4 contig as the newt orthologue of mammalian Gas6 with an immeasurable E-value (Figure 10).

The ORF finder software (http://www.ncbi.nlm.nih.gov/gorf/gorf.html) was utilized to identify unbroken reading frame(s), and to verify sequence orientation and the BLASTX 'hits.' The ORF search identified one major reading frame, with 2 putative MET translational start sites (data not shown). Subsequent BLASTP analysis confirmed that this open reading frame was the one which showed homology to mammalian Gas6 (data not shown), affirming the BLASTX search results.

Figure 10. BLASTX identifies the SR4 contig as the newt orthologue of mammalian growth arrest specific 6 (Gas6). Shown is the sequence with highest similarity to the SR4 contig. The BLASTX search was performed with the default parameters with complexity filter switched off.

gi|16923942|ref|NP_476441.1| growth arrest specific 6 [Rattus norvegicus]
Length = 674
Score = 906 bits (2342), Expect = 0.0
Identities = 428/664 (64%), Positives = 523/664 (78%), Gaps = 1/664 (0%)
Frame = +3

```
Query: 444  ALLGAALLFVLLAADPAQGTIVLPAKEASQFLRSRQRRANQIFEETKQGHLERECVEERC 623
            A LG ALL +LLA++ +  T++L A+EA+QFLR RQRRA Q+FEE KQGHLERECVEE C
Sbjct: 9    AALGTALLLLLLASESSH-TVLLRAREAAQFLRPRQRRAYQVFEEAKQGHLERECVEEVC 67

Query: 624  SREEAREVFENDPETEYFYDRYLECIKLFGSPYARNPGLITCVHNLPNQCSPNPCFKDGS 803
            S+EEAREVFENDPET+YFY RY EC++ +G P  +NP   TCV NLP+QC+PNPC K G+
Sbjct: 68   SKEEAREVFENDPETDYFYPRYQECMRKYGRPEDKNPNFATCVKNLPDQCTPNPCDKKGT 127

Query: 804  TSCEDQKGDFYCHCKLGWIGKKCDADKDECFVNNGGCNQICLNKPGSYHCSCFSGYALQA 983
              C+D  G+F+C CK GW G+ CD D +EC   NGGC+Q+C NKPGS+ C+C SG++LQ+
Sbjct: 128  QLCQDLMGNFFCLCKDGWGGRLCDKDVNECSQKNGGCSQVCHNKPGSFQCACHSGFSLQS 187

Query: 984  NNRICEDIDECKDSPTICGTAQCRNHISSYSCHCDKGYKYDEVAKACVDVDECEDKPCEQ 1163
            +N+ C+DIDEC DS T CG A+C+N   SYSC CDKGY Y    K C DVDEC+   CEQ
Sbjct: 188  DNKSCQDIDECTDSDT-CGDARCKNLPGSYSCLCDKGYTYSSKEKTCQDVDECQQDRCEQ 246

Query: 1164 TCVNTLGSYTCHCDGRDGVKLSHDMNNCEDILPCVSLAIEKSIKSLYLGRMFSGTPVIWR 1343
            TCVN+ GSYTCHC+GR G+KLS DM+ CEDILPCV  ++ KS+KSLYLGRMFSGTPVI
Sbjct: 247  TCVNSPGSYTCHCNGRGGLKLSPDMDTCEDILPCVPFSMAKSVKSLYLGRMFSGTPVIRL 306

Query: 1344 RFKRKQPTRFVAEFDFRTFDPEGVLFFAGGHQDSTWIVLALRNGRLELQLKYNGIGRVTS 1523
            RFKR QPTR +AEFDFRTFDPEGVLFFAGG  DSTWIVL LR GRLELQL+YNG+GR+TS
Sbjct: 307  RFKRLQPTRLLAEFDFRTFDPEGVLFFAGGRSDSTWIVLGLRAGRLELQLRYNGVGRITS 366

Query: 1524 SGPLINHGMWQMISVEELERSLVIKVNKEAVMKIAVSGELFTFEKGLYQLNLTVGGIPFK 1703
            SGP INHGMWQ ISVEEL+R+LVIKVNK+AVMKIAV+G LF  E+GLY LNLTVGGIPFK
Sbjct: 367  SGPTINHGMWQTISVEELDRNLVIKVNKDAVMKIAVAGGLFQLERGLYHLNLTVGGIPFK 426

Query: 1704 HNELNQPINPRLDGCMRGWNWLNGEDSTTQETVRLHEKMQCYAVAGRGSFYPGKGFAFFN 1883
             ++L QPINPRLDGCMR WNWLNGEDS  QETV+ + KMQC++V  RGSF+PG GFAF++
Sbjct: 427  ESDLVQPINPRLDGCMRSWNWLNGEDSAIQETVKANTKMQCFSVTERGSFFPGNGFAFYS 486

Query: 1884 IGYTASSGEEQADKNWTVALTAEIRPAVDTGVLFALVNDDNVVPLSLSLIDYHSSTKTKQ 2063
            + YT +S +   +  W V + A IRPA DTGVL ALV D +VV LS++L+DYHS+ K K+
Sbjct: 487  LNYTRTSLDVGTETTWEVEVVARIRPATDTGVLMALVGDKDVVLLSVALVDYHSTKKLKK 546

Query: 2064 QLILLAIGKTIVSSLEVNVCDN-DHSLALFVNKQDIVLTVDGIAGQSEVNNMQLEASLKL 2240
            QL++LA+    ++ +E+ VCD+ +H++ + +   +  L VDG  GQSEV+  QL+  L L
Sbjct: 547  QLVVLAVENVALALMEIKVCDSQEHTVTVSLRDGEATLEVDGTKGQSEVSTAQLQERLDL 606

Query: 2241 LNEHLQRGVKTYLGGLPDVEVTSTPVTAFYHGCMTIKMNEKPLDLDDALYKHSDITSHSC 2420
            L   LQ  V T++GGLPDV+VTSTPVTAFY GCMT+++N K LDLD A YKHSDITSHSC
Sbjct: 607  LKTRLQGSVLTFVGGLPDVQVTSTPVTAFYRGCMTLEVNGKTLDLDTASYKHSDITSHSC 666

Query: 2421 PPVD 2432
            PPV+
Sbjct: 667  PPVE 670
```

Figure 11. Results of the conserved domain and database search of the SR4 full-length contig revealed a γ-carboxyglutmaic acid (GLA) domain followed by 4 tandem repeats of epidermal-like growth factor (EGF) modules and 2 laminin G-like (LamG) domains.

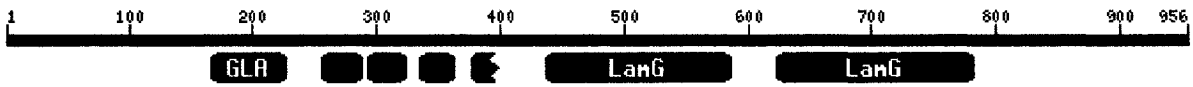

gnl|CDD|61, smart00069, GLA, Domain containing Gla (gamma-carboxyglutamate) residues
CD-Length = 65 residues, 98.5% aligned Score = 80.3 bits (198), Expect = 8e-16
Query: 165 GTIVLPAKEASQFLRSRQRRAN-QIFEETKQGHLERECVEERCSREEAREVFENDPETEY 223
Sbjct: 1 GSVFLSRQEANKVLR-RQRRANAFLLEELRPGNLERECQEEICSLEEAREVFEDNEGTDE 59
Query: 224 FYDRY 228
Sbjct: 60 FYRRY 64

gnl|CDD|14791, cd00054, EGF_CA, Calcium-binding EGF-like domain
CD-Length = 38 residues, only 76.3% aligned Score = 38.7 bits (90), Expect = 0.003
Query: 375 DVDECEDK-PCE--QTCVNTLGSYTCHCD 400
Sbjct: 1 DIDECASGNPCQNGGTCVNTVGSYRCSCP 29
gnl|CDD|14791, cd00054, EGF_CA, Calcium-binding EGF-like domain
CD-Length = 38 residues, 92.1% aligned Score = 38.3 bits (89), Expect = 0.004
Query: 292 DKDECFVNNG-GCNQICLNKPGSYHCSCFSGYALQ 325
Sbjct: 1 DIDECASGNPCQNGGTCVNTVGSYRCSCPPGYTGR 35
gnl|CDD|14791, cd00054, EGF_CA, Calcium-binding EGF-like domain,
CD-Length = 38 residues, 84.2% aligned Score = 37.9 bits (88), Expect = 0.006
Query: 333 DIDECKDSPTICGTAQCRNHISSYSCHCDKGY 364
Sbjct: 1 DIDECASGNPCQNGGTCVNTVGSYRCSCPPGY 32
gnl|CDD|14791, cd00054, EGF_CA, Calcium-binding EGF-like domain
CD-Length = 38 residues, 94.7% aligned Score = 37.6 bits (87), Expect = 0.007
Query: 254 NQC-SPNPCFKDGSTSCEDQKGDFYCHCKLGWIGKKCD 290
Sbjct: 3 DECASGNPCQNGGT--CVNTVGSYRCSCPPGYTGRNCE 38

gnl|CDD|5359, cd00110, LamG, Laminin G domain;
CD-Length = 151 residues, 99.3% aligned Score = 107 bits (267), Expect = 9e-24
Query: 435 GRMFSGTPVIWRRFKRKQPTRFVAEFDFRTFDPEGVLFFAGGHQDSTWIVLALRNGRLEL 494
Sbjct: 1 GVSFSGSSYVRLPTLPAPRTRLSISFSFRTTSPNGLLLYAGSQNGGDFLALELEDGRLVL 60
Query: 495 QLKYNGIGRVTSSGPLINHGMWQMISVEELERSLVIKVNKEAVMKIAVSGELFTFEKGLY 554
Sbjct: 61 RYDLGSGSLVLSSKTPLNDGQWHSVSVERNGRSVTLSVDGERVVESGSPGGSALLNL--- 117
Query: 555 QLNLTVGGIPFKHNELNQPINPRLDGCMRGWNW 587
Sbjct: 118 DGPLYLGGLPEDLKSPGLPVSPGFVGCIRDLKV 150
gnl|CDD|5359, cd00110, LamG, Laminin G domain;
CD-Length = 151 residues, 100.0% aligned Score = 52.8 bits (126), Expect = 2e-07
Query: 621 GFAFFNIGYTASSGEEQADKNWTVALTAEIRPAVDTGVLFALVNDDNVVPLSLSLIDYHS 680
Sbjct: 1 GVSFSGSSYVRLPTLPAPRTRLSISF--SFRTTSPNGLLLYAGSQNGGDFLALELEDGRL 58
Query: 681 STKTKQQLILLAIGKTIVSSLEVNVCDN-DHSLALFVNKQDIVLTVDGIAGQSEVNNMQL 739
Sbjct: 59 VLRYD-----LGSGSLVLSS-KTPLNDGQWHSVSVERNGRSVTLSVDGER--------VV 104
Query: 740 EASLKLLNEHLQRGVKTYLGGLPD-VEVTSTPVTAFYHGCM-TIKMN 784
Sbjct: 105 ESGSPGGSALLNLDGPLYLGGLPEDLKSPGLPVSPGFVGCIRDLKVN 151

Figure 12. Multiple alignment of NvGas6 amino acid sequence with mammalian Gas6 sequences. Yellow shading reveals areas of amino acid identity. The red boxes represent approximate areas of each Gas6 domain. The GLA domain represents the γ-carboxyglutamic acid module, EGF_CA is epidermal-like growth factor domains and LamG are laminin G-like domains. Blue asterisks identify key conserved residues of the GLA propeptide. Red asterisks identify Gla residues. Blue numbers identify conserved cysteine residues within each EGF_CA tandem repeat. The analysis was performed with the CLUSTALV algorithm on MegAlign (DNAStar) with the default parameters. *N. viridescens* (red spotted newt, NvGas6), *H. sapiens* (human, NP_062394), *R. rattus* (Norway rat, NP_476441) and *M. musculus* (mouse, AAH05444).

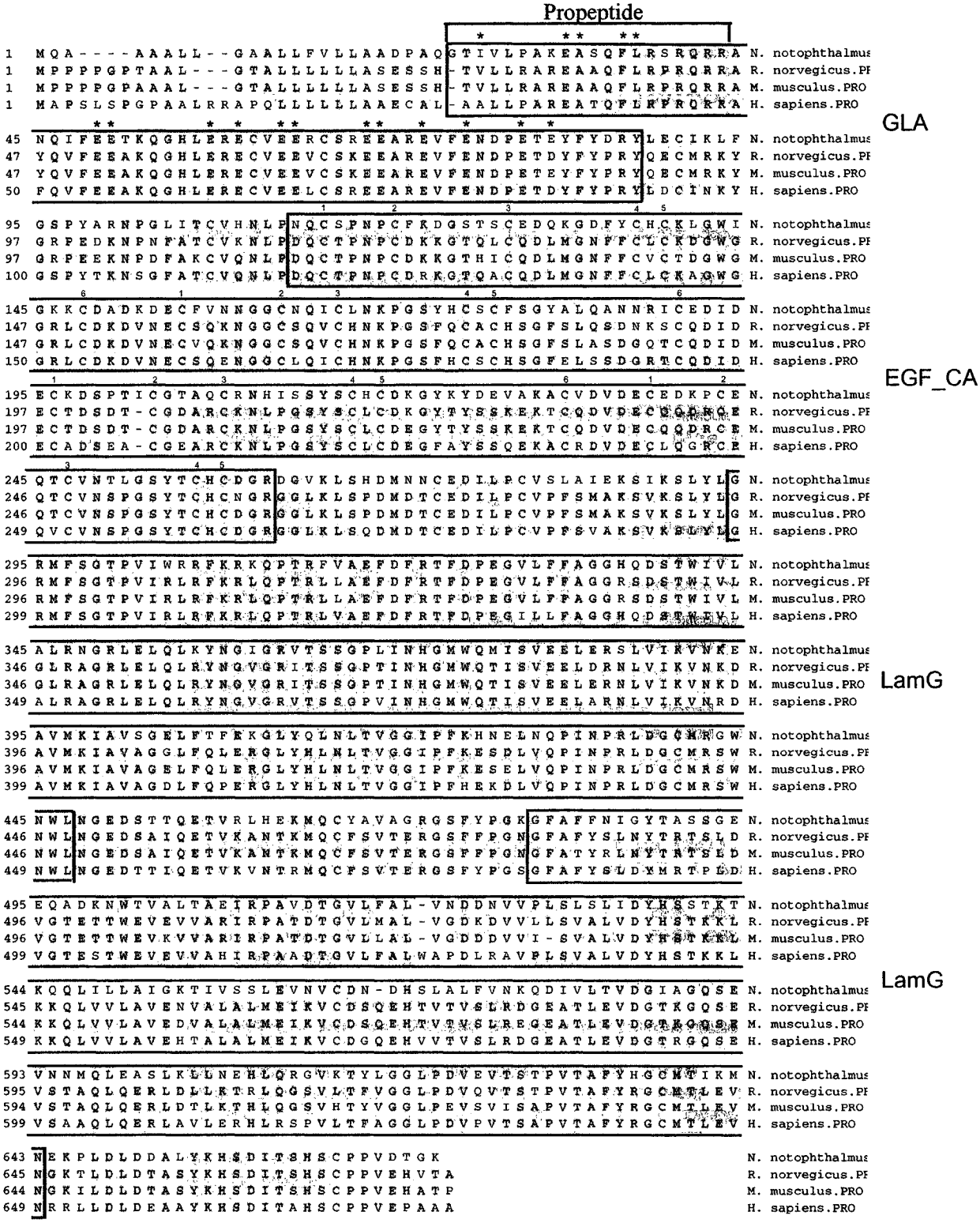
Propeptide
GLA
EGF_CA
LamG
LamG

The conserved domain database and search tool (http://www.ncbi.nlm.nih.gov/Structure/cdd/wrpsb.cgi) was utilized to identify potential domain sites. As homologous proteins commonly have conserved modules or domains, this information provides additional empirical evidence towards the identity of the SR4 contig. Translating the whole cDNA to an amino acid sequence in the +3 reading frame identified 5 major domain regions: one GLA, 4 EGF-CA and 2 LamG domains (Figure 11), which correspond to the domains found in Gas6 and protein S. However, the cDNA is unlikely to be the newt orthologue of protein S as SR4 lacks the consensus to be susceptible to trypsin cleavage (data not shown).

Combined, the above analyses verified that the SR4 cDNA is a newt homologue of Gas6 (NvGas6). Although NvGas6 shows 77-78% similarity with mammalian Gas6, it also exhibits close similarity to human protein S (64%). Of particular interest is the significant similarity to an unknown protein from *Danio rerio* (70%), which is most likely to be the zebrafish homologue of Gas6. Multiple alignments with known Gas6 genes in other species showed that the major domains are conserved, including key residues in the GLA propeptide sequence and cysteine sites in the EGF_CA modules (Figure 12), suggesting significant evolutionary conservation across taxa.

3.4 Gas6 Expression Analysis Using the Real-Time qPCR Method

3.4.1 Preliminary Real-Time RT-qPCR Analysis

The method used in this thesis is based on the relative quantification approach by the comparative threshold cycle (C_T) method (Livak and Schmittgen 2001) using the SYBR Green I dye, which is similar to the standard curve method except that algebraic formulas are utilized. In order to use this method, a validation experiment must be performed, demonstrating that the PCR efficiency of each gene approaches 100% and relative PCR efficiencies (i.e., gene of interest and normalization factor) are approximately equal (slope

is less than 0.1). The NvGas6 primers are an acceptable combination, with a PCR efficiency of 96.0% and $R^2 = 0.988$ (Figure 13a). An efficiency plot (i.e., ΔC_T versus log cDNA) of *NvGas6* and housekeeping genes *NvGAPDH* and *Nvβ-actin* yielded absolute slope values of 0.114 ($F = 2.38$, $df = 1,19$, $p_r = 0.143$, $R^2 = 0.111$) and 0.0148 ($F = 0.042$, $df = 1,19$, $p_r = 0.844$, $R^2 = 0.00218$), respectively (Figure 13b). With *NvGas6-Nvβ-actin* almost at zero, normalization of *NvGas6* to *Nvβ-actin* is permitted. Although the *NvGas6-NvGAPDH* PCR efficiency is above 0.1, *NvGas6* was still normalized to *Nvβ-NvGAPDH* because the 0.1 cut-off is a conservative and arbitrary value, the p_r value is insignificant, and was used to determine if the same profile exists for another normalization gene. Repeating the validation experiment with different first strand sources resulted in similar values (data not shown).

3.4.2 B1H1 *NvGas6* Expression Profile

Real-time RT-qPCR analysis was performed to delineate the *NvGas6* expression profile under various B1H1 cell culture conditions, including subconfluent and confluent cultures, myotubes (induced by exposure to low serum conditions for 4 and 8 d), and serum resupplemented myotubes. The real-time analysis shows that expression increases with myogenesis and decreases upon serum resupplementation of myotubes (Figure 14a). There is a significant increase in expression between subconfluent cells and both 4 day and 8 day myotubes (t-test = -9.53, df = 2, p = 0.011 and t-test = -5.02, df = 2 p = 0.027, respectively) and a concomitant decrease of *NvGas6* expression from myogenesis to cell cycle reentry (t-test = 4.91, df = 2, p = 0.039). All replications had the same general profile.

3.4.3 Limb Regeneration *NvGas6* Expression Profile

The *NvGas6* expression profile during forelimb regeneration illustrates increasing *NvGas6* expression from intact limb up to 21 days, a peak at 21d PA and decreasing expression at the palette stage of regeneration (Figure 14b). There is a statistically

Figure 13. A real-time RT-qPCR efficiency plot of *NvGas6*. a) Real-time analysis of *NvGas6* over a range of concentrations of B1H1 cell cDNA revealed that the primer combination is an ideal candidate for RT-qPCR with a PCR efficiency of 96%. Amplification efficiency was determined by the equation $E = [10^{(-1/slope)} - 1]$. b) A comparative RT-qPCR efficiency plot between *NvGas6* and normalisation genes *NvGAPDH* and *Nvβ-actin*. Over a 500-fold concentration difference, the slopes were ≤ 0.1, with $p_r \geq 0.1$. Thus, using the $\Delta\Delta C_T$ method of quantifying real-time results is valid. The dotted line represents the mean of ΔC_T values.

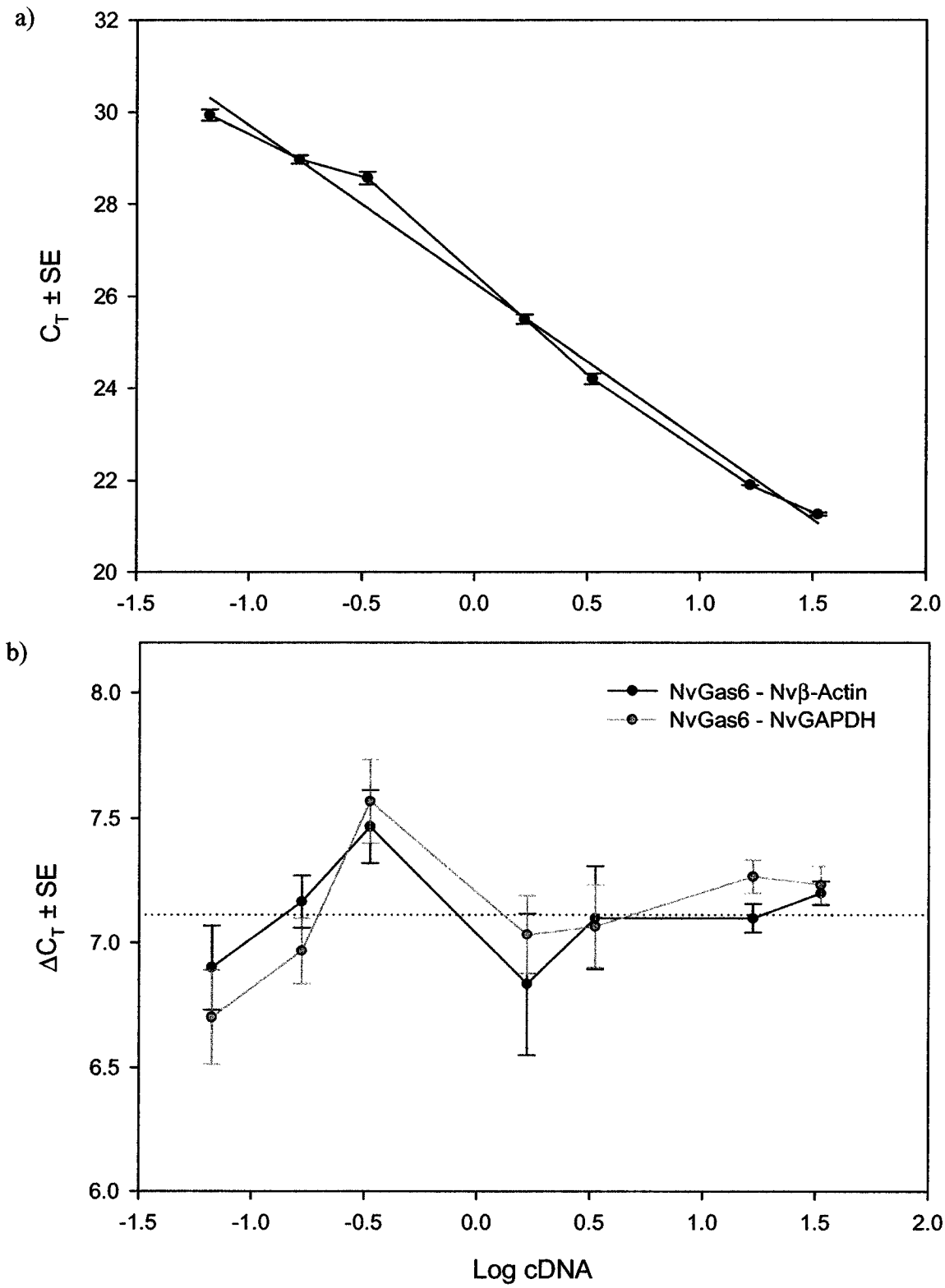
a)
32
30
28
26
24
22
20
$C_T \pm SE$
-1.5
-1.0
-0.5
0.0
0.5
1.0
1.5
2.0
b)
8.0
7.5
7.0
6.5
6.0
$\Delta C_T \pm SE$
NvGas6 - Nvβ-Actin
NvGas6 - NvGAPDH
Log cDNA

Figure 14. Real-time expression profile of *NvGas6* under different B1H1 cell conditions and during forelimb regeneration. a) There is an increase in *NvGas6* expression during the formation of myotubes and cell cycle arrest, with a concomitant decrease during cell cycle reentry. Cell conditions are: subconfluent (Sub, ≤60%) and confluent states (Con, ≥80%), 4 and 8 day old myotubes (4 d Myo and 8 d Myo, respectively), and serum resupplemented myotubes (Myo Res). *NvGas6* was normalized to *NvGAPDH*, and is relative to subconfluent cells. Dotted line represents relative expression level of 1.0. b) *NvGas6* expression increases upon amputation, peaks at 21 day postamputation and decreases at the palette stage. *NvGas6* was normalized to *NvGAPDH* and *Nvβ-Actin*, and is relative to intact limbs.

a)

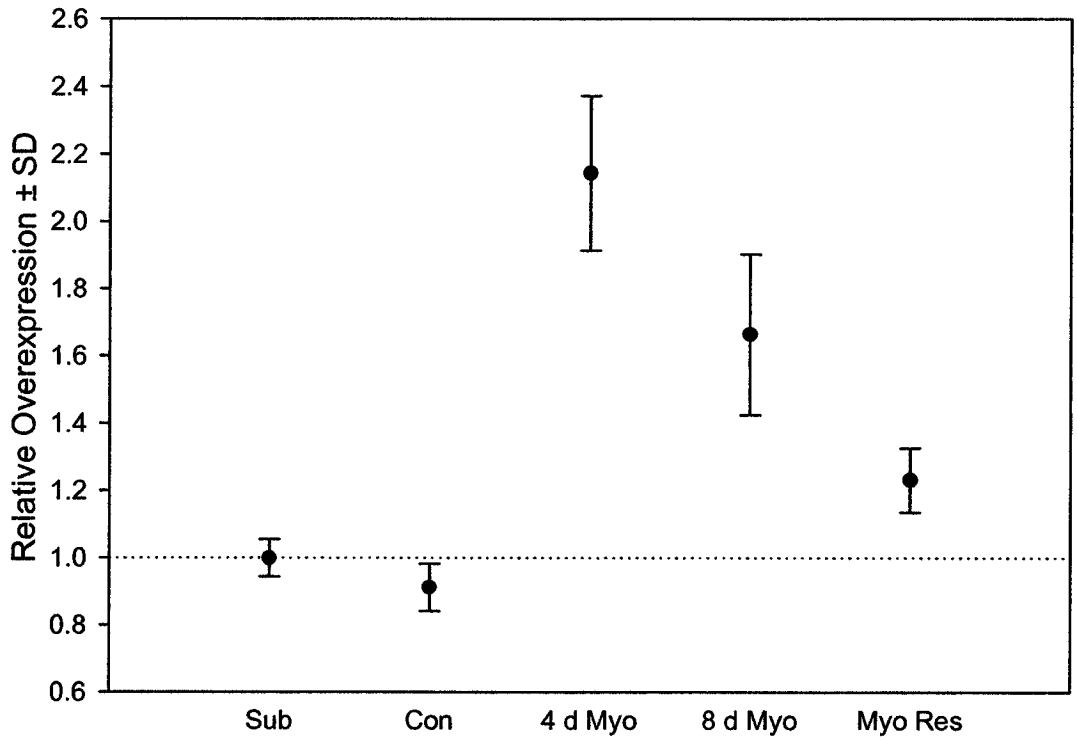
Relative Overexpression ± SD
2.6
2.4
2.2
2.0
1.8
1.6
1.4
1.2
1.0
0.8
0.6
Sub
Con
4 d Myo
8 d Myo
Myo Res

b)

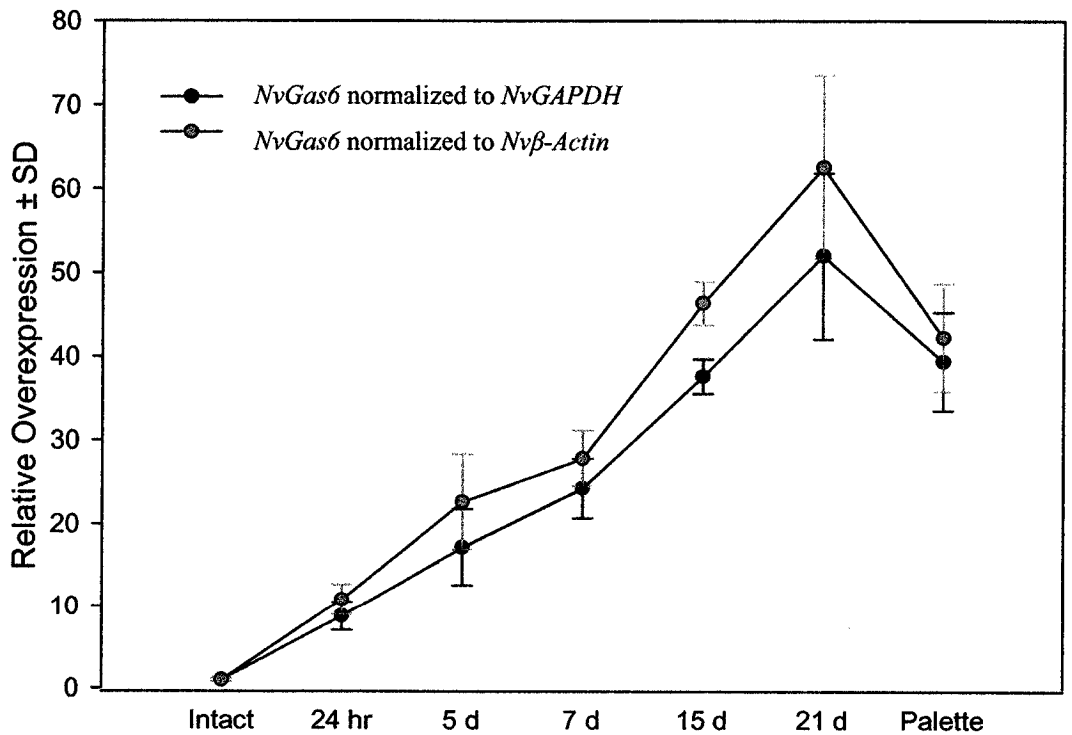
Relative Overexpression ± SD
80
70
60
50
40
30
20
10
0
NvGas6 normalized to NvGAPDH
NvGas6 normalized to Nvβ-Actin
Intact
24 hr
5 d
7 d
15 d
21 d
Palette

significant difference in all regenerative samples compared to intact limbs. Due to differential regenerative rates (Iten and bryant 1973) between animals and under different environmental conditions, the RT-qPCR experiments were repeated with different RNA sources, and the results were consistent.

3.5 Southern Analysis

To identify single copy sequences within the *NvGas6* transcript that would serve as an ideal probe for *in situ* hybridization analysis, newt genomic DNA was labelled and hybridized to a southern blot containing restriction digests of the *NvGas6* cDNA. In this analysis, any fragments which contain single copy nonrepetitive cDNA do not hybridize to the probe. After 2 days of exposure, the only band observed on the blot was a ~ 340 bp band, corresponding to a juxtaposition of vector and 3′ cDNA fragment sequence (data not shown). Since there were no observable bands in any of the digested fragments, this suggested that any region of the *NvGas6* clone could be utilized for *in situ* hybridization probe synthesis. Concordantly, as previous authors have utilized a probe spanning all 4 EGF_CA regions and part of the first LamG domains region for mammalian Gas6 in situ hybridization (Prieto et al. 1999), the region downstream of the EGF_CA domain, comprising the loop region and the first LamG domain was selected for the *in situ* hybridization probe. Of particular importance is the inclusion of the loop region, as homology to protein S is lowest in this region.

3.6 In situ Hybridization Analysis

NvGas6 is expressed at the epidermal and dermal layers, and within the distal mesenchymal cells and differentiating structures (Figure 15). Throughout all regenerative time points, staining was observed in the epithelial and dermal layers, including the stratum spongiosum and stratum compactum. There was also occasional weak staining in the intact

Figure 15. *NvGas6 in situ* hybridization analysis during newt forelimb regeneration. (a) Staining in the 24-hour regenerate. The staining throughout the bone is probably nonspecific staining due to incomplete PVA dissolution. (b) Expression within the migrating wound epithelium (arrow points to individual epidermal cells). (c) 24-hr sense control. (d) Expression in the 7-day regenerate is found in the epidermal layer and mesenchymal cells. (e) Magnification of the boxed region in (d) showing staining within the distal mesenchymal cells that correspond to dedifferentiated cells and proliferating blastemal cells. (f) 7-day sense control. (g) Staining in the 15-day regenerate is located throughout the blastema, dedifferentiating cells and periosteum. (h) Magnification of box A in (g) showing expression within the blastemal and dedifferentiating cells. (j) Magnification of box B in (g) showing expression in the dermal gland. The arrow represents positive staining in the dermal gland. (i and k) 15-day sense control. (l) Staining in the 21-day regenerate, which displays high *NvGas6* expression in the blastema (m; boxed region in (l)). (n) 21-day sense control (o) Staining at the palette stage regenerate, with *NvGas6* transcripts located in condensing cartilage (C) and differentiating myotubes (M) and distal blastemal cells (p and r; boxed regions A and B in (o), respectively). (q) and (s) are palette stage controls for (p) and (r), respectively. Dotted lines represent approximate amputation plane.

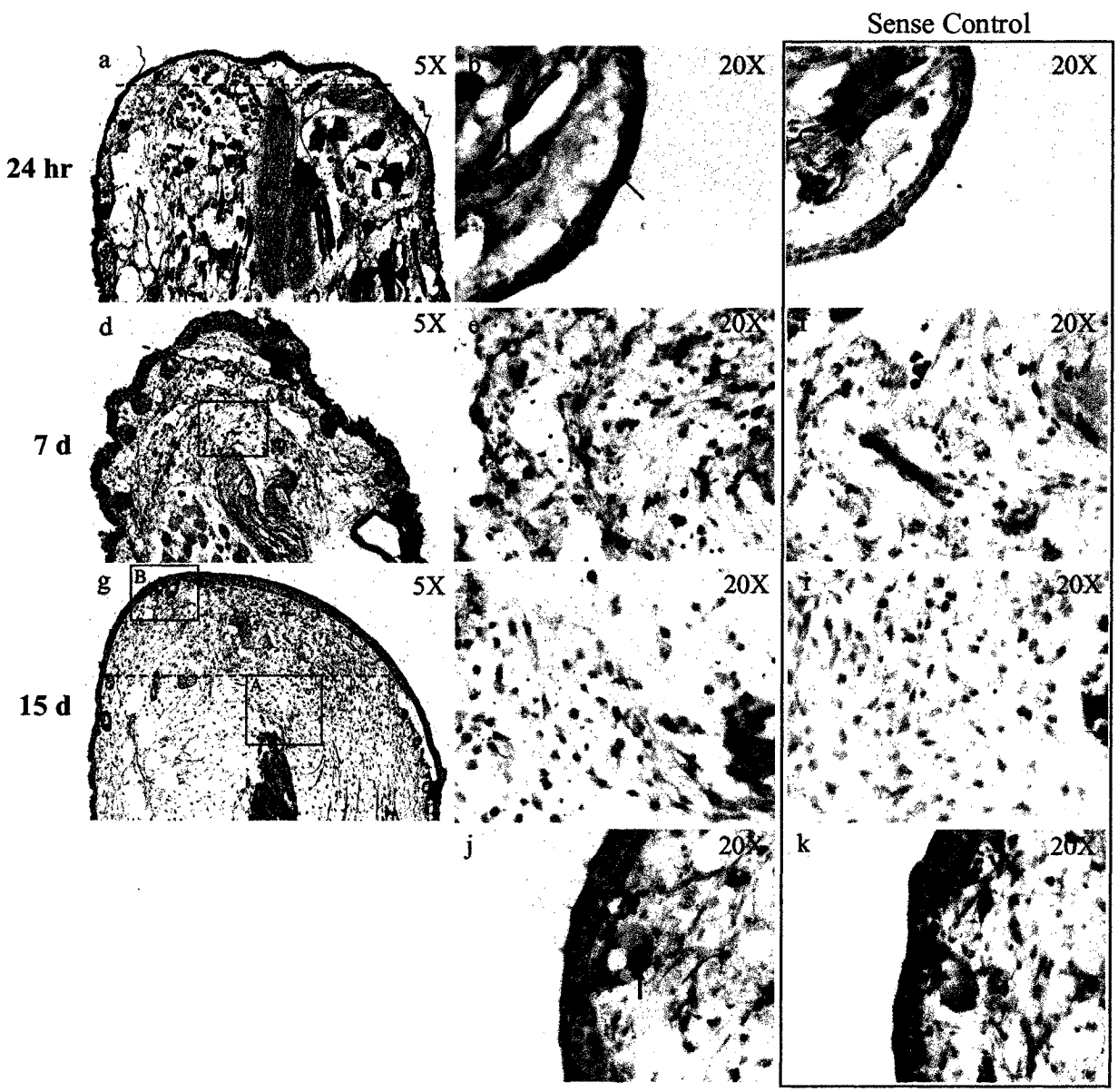
Sense Control
24 hr
7 d
15 d
a
5X
b
20X
c
20X
d
5X
e
20X
f
20X
g
5X
B
A
20X
i
20X
j
20X
k
20X

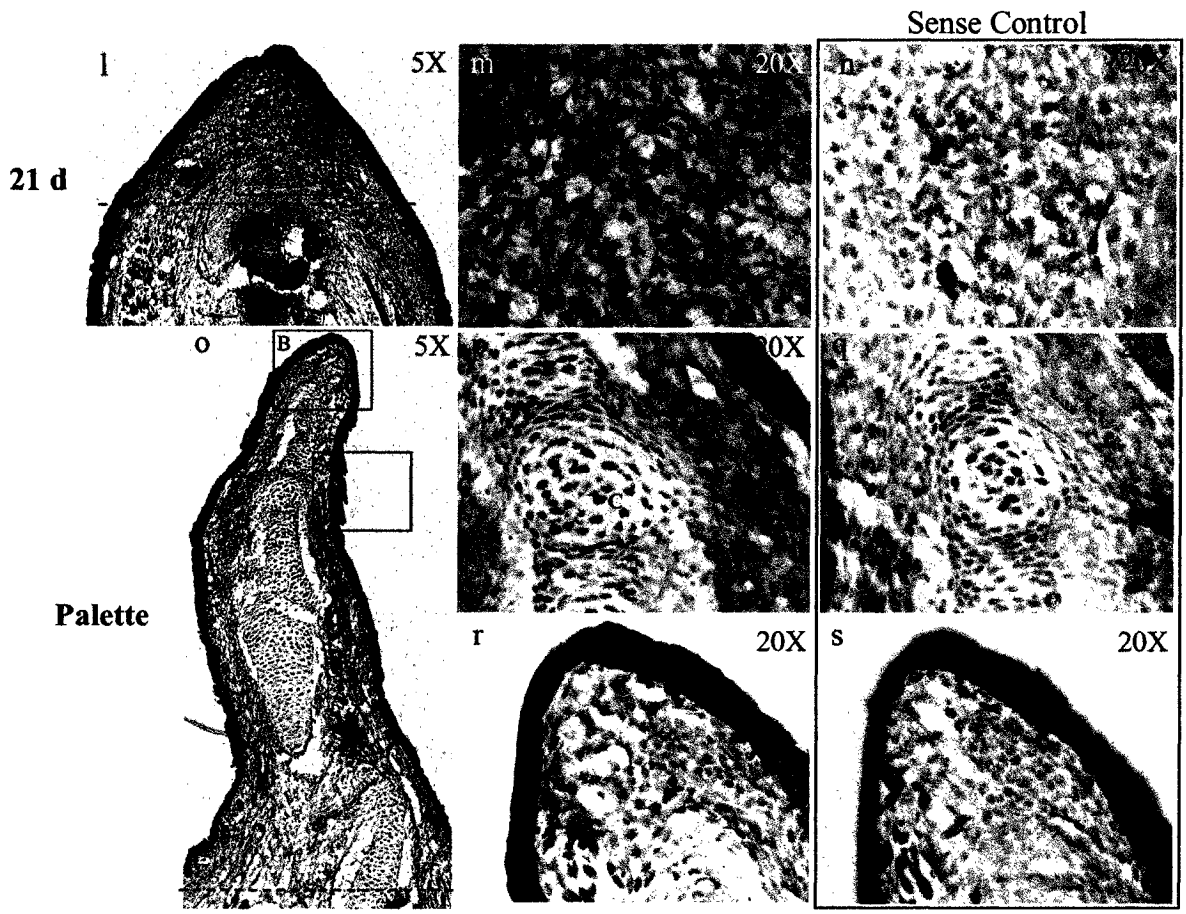
Sense Control
21 d
l
5X
m
20X
n
20X
o
B
5X
Palette
20X
r
20X
s
20X

muscles and dermal glands. At 24 hours PA, the regenerate is undergoing wound healing and the epithelium has migrated over the open wound. *NvGas6* expression is only observed in the WE, and in the dermal and epidermal layers of the stump. At 7 days PA, wound healing is complete and the cells are undergoing dedifferentiation. At this stage, staining was first observed in the distal stump in loose aggregation of mesenchymal cells that include dedifferentiating cells and accumulating blastemal cells. The 15 day regenerate is denoted by maximal dedifferentiation, with the formation of a well-defined blastema. At this point, there was heavier staining in tissues distal to the bone that included blastemal and dedifferentiating cells. As well, there were a few positive cells in the periosteum. The 21 day regenerate is characterized by maximal blastema cell proliferation, and had the same pattern as the 15 day regenerate, with the exception that staining of the mesenchymal cells was stronger due to aggregation of blastemal cells. Also apparent at this time point is decreased staining in areas that are lateral to the bone. After 21 d PA, blastema cell proliferation is rapidly decreasing, and these cells are differentiating into the structures that give rise to the regenerate. Concordantly, staining in the distal stump tissues at the palette stage was limited to fewer distal mesenchymal cells, and was observed in both condensing chondrocytes and differentiating myotubes.

4. DISCUSSION

4.1 Identification of SR4 as NvGas6

The SR4 fragment was identified as the newt orthologue of mammalian growth arrest-specific 6. This is the first *Gas6* gene cloned in the lower tetrapods. It is surprising that the sequence is so well conserved (78% similarity when considering substitutions) given that evolutionary divergence occurred over 240 million years ago (Pough et al. 1999).

The GLA domain is highly conserved, more so than the other NvGas6 modules. NvGas6 appears to contain the propeptide sequence, which includes a well-conserved phenylalanine site that is present in almost all chordate GLA domains with several key hydrophobic residues (Figure 12, Furie et al. 1999; Bandyopadhyay et al. 2002; Wang et al. 2003). The propeptide sequence is believed to anchor the substrate to γ-glutamylcarboxylase, the enzyme that accomplishes the GLU to GLA modification, and mutation of this site results in a mature protein that is deficient or lacking GLA residues (Furie et al. 1999). The presence of the propeptide within the GLA domain partially explains why the amino terminus of the protein is not well conserved. The well-conserved propeptide suggests that NvGas6 may be able to react with human carboxylase, since a tunicate polypeptide containing a GLA domain that has the same key conserved sites was able to serve as a substrate for human carboxylase (Wang et al. 2003).

NvGas6 also shows high conservation of its EGF_CA and LamG domains. Like the other Gas6 sequences, NvGas6 contains 4 EGF_CA modules in tandem. Within the EGF_CA domains, NvGas6 shows conservation of the 5-6 core cysteines that can form 3 disulfide bridges (Figure 12). Similarly, the LamG domains are highly conserved, with almost 100% sequence similarity to LamG consensus. Of the 2 LamG domains, the first is most highly conserved compared to mammalian Gas6. It can be speculated that this may be due to the importance of the first domain in receptor binding wheras the second domain is

required for proper folding and/or receptor interaction (Sasaki et al. 2002). The overall similarity suggests that recombinant mammalian Gas6 may be used in newt functional experiments.

4.2 Real-Time Expression in B1H1 Cell Line

A long-term polyclonal blastema cell line, B1H1, was used in characterizing the role of NvGas6 under states of proliferation, myogenesis and cell cycle reentry. Extensive characterization of this line has been done by Ferretti and Brockes (1988), Maier and Miller (1992) and S. Vascotto (Unpublished results) The B1H1 is cell line comprised of pleiomorphic, bipolar, signet and giant cells. Signet and giant cells represent less than 10% in all culture conditions. A unique feature of B1H1 cells is that cells proliferate under high serum conditions, can be induced to form postmitotic myotubes under both confluent and low serum conditions, and transverse the S-phase upon serum resupplementation. As such, this cell line represents an appropriate system to identify proliferation, dedifferentiation, cell cycle reentry and survival-specific genes.

The composition of the heterogeneous cell line changes during cell culture manipulations. The "subconfluent" classification was used to identify cultures that were less than 70% confluent, while "confluent" status referred to cultures between 85-100% confluency. B1H1 composition under these conditions consisted mainly of pleiomorphic cells, with scattered bipolar, signet and giant cells. To be classified as 4 day myotubes, confluent B1H1 cells were in low serum conditions for 4 days, and 8 day myotubes represented B1H1 cells under low serum conditions for 8 days. 8 day myotubes are 'more' mature myotubes as demonstrated by *myosin heavy chain* and *Nvβ-actin* expression profiles (S. Vascotto, unpublished results; Appendix I). In 4 day myotubes, the culture composition consisted of equal amounts of pleiomorphic and bipolar cells, with myotubes representing ~10% of the cells in the cutlure. On the other hand, in 8 day myotubes, the composition of

plieomorphic, bipolar cells and myotubes were equal. However, the proportional myotube increase could be a result of cell death of the pleiomorphic or bipolar cells under low serum conditions since there is a noticeable increase of floating cells in the medium. Finally, a serum resupplemented culture involved 4 day myotubes that were subsequently exposed to high serum conditions for 4 days. This typically resulted an increase of pleiomorphic cells, with bipolar and myotube levels the same as 4 day myotubes. This most likely results from the remaining pleiomorphic cells reentering the cell cycle.

Real-time RT-qPCR analysis during different B1H1 culture states reveals that *NvGas6* expression increases during myogenesis and decreases upon serum resupplementation. It is interesting that there is a low level of upregulation from proliferating to myogenesis conditions. If NvGas6 is associated with a specific cell type, this result may be due to an increase in both myotube formation and bipolar cell composition, and a concomitant decrease in pleiomorphic cells. Cell culture *in situ* hybridization or immunohistochemistry would partially settle this issue. In any case, it is unlikely that NvGas6 is acting as a mitogen as expression is not upregulated during both proliferation and cell cycle reentry. Similarly, it is unlikely that NvGas6 is a dedifferentiation-inducing factor and is required for cell cycle progression. It is also unlikely that NvGas6 modulates differentiation as expression decreases during prolonged exposure to low serum conditions. However, it must be kept in mind that this result may be due to death of cells that highly express *NvGas6*, leading to lower overall expression levels when taken as a whole. Performing a cell culture *in situ* hybridization analysis in combination with TUNEL analysis to evaluate cell death would resolve some of these issues. The most likely role for NvGas6 is as a prosurvival factor. Upregulation during exposure to low serum conditions could be a direct result of stress due to nutrient depletion.

In this scenario, resupplementing cells with serum would alleviate the nutrient deficiency and lead to downregulation of *NvGas6*.

Reducing the serum in cell culture medium deprives cells of essential nutrients and growth factors. As a result, cells typically respond by induction of numerous antiapoptotic and growth arrest factors, including Gas6 (Manfioletti et al. 1990; Manfioletti et al. 1993; Shugart et al. 1995; Fleming et al. 1998; Hogg et al. 1999), which leads to growth arrest and prevention of apoptosis or repression of proapoptotic molecules (Baek et al. 2000; Izuishi et al. 2000; Mastrangelo et al. 2000; Reshkin et al. 2000). It is, therefore, not surprising that *NvGas6* expression increases upon serum withdrawal.

NvGas6 may have another role during proliferation and differentiation by controlling cell migration and adhesion. Gas6 has an important role in these events in endothelial vascular smooth muscle cells and GnRH neurons, which involves transcriptional activation and cytoskeletal alterations that leads to migration and modulates adhesion (Chen et al. 1997; McCloskey et al. 1997; Nakano et al. 1997; Avanzi et al. 1998; Fang et al. 1998; Fridell et al. 1998; Melaragno et al. 1998; Allen et al. 1999; Allen et al. 2000; Yin et al. 2000; Wimmel et al. 2001; Allen et al. 2002). Alignment and fusion in B1H1 cells would certainly involve differential gene expression and cytoskeletal rearrangement. Thus, upregulation may be partially due to alignment and fusion during myogenesis. It must be noted that the prosurvival effect is still present during migration in the vascular smooth muscles and GnRH neurons; inhibiting Gas6 leads to lower migratory and adhesion events and susceptibility to conditions of growth arrest. It may be that NvGas6 has both survival and migration and adhesion effects in B1H1 cells. NvGas6 may promote survival during serum depletion and is downregulated upon serum resupplementation. In addition, NvGas6 may be required for cellular migration and adhesion, leading to myotubes fusion, and as the fusion events are decreasing (in 8 day myotubes), *NvGas6* is downregulated.

4.3 Expression in Newt Regenerating Forelimbs

Overall, during limb regeneration, *NvGas6* expression steadily increases from amputation to the late bud stage, and decreases at the palette stage. Not surprisingly, it is also expressed in intact limbs. The expression profiles and their relevance will be discussed in detail below.

NvGas6 is upregulated within 24 hr PA, and is likely participating in the initial coagulation response. Gas6 is stored in the α-granules of platelets (Angelillo-Scherrer et al. 2001), is released during platelet activation (Ishimoto and Nakano 2000; Ishimoto et al. 2000) and binds to phosphatidylserine (Nakano et al. 1997) and its associated RTKs (Angelillo-Scherrer et al. 2001). Since phosphatidylserine is normally positioned in the inner leaflet of the plasma membrane and exposure results in macrophage engulfment, it was proposed that Gas6 might function in apoptotic cell clearance. Since amputation leads to massive apoptosis within the first 3 days PA (Vlaskin et al., manuscript in preparation) and has a role in macrophage engulfment, it would make sense that *NvGas6* expression should be upregulated early in the regeneration response.

As regeneration proceeds through the wound healing stage (up to 5 days PA), *NvGas6* expression increases almost 20-fold. NvGas6 might have a role during this stage in influencing macrophage activation and mediating survival of the remaining cells located at the wound stump. Although I did not find any significant *in situ* staining in the mesenchymal cells during wound healing, there was significant expression in the WE, the dermal layer beneath the WE and in the forming AEC. This may be relevant to both survival and migratory activities since wound healing involves migration of the stump epithelial cells to cover the wound surface. Although the *in situ* hybridization did not detect very much expression in the mesenchymal cells, there most likely is expression in cells surrounding the wound site because many of these cells are undergoing apoptosis. The lack

of staining may be due to the limits of detection of the *in situ* hybridization technique. Repeating the *in situs* and developing the colourimetric reaction for an extended period of time might alleviate this problem. Alternatively, immunohistochemistry for Gas6 on frozen sections can be performed to localize NvGas6 at the protein level.

There is marked *NvGas6* expression in the distal mesenchymal cells from 7 to 21 days PA. At this time, distal stump tissues are beginning to dedifferentiate, migrate and proliferate to form the blastema. There is a noticeable increase in expression intensity as regeneration progresses, likely due to increased aggregation of blastemal cells as maximal cell proliferation and highest aggregation occurs during the late bud stage (Iten and Bryant 1973). Cellular proliferation is often associated with increased expression of survival and antiapoptotic factors (Nickoloff et al. 2002; Borgne et al. 2003; Calo et al. 2003; Gaur et al. 2003; Klein et al. 2003). Thus, it may be possible that NvGas6 is promoting survival of these proliferating cells. In addition, dedifferentiating and migrating dedifferentiated cells produce NvGas6. As shown *in vitro*, it is unlikely that NvGas6 participates during the dedifferentiation process. Thus, *NvGas6* may facilitate survival and blastemal aggregation via adhesion and migration of dedifferentiated cells.

By the palette stage, overall *NvGas6* expression declines, with the majority of regeneration-related expression in condensing cartilage, differentiating myotubes and distal mesenchymal cells. There is a marked drop of expression in blastemal cells. At this point, proliferation is declining at a rapid rate, and blastemal cells are beginning to reconstruct lost tissues (Iten and Bryant 1973). In other systems, Gas6 mediates the survival and mitogenic activities in chondrocytes (Loeser et al. 1997), and stimulates osteoclast function (Nakamura et al. 1998; Katagiri et al. 2001). At this stage in regeneration, it can be hypothesized that the role of NvGas6 is to modulate differentiation or survival of the differentiating cells.

4.4 A Hypothesis for NvGas6 in Regeneration

Overall, it appears that NvGas6 is an important factor in the regenerative process. The fact that proliferating blastemal cells strongly express *NvGas6 in vivo* and *NvGas6* is upregulated during differentiation *in vitro* suggests that the roles for NvGas6 during regeneration may be to mediate cellular survival, adhesion and migration. As differentiation progresses, NvGas6 is no longer required and is downregulated. Interestingly, Gas6 and its associated receptors are overexpressed in many cancer cell lines and have similar roles in survival, adhesion and migration (Chapter 1.3.2). A regeneration blastema has often been compared with a tumour whereby similar events are occurring, such as ECM alteration, dedifferentiation, proliferation, vascularization and innervation. It may not be surprising, then, that the roles for NvGas6 that have been proposed in this study are similar to those proposed for tumours.

4.5 Future Directions

The results presented in this thesis suggest a role for an RTK ligand during newt forelimb regeneration. However, in order to understand the role of NvGas6 at the ligand, receptor and signal transduction levels in regeneration, several experiments must be performed. They are outlined below.

4.5.1 Detection of NvGas6 at the Protein Level

Analysis at the protein level must be performed to confirm the mRNA results. The presence of a mRNA is not always indicative of the site or level of protein activity. Stability of mRNA and posttranslational modifications of proteins may all play roles in gene activity. As NvGas6 is relatively conserved in relation to mammalian Gas6, one may be able to use antibodies specific for Gas6 in newt studies. Commercially available antibodies are raised against an epitope where NvGas6 shares 7 out of 8 residues at the amino termini. If the

commercial antibody does not work with NvGas6, then antibodies against specific NvGas6 epitopes would need to be designed.

Once antibodies are obtained, several experiments can be performed. Western blots of different B1H1 culture states and regenerative time points can be probed with an antibody to determine expression profiles at the protein level. Immunohistochemistry could be used to identify temporal and spatial profiles of protein expression. This would complement the mRNA expression profiles obtained in this thesis.

4.5.2 NvGas6 Functional Analysis

While both mRNA and protein expression analyses would provide a hypothesis for the NvGas6 function, further analyses are required to verify the predictions of the hypothesis. This can be accomplished by overexpression or downregulation of NvGas6. Overexpression may be possible through the use of recombinant mammalian Gas6 in newt cells since the primary sequence is highly conserved and the tertiary structure is most likely the same. Alternatively, pseudotyped retroviruses can be used to overexpress *NvGas6* in newt cells. With these approaches, one can directly observe the effects of (Nv)Gas6 *in vitro* under different B1H1 conditions. One would expect that if NvGas6 is involved in cellular migration and adhesion, that upregulation of NvGas6 expression may induce precocious myotube formation. One can also induce apoptosis in B1H1 cells (e.g., through hypoxia) to verify if NvGas6 is a *bona fide* prosurvival factor. *In vivo*, infected B1H1 cells transfected with pseudotyped retroviruses expressing a tagged NvGas6 can be implanted beneath the wound epidermis. Both immunohistochemisty and *in situ* hybridization analysis can be carried out regarding final locality and the effects of NvGas6 on surrounding cells.

Downregulation of NvGas6 may be achieved using morpholinos *in vitro*. Decreasing NvGas6 protein levels should result in higher cell death and/or inhibition of differentiation. Another method is to use γ-carboxylase inhibitors (e.g., warfarin (3-[alpha-acetonyl-benzyl-

4-hydroxycoumarin])), or the Gas6 antibodies themselves *in vitro*. Most of the studies that examined the role of Gas6 in multiple systems used these latter strategies to 'knockdown' Gas6 at the posttranslational and protein level.

Finally, performing a migration assay can reveal if NvGas6 has chemoattractant effects *in vitro*. This could be performed in a Boyden chamber. This entails depositing NvGas6 on the bottom of a cell culture dish, a permeable membrane placed above the deposit and B1H1 cells seeded on top of the membrane. If B1H1 cells are chemoattracted to (Nv)Gas6, then the cells will migrate through the membrane pores.

4.5.3 Cloning and Characterization of NvGas6 Downstream Effectors

In order to completely understand the role of NvGas6, the associated RTKs must be cloned and characterized. The multifunctional capability of Gas6 is due to differential binding to multiple receptors and unique signal transduction events. Fortunately, RTKs are highly conserved throughout invertebrates and vertebrates (Hanks et al. 1988). Therefore, it should be relatively easy to design degenerate primers to isolate individual newt RTKs. Upon isolation, characterization of these RTKs can be done at the RNA and protein levels in similar experiments as discussed above.

Similarly, the downstream targets need to be cloned and characterized. This may not be a straightforward task as it is unknown if the effectors are evolutionary conserved as most were isolated in human and mouse. Nevertheless, many of the downstream target binding sites are conserved. Performing library screens with sequences that have regions of high conservation is the best approach towards cloning these downstream effectors. Alternatively, one can hope that antibodies used for these downstream effectors will cross-react with the newt orthologues.

5. REFERENCES

Albert, P., B. Boilly, J. Courty and D. Barritault (1987). "Stimulation in cell culture of mesenchymal cells of newt limb blastemas by EDGF I or II (basic or acidic FGF)." Cell Differ **21**(1): 63-8.

Allen, M. P., D. A. Linseman, H. Udo, M. Xu, J. B. Schaack, B. Varnum, E. R. Kandel, K. A. Heidenreich and M. E. Wierman (2002). "Novel mechanism for gonadotropin-releasing hormone neuronal migration involving Gas6/Ark signaling to p38 mitogen-activated protein kinase." Mol Cell Biol **22**(2): 599-613.

Allen, M. P., M. Xu, D. A. Linseman, J. E. Pawlowski, G. M. Bokoch, K. A. Heidenreich and M. E. Wierman (2002). "Adhesion-related kinase repression of gonadotropin-releasing hormone gene expression requires Rac activation of the extracellular signal-regulated kinase pathway." J Biol Chem **277**(41): 38133-40.

Allen, M. P., M. Xu, C. Zeng, S. A. Tobet and M. E. Wierman (2000). "Myocyte enhancer factors-2B and -2C are required for adhesion related kinase repression of neuronal gonadotropin releasing hormone gene expression." J Biol Chem **275**(50): 39662-70.

Allen, M. P., C. Zeng, K. Schneider, X. Xiong, M. K. Meintzer, P. Bellosta, C. Basilico, B. Varnum, K. A. Heidenreich and M. E. Wierman (1999). "Growth arrest-specific gene 6 (Gas6)/adhesion related kinase (Ark) signaling promotes gonadotropin-releasing hormone neuronal survival via extracellular signal-regulated kinase (ERK) and Akt." Mol Endocrinol **13**(2): 191-201.

Altizer, A. M., S. G. Stewart, B. K. Albertson and R. B. Borgens (2002). "Skin flaps inhibit both the current of injury at the amputation surface and regeneration of that limb in newts." J Exp Zool **293**(5): 467-77.

Angelillo-Scherrer, A., P. de Frutos, C. Aparicio, E. Melis, P. Savi, F. Lupu, J. Arnout, M. Dewerchin, M. Hoylaerts, J. Herbert, D. Collen, B. Dahlback and P. Carmeliet (2001). "Deficiency or inhibition of Gas6 causes platelet dysfunction and protects mice against thrombosis." Nat Med **7**(2): 215-21.

Avanzi, G. C., M. Gallicchio, F. Bottarel, L. Gammaitoni, G. Cavalloni, D. Buonfiglio, M. Bragardo, G. Bellomo, E. Albano, R. Fantozzi, G. Garbarino, B. Varnum, M. Aglietta, G. Saglio, U. Dianzani and C. Dianzani (1998). "GAS6 inhibits granulocyte adhesion to endothelial cells." Blood **91**(7): 2334-40.

Avanzi, G. C., M. Gallicchio, G. Cavalloni, L. Gammaitoni, F. Leone, A. Rosina, R. Boldorini, G. Monga, L. Pegoraro, B. Varnum and M. Aglietta (1997). "GAS6, the ligand of Axl and Rse receptors, is expressed in hematopoietic tissue but lacks mitogenic activity." Exp Hematol **25**(12): 1219-26.

Baek, J. H., J. E. Jang, C. M. Kang, H. Y. Chung, N. D. Kim and K. W. Kim (2000). "Hypoxia-induced VEGF enhances tumor survivability via suppression of serum deprivation-induced apoptosis." Oncogene **19**(40): 4621-31.

Bandyopadhyay, P. K., J. E. Garrett, R. P. Shetty, T. Keate, C. S. Walker and B. M. Olivera (2002). "gamma -Glutamyl carboxylation: An extracellular posttranslational modification that antedates the divergence of molluscs, arthropods, and chordates." Proc Natl Acad Sci U S A **99**(3): 1264-9.

Beauchemin, M. and P. Savard (1992). "Two distal-less related homeobox-containing genes expressed in regeneration blastemas of the newt." Dev Biol **154**(1): 55-65.

Bellosta, P., M. Costa, D. A. Lin and C. Basilico (1995). "The receptor tyrosine kinase ARK mediates cell aggregation by homophilic binding." Mol Cell Biol **15**(2): 614-25.

Bellosta, P., Q. Zhang, S. P. Goff and C. Basilico (1997). "Signaling through the ARK tyrosine kinase receptor protects from apoptosis in the absence of growth stimulation." Oncogene **15**(20): 2387-97.

Berclaz, G., H. J. Altermatt, V. Rohrbach, I. Kieffer, E. Dreher and A. C. Andres (2001). "Estrogen dependent expression of the receptor tyrosine kinase axl in normal and malignant human breast." Ann Oncol **12**(6): 819-24.

Berkner, K. L. (2000). "The vitamin K-dependent carboxylase." J Nutr **130**(8): 1877-80.

Blume-Jensen, P. and T. Hunter (2001). "Oncogenic kinase signalling." Nature **411**(6835): 355-65.

Bode, H. R. (2003). "Head regeneration in Hydra." Dev Dyn **226**(2): 225-36.

Booth, S. L. (1997). "Skeletal functions of vitamin K-dependent proteins: not just for clotting anymore." Nutr Rev **55**(7): 282-4.

Borgne, A. and R. M. Golsteyn (2003). "The role of cyclin-dependent kinases in apoptosis Prog Cell Cycle Res **5**(8): 453-9.

Brockes, J. P. (1987). "The nerve dependence of amphibian limb regeneration." J Exp Biol **132**: 79-91.

Brockes, J. P. and A. Kumar (2002). "Plasticity and reprogramming of differentiated cells in amphibian regeneration." Nat Rev Mol Cell Biol **3**(8): 566-74.

Bryan, J. T. and M. I. Morasso (2000). "The Dlx3 protein harbors basic residues required for nuclear localization, transcriptional activity and binding to Msx1." J Cell Sci **113 (Pt 22)**: 4013-23.

Calo, V., M. Migliavacca, V. Bazan, M. Macaluso, M. Buscemi, N. Gebbia, A. Russo, B. Klein, K. Tarte, M. Jourdan, K. Mathouk, J. Moreaux, E. Jourdan, E. Legouffe, J. De Vos, J. F. Rossi, B. J. Nickoloff, J. Z. Qin, V. Chaturvedi, P. Bacon, J. Panella and M. F. Denning (2003). "STAT proteins: from normal control of cellular events to tumorigenesis Survival and proliferation factors of normal and malignant plasma cells
Life and death signaling pathways contributing to skin cancer." J Cell Physiol **197**(2): 157-68.

Camenisch, T. D., B. H. Koller, H. S. Earp and G. K. Matsushima (1999). "A novel receptor tyrosine kinase, Mer, inhibits TNF-alpha production and lipopolysaccharide-induced endotoxic shock." J Immunol **162**(6): 3498-503.

Chan, M. C., J. P. Mather, G. McCray and W. M. Lee (2000). "Identification and regulation of receptor tyrosine kinases Rse and Mer and their ligand Gas6 in testicular somatic cells." J Androl **21**(2): 291-302.

Chen, J., K. Carey and P. J. Godowski (1997). "Identification of Gas6 as a ligand for Mer, a neural cell adhesion molecule related receptor tyrosine kinase implicated in cellular transformation." Oncogene **14**(17): 2033-9.

Chen, W. S., H. J. Kung, W. K. Yang and W. Lin (1999). "Comparative tyrosine-kinase profiles in colorectal cancers: enhanced arg expression in carcinoma as compared with adenoma and normal mucosa." Int J Cancer **83**(5): 579-84.

Christensen, R. N., M. Weinstein and R. A. Tassava (2001). "Fibroblast growth factors in regenerating limbs of Ambystoma: cloning and semi-quantitative RT-PCR expression studies." J Exp Zool **290**(5): 529-40.

Cohen, P. L., R. Caricchio, V. Abraham, T. D. Camenisch, J. C. Jennette, R. A. Roubey, H. S. Earp, G. Matsushima and E. A. Reap (2002). "Delayed apoptotic cell clearance and lupus-like autoimmunity in mice lacking the c-mer membrane tyrosine kinase." J Exp Med **196**(1): 135-40.

Collett, G., A. Wood, M. Y. Alexander, B. C. Varnum, R. P. Boot-Handford, V. Ohanian, J. Ohanian, Y. W. Fridell and A. E. Canfield (2003). "Receptor tyrosine kinase Axl modulates the osteogenic differentiation of pericytes." Circ Res **92**(10): 1123-9.

Costa, M., P. Bellosta and C. Basilico (1996). "Cleavage and release of a soluble form of the receptor tyrosine kinase ARK in vitro and in vivo." J Cell Physiol **168**(3): 737-44.

Crosier, K. E. and P. S. Crosier (1997). "New insights into the control of cell growth; the role of the AxI family." Pathology **29**(2): 131-5.

Crosier, P. S., S. A. Freeman, D. Orlic, D. M. Bodine and K. E. Crosier (1996). "The Dtk receptor tyrosine kinase, which binds protein S, is expressed during hematopoiesis." Exp Hematol **24**(2): 318-23.

Dahlback, B. (2000). "Blood coagulation." Lancet **355**(9215): 1627-32.

D'Arcangelo, D., C. Gaetano and M. C. Capogrossi (2002). "Acidification prevents endothelial cell apoptosis by Axl activation." Circ Res **91**(7): e4-12.

D'Cruz, P. M., D. Yasumura, J. Weir, M. T. Matthes, H. Abderrahim, M. M. LaVail and D. Vollrath (2000). "Mutation of the receptor tyrosine kinase gene Mertk in the retinal dystrophic RCS rat." Hum Mol Genet **9**(4): 645-51.

Demarchi, F., R. Verardo, B. Varnum, C. Brancolini and C. Schneider (2001). "Gas6 anti-apoptotic signaling requires NF-kappa B activation." J Biol Chem **276**(34): 31738-44.

Diehl, A. M. (2002). "Liver regeneration." Front Biosci **7**: e301-14.

Dirks, W., D. Rome, F. Ringel, K. Jager, R. A. MacLeod and H. G. Drexler (1999). "Expression of the growth arrest-specific gene 6 (GAS6) in leukemia and lymphoma cell lines." Leuk Res **23**(7): 643-51.

Dungan, K. M., T. Y. Wei, J. D. Nace, M. L. Poulin, I. M. Chiu, J. C. Lang and R. A. Tassava (2002). "Expression and biological effect of urodele fibroblast growth factor 1: relationship to limb regeneration." J Exp Zool **292**(6): 540-54.

Dunis, D. A. and M. Namenwirth (1977). "The role of grafted skin in the regeneration of x-irradiated axolotl limbs." Dev Biol **56**(1): 97-109.

Echeverri, K. and E. M. Tanaka (2002). "Ectoderm to mesoderm lineage switching during axolotl tail regeneration." Science **298**(5600): 1993-6.

Fang, Z., X. Xiong, A. James, D. F. Gordon and M. E. Wierman (1998). "Identification of novel factors that regulate GnRH gene expression and neuronal migration." Endocrinology **139**(8): 3654-7.

Fedi, P., A. C. Kimmelman and S. A. Aaronson (2000). Growth factor signal transduction in cancer. Cancer Medicine. T. S. Gansler: 33-55.

Ferretti, P. and J. P. Brockes (1988). "Culture of newt cells from different tissues and their expression of a regeneration-associated antigen." J Exp Zool **247**(1): 77-91.

Fleming, J. V., S. M. Hay, D. N. Harries and W. D. Rees (1998). "Effects of nutrient deprivation and differentiation on the expression of growth-arrest genes (gas and gadd) in F9 embryonal carcinoma cells." Biochem J **330 (Pt 1)**: 573-9.

Fridell, Y. W., J. Villa, Jr., E. C. Attar and E. T. Liu (1998). "GAS6 induces Axl-mediated chemotaxis of vascular smooth muscle cells." J Biol Chem **273**(12): 7123-6.

Furie, B., B. A. Bouchard and B. C. Furie (1999). "Vitamin K-dependent biosynthesis of gamma-carboxyglutamic acid." Blood **93**(6): 1798-808.

Gal, A., Y. Li, D. A. Thompson, J. Weir, U. Orth, S. G. Jacobson, E. Apfelstedt-Sylla and D. Vollrath (2000). "Mutations in MERTK, the human orthologue of the RCS rat retinal dystrophy gene, cause retinitis pigmentosa." Nat Genet **26**(3): 270-1.

Gaur, U. and B. B. Aggarwal, (2003). "Regulation of proliferation, survival and apoptosis by members of the TNF superfamily" Biochem Pharmacol **66**(8): 1403-8.

Georgescu, M. M., K. H. Kirsch, T. Shishido, C. Zong and H. Hanafusa (1999). "Biological effects of c-Mer receptor tyrosine kinase in hematopoietic cells depend on the Grb2 binding site in the receptor and activation of NF-kappaB." Mol Cell Biol **19**(2): 1171-81.

Goldring, K., T. Partridge and D. Watt (2002). "Muscle stem cells." J Pathol **197**(4): 457-67.

Gonzales, M., B. Weksler, D. Tsuruta, R. D. Goldman, K. J. Yoon, S. B. Hopkinson, F. W. Flitney and J. C. Jones (2001). "Structure and function of a vimentin-associated matrix adhesion in endothelial cells." Mol Biol Cell **12**(1): 85-100.

Goruppi, S., C. Chiaruttini, M. E. Ruaro, B. Varnum and C. Schneider (2001). "Gas6 induces growth, beta-catenin stabilization, and T-cell factor transcriptional activation in contact-inhibited C57 mammary cells." Mol Cell Biol **21**(3): 902-15.

Goruppi, S., E. Ruaro and C. Schneider (1996). "Gas6, the ligand of Axl tyrosine kinase receptor, has mitogenic and survival activities for serum starved NIH3T3 fibroblasts." Oncogene **12**(3): 471-80.

Goruppi, S., E. Ruaro, B. Varnum and C. Schneider (1997). "Requirement of phosphatidylinositol 3-kinase-dependent pathway and Src for Gas6-Axl mitogenic and survival activities in NIH 3T3 fibroblasts." Mol Cell Biol **17**(8): 4442-53.

Goruppi, S., E. Ruaro, B. Varnum and C. Schneider (1999). "Gas6-mediated survival in NIH3T3 cells activates stress signalling cascade and is independent of Ras." Oncogene **18**(29): 4224-36.

Goruppi, S., H. Yamane, P. Marcandalli, A. Garcia, C. Clogston, M. Gostissa, B. Varnum and C. Schneider (1997). "The product of a gas6 splice variant allows the release of the domain responsible for Axl tyrosine kinase receptor activation." FEBS Lett **415**(1): 59-63.

Graham, D. K., T. L. Dawson, D. L. Mullaney, H. R. Snodgrass and H. S. Earp (1994). "Cloning and mRNA expression analysis of a novel human protooncogene, c-mer." Cell Growth Differ **5**(6): 647-57.

Greenhalgh, D. G. (1998). "The role of apoptosis in wound healing." Int J Biochem Cell Biol **30**(9): 1019-30.

Gulati, A. K., A. A. Zalewski and A. H. Reddi (1983). "An immunofluorescent study of the distribution of fibronectin and laminin during limb regeneration in the adult newt." Dev Biol **96**(2): 355-65.

Guttridge, K. L., J. C. Luft, T. L. Dawson, E. Kozlowska, N. P. Mahajan, B. Varnum and H. S. Earp (2002). "Mer receptor tyrosine kinase signaling: prevention of apoptosis and alteration of cytoskeletal architecture without stimulation or proliferation." J Biol Chem **277**(27): 24057-66.

Hall, M. O., M. S. Obin, A. L. Prieto, B. L. Burgess and T. A. Abrams (2002). "Gas6 binding to photoreceptor outer segments requires gamma-carboxyglutamic acid (Gla) and Ca(2+) and is required for OS phagocytosis by RPE cells in vitro." Exp Eye Res **75**(4): 391-400.

Han, M. J., J. Y. An and W. S. Kim (2001). "Expression patterns of Fgf-8 during development and limb regeneration of the axolotl." Dev Dyn **220**(1): 40-8.

Hanken, J. (1986). Developmental evidence for amphibian origins. Evolutionary Biology. M. K. Hecht, B. Wallace and G. T. Prance. New York, Plenum Press: 389-417.

Hanks, S. K., A. M. Quinn and T. Hunter (1988). "The protein kinase family: conserved features and deduced phylogeny of the catalytic domains." Science **241**(4861): 42-52.

Hay, E. D. (1959). "Electron microscopic observations of muscle dedifferentiation in regenerating *Amblystoma* limbs." Dev Biol **1**: 555-85.

Hay, E. D. and D. A. Fischman (1961). "Origin of the blastema in regenerating limbs of the newt *Triturus viridescens*: an autoradiographic study using tritiated thymidine to follow cell proliferation and migration." Dev Biol **3**: 26-59.

Healy, A. M., J. J. Schwartz, X. Zhu, B. E. Herrick, B. Varnum and H. W. Farber (2001). "Gas 6 promotes Axl-mediated survival in pulmonary endothelial cells." Am J Physiol Lung Cell Mol Physiol **280**(6): L1273-81.

Hogg, N., J. Browning, T. Howard, C. Winterford, D. Fitzpatrick and G. Gobe (1999). "Apoptosis in vascular endothelial cells caused by serum deprivation, oxidative stress and transforming growth factor-beta." Endothelium **7**(1): 35-49.

Hubbard, S. R. and J. H. Till (2000). "Protein tyrosine kinase structure and function." Annu Rev Biochem **69**: 373-98.

Ishimoto, Y. and T. Nakano (2000). "Release of a product of growth arrest-specific gene 6 from rat platelets." FEBS Lett **466**(1): 197-9.

Ishimoto, Y., K. Ohashi, K. Mizuno and T. Nakano (2000). "Promotion of the uptake of PS liposomes and apoptotic cells by a product of growth arrest-specific gene, gas6." J Biochem (Tokyo) **127**(3): 411-7.

Iten, L. E. and P. J. Bryant (1973). "Forelimb regeneration from different levels of amputation in the newt *Notophthalmus viridescens*: length, rate and stages." Wilhelm Roux' Archiv **173**: 263-82.

Ito, M., M. Nakashima, T. Nakayama, A. Ohtsuru, Y. Nagayama, N. Takamura, E. P. Demedchik, I. Sekine and S. Yamashita (2002). "Expression of receptor-type tyrosine kinase, axl, and its ligand, gas6, in pediatric thyroid carcinomas around chernobyl." Thyroid **12**(11): 971-5.

Ito, T., M. Ito, S. Naito, A. Ohtsuru, Y. Nagayama, T. Kanematsu, S. Yamashita and I. Sekine (1999). "Expression of the Axl receptor tyrosine kinase in human thyroid carcinoma." Thyroid **9**(6): 563-7.

Izuishi, K., K. Kato, T. Ogura, T. Kinoshita and H. Esumi (2000). "Remarkable tolerance of tumor cells to nutrient deprivation: possible new biochemical target for cancer therapy." Cancer Res **60**(21): 6201-7.

Jacob, A. N., J. Kalapurakal, W. R. Davidson, G. Kandpal, N. Dunson, Y. Prashar and R. P. Kandpal (1999). "A receptor tyrosine kinase, UFO/Axl, and other genes isolated by a modified differential display PCR are overexpressed in metastatic prostatic carcinoma cell line DU145." Cancer Detect Prev **23**(4): 325-32.

Katagiri, M., Y. Hakeda, D. Chikazu, T. Ogasawara, T. Takato, M. Kumegawa, K. Nakamura and H. Kawaguchi (2001). "Mechanism of stimulation of osteoclastic bone resorption through Gas6/Tyro 3, a receptor tyrosine kinase signaling, in mouse osteoclasts." J Biol Chem **276**(10): 7376-82.

Kato, T., K. Miyazaki, K. Shimizu-Nishikawa, K. Koshiba, M. Obara, H. K. Mishima and K. Yoshizato (2003). "Unique expression patterns of matrix metalloproteinases in regenerating newt limbs." Dev Dyn **226**(2): 366-76.

Kishi, Y. A., H. Funakoshi, K. Matsumoto and T. Nakamura (2002). "Molecular cloning, expression and partial characterization of Xksy, Xenopus member of the Sky family of receptor tyrosine kinases." Gene **288**(1-2): 29-40.

Klein, B., K. Tarte, M. Jourdan, K. Mathouk, J. Moreaux, E. Jourdan, E. Legouffe, J. De Vos, J. F. Rossi, B. J. Nickoloff, J. Z. Qin, V. Chaturvedi, P. Bacon, J. Panella and M. F. Denning (2003). "Survival and proliferation factors of normal and malignant plasma cells Life and death signaling pathways contributing to skin cancer." Int J Hematol **78**(2): 106-13.

Kozak, M. (1999). "Initiation of translation in prokaryotes and eukaryotes." Gene **234**(2): 187-208.

Kulman, J. D., J. E. Harris, B. A. Haldeman and E. W. Davie (1997). "Primary structure and tissue distribution of two novel proline-rich gamma-carboxyglutamic acid proteins." Proc Natl Acad Sci U S A **94**(17): 9058-62.

Kulman, J. D., J. E. Harris, L. Xie and E. W. Davie (2001). "Identification of two novel transmembrane gamma-carboxyglutamic acid proteins expressed broadly in fetal and adult tissues." Proc Natl Acad Sci U S A **98**(4): 1370-5.

Kumar, A., C. P. Velloso, Y. Imokawa and J. P. Brockes (2000). "Plasticity of retrovirus-labelled myotubes in the newt limb regeneration blastema." Dev Biol **218**(2): 125-36.

Lan, Z., H. Wu, W. Li, S. Wu, L. Lu, M. Xu and W. Dai (2000). "Transforming activity of receptor tyrosine kinase tyro3 is mediated, at least in part, by the PI3 kinase-signaling pathway." Blood **95**(2): 633-8.

Lee, W. P., Y. Liao, D. Robinson, H. J. Kung, E. T. Liu and M. C. Hung (1999). "Axl-gas6 interaction counteracts E1A-mediated cell growth suppression and proapoptotic activity." Mol Cell Biol **19**(12): 8075-82.

Lee, W. P., Y. Wen, B. Varnum and M. C. Hung (2002). "Akt is required for Axl-Gas6 signaling to protect cells from E1A-mediated apoptosis." Oncogene **21**(3): 329-36.

Li, R., J. Chen, G. Hammonds, H. Phillips, M. Armanini, P. Wood, R. Bunge, P. J. Godowski, M. X. Sliwkowski and J. P. Mather (1996). "Identification of Gas6 as a growth factor for human Schwann cells." J Neurosci **16**(6): 2012-9.

Livak, K. J. and T. D. Schmittgen (2001). "Analysis of relative gene expression data using real-time quantitative PCR and the 2(-Delta Delta C(T)) Method." Methods **25**(4): 402-8.

Liversage, R. (1991). Origin of the blastema cells in epimorphic regeneration of urodele appendages: a history of ideas. A History of Regeneration Research. C. E. Dinsmore. London, Cambridge University Press: 179-99.

Lo, D. C., F. Allen and J. P. Brockes (1993). "Reversal of muscle differentiation during urodele limb regeneration." Proc Natl Acad Sci U S A **90**(15): 7230-4.

Loeser, R. F., B. C. Varnum, C. S. Carlson, M. B. Goldring, E. T. Liu, S. Sadiev, T. E. Kute and R. Wallin (1997). "Human chondrocyte expression of growth-arrest-specific gene 6 and

the tyrosine kinase receptor axl: potential role in autocrine signaling in cartilage." Arthritis Rheum **40**(8): 1455-65.

Lu, Q., M. Gore, Q. Zhang, T. Camenisch, S. Boast, F. Casagranda, C. Lai, M. K. Skinner, R. Klein, G. K. Matsushima, H. S. Earp, S. P. Goff and G. Lemke (1999). "Tyro-3 family receptors are essential regulators of mammalian spermatogenesis." Nature **398**(6729): 723-8.

Lu, Q. and G. Lemke (2001). "Homeostatic regulation of the immune system by receptor tyrosine kinases of the Tyro 3 family." Science **293**(5528): 306-11.

Maier, C. E. and R. H. Miller (1992). "In vitro and in vivo characterization of blastemal cells from regenerating newt limbs." J Exp Zool **262**(2): 180-92.

Manfioletti, G., C. Brancolini, G. Avanzi and C. Schneider (1993). "The protein encoded by a growth arrest-specific gene (gas6) is a new member of the vitamin K-dependent proteins related to protein S, a negative coregulator in the blood coagulation cascade." Mol Cell Biol **13**(8): 4976-85.

Manfioletti, G., M. E. Ruaro, G. Del Sal, L. Philipson and C. Schneider (1990). "A growth arrest-specific (gas) gene codes for a membrane protein." Mol Cell Biol **10**(6): 2924-30.

Manly, B. F. J. (1997). RT Program Manual. Cheyenne, Wyoming, USA.

Mark, M. R., J. Chen, R. G. Hammonds, M. Sadick and P. J. Godowsk (1996). "Characterization of Gas6, a member of the superfamily of G domain-containing proteins, as a ligand for Rse and Axl." J Biol Chem **271**(16): 9785-9.

Mastrangelo, A. J., J. M. Hardwick, S. Zou and M. J. Betenbaugh (2000). "Part II. Overexpression of bcl-2 family members enhances survival of mammalian cells in response to various culture insults." Biotechnol Bioeng **67**(5): 555-64.

McCloskey, P., Y. W. Fridell, E. Attar, J. Villa, Y. Jin, B. Varnum and E. T. Liu (1997). "GAS6 mediates adhesion of cells expressing the receptor tyrosine kinase Axl." J Biol Chem **272**(37): 23285-91.

McCloskey, P., J. Pierce, R. A. Koski, B. Varnum and E. T. Liu (1994). "Activation of the Axl receptor tyrosine kinase induces mitogenesis and transformation in 32D cells." Cell Growth Differ **5**(10): 1105-17.

Melaragno, M. G., Y. W. Fridell and B. C. Berk (1999). "The Gas6/Axl system: a novel regulator of vascular cell function." Trends Cardiovasc Med **9**(8): 250-3.

Melaragno, M. G., D. A. Wuthrich, V. Poppa, D. Gill, V. Lindner, B. C. Berk and M. A. Corson (1998). "Increased expression of Axl tyrosine kinase after vascular injury and regulation by G protein-coupled receptor agonists in rats." Circ Res **83**(7): 697-704.

Meric, F., W. P. Lee, A. Sahin, H. Zhang, H. J. Kung and M. C. Hung (2002). "Expression profile of tyrosine kinases in breast cancer." Clin Cancer Res **8**(2): 361-7.

Mescher, A. L. (1976). "Effects on adult newt limb regeneration of partial and complete skin flaps over the amputation surface." J Exp Zool **195**(1): 117-28.

Mescher, A. L. (1996). "The cellular basis of limb regeneration in urodeles." Int J Dev Biol **40**(4): 785-95.

Mescher, A. L., G. W. White and J. J. Brokaw (2000). "Apoptosis in regenerating and denervated, nonregenerating urodele forelimbs." Wound Repair Regen **8**(2): 110-6.

Miyazaki, K., K. Uchiyama, Y. Imokawa and K. Yoshizato (1996). "Cloning and characterization of cDNAs for matrix metalloproteinases of regenerating newt limbs." Proc Natl Acad Sci U S A **93**(13): 6819-24.

Mullen, L. M., S. V. Bryant, M. A. Torok, B. Blumberg and D. M. Gardiner (1996). "Nerve dependency of regeneration: the role of Distal-less and FGF signaling in amphibian limb regeneration." Development **122**(11): 3487-97.

Nace, J. D. and R. A. Tassava (1995). "Examination of fibronectin distribution and its sources in the regenerating newt limb by immunocytochemistry and in situ hybridization." Dev Dyn **202**(2): 153-64.

Nagata, K., K. Ohashi, T. Nakano, H. Arita, C. Zong, H. Hanafusa and K. Mizuno (1996). "Identification of the product of growth arrest-specific gene 6 as a common ligand for Axl, Sky, and Mer receptor tyrosine kinases." J Biol Chem **271**(47): 30022-7.

Nakamura, Y. S., Y. Hakeda, N. Takakura, T. Kameda, I. Hamaguchi, T. Miyamoto, S. Kakudo, T. Nakano, M. Kumegawa and T. Suda (1998). "Tyro 3 receptor tyrosine kinase and its ligand, Gas6, stimulate the function of osteoclasts." Stem Cells **16**(3): 229-38.

Nakano, T., K. Higashino, N. Kikuchi, J. Kishino, K. Nomura, H. Fujita, O. Ohara and H. Arita (1995). "Vascular smooth muscle cell-derived, Gla-containing growth-potentiating factor for Ca(2+)-mobilizing growth factors." J Biol Chem **270**(11): 5702-5.

Nakano, T., Y. Ishimoto, J. Kishino, M. Umeda, K. Inoue, K. Nagata, K. Ohashi, K. Mizuno and H. Arita (1997). "Cell adhesion to phosphatidylserine mediated by a product of growth arrest-specific gene 6." J Biol Chem **272**(47): 29411-4.

Nakano, T., K. Kawamoto, K. Higashino and H. Arita (1996). "Prevention of growth arrest-induced cell death of vascular smooth muscle cells by a product of growth arrest-specific gene, gas6." FEBS Lett **387**(1): 78-80.

Nakano, T., K. Kawamoto, J. Kishino, K. Nomura, K. Higashino and H. Arita (1997). "Requirement of gamma-carboxyglutamic acid residues for the biological activity of Gas6: contribution of endogenous Gas6 to the proliferation of vascular smooth muscle cells." Biochem J **323 (Pt 2)**: 387-92.

Nakano, T., J. Kishino and H. Arita (1996). "Characterization of a high-affinity and specific binding site for Gas6." FEBS Lett **387**(1): 75-7.

Nemoto, T., K. Ohashi, T. Akashi, J. D. Johnson and K. Hirokawa (1997). "Overexpression of protein tyrosine kinases in human esophageal cancer." Pathobiology **65**(4): 195-203.

Neufeld, D. A. and F. A. Day (1996). "Perspective: a suggested role for basement membrane structures during newt limb regeneration." Anat Rec **246**(2): 155-61.

Nickoloff, B. J., J. Z. Qin, V. Chaturvedi, P. Bacon, J. Panella and M. F. Denning (2002). "Life and death signaling pathways contributing to skin cancer." J Investig Dermatol Symp Proc **7**(1): 27-35.

O'Bryan, J. P., R. A. Frye, P. C. Cogswell, A. Neubauer, B. Kitch, C. Prokop, R. Espinosa, 3rd, M. M. Le Beau, H. S. Earp and E. T. Liu (1991). "axl, a transforming gene isolated from primary human myeloid leukemia cells, encodes a novel receptor tyrosine kinase." Mol Cell Biol **11**(10): 5016-31.

O'Donnell, K., I. C. Harkes, L. Dougherty and I. P. Wicks (1999). "Expression of receptor tyrosine kinase Axl and its ligand Gas6 in rheumatoid arthritis: evidence for a novel endothelial cell survival pathway." Am J Pathol **154**(4): 1171-80.

Onda, H., M. L. Poulin, R. A. Tassava and I. M. Chiu (1991). "Characterization of a newt tenascin cDNA and localization of tenascin mRNA during newt limb regeneration by in situ hybridization." Dev Biol **148**(1): 219-32.

Poss, K. D., J. Shen, A. Nechiporuk, G. McMahon, B. Thisse, C. Thisse and M. T. Keating (2000). "Roles for Fgf signaling during zebrafish fin regeneration." Dev Biol **222**(2): 347-58.

Pough, F. H., C. M. Janis and J. B. Heiser (1999). Vertebrate life. Upper Saddle River, Prentice Hall.

Poulin, M. L., K. M. Patrie, M. J. Botelho, R. A. Tassava and I. M. Chiu (1993). "Heterogeneity in the expression of fibroblast growth factor receptors during limb regeneration in newts (Notophthalmus viridescens)." Development **119**(2): 353-61.

Prieto, A. L., J. L. Weber, S. Tracy, M. J. Heeb and C. Lai (1999). "Gas6, a ligand for the receptor protein-tyrosine kinase Tyro-3, is widely expressed in the central nervous system." Brain Res **816**(2): 646-61.

Rageh, M. A., L. Mendenhall, E. E. Moussad, S. E. Abbey, A. L. Mescher and R. A. Tassava (2002). "Vasculature in pre-blastema and nerve-dependent blastema stages of regenerating forelimbs of the adult newt, Notophthalmus viridescens." J Exp Zool **292**(3): 255-66.

Rao, Z., P. Handford, M. Mayhew, V. Knott, G. G. Brownlee and D. Stuart (1995). "The structure of a Ca(2+)-binding epidermal growth factor-like domain: its role in protein-protein interactions." Cell **82**(1): 131-41.

Repesh, L. A., T. J. Fitzgerald and L. T. Furcht (1982). "Changes in the distribution of fibronectin during limb regeneration in newts using immunocytochemistry." Differentiation **22**(2): 125-31.

Repesh, L. A. and J. C. Oberpriller (1978). "Scanning electron microscopy of epidermal cell migration in wound healing during limb regeneration in the adult newt, Notophthalmus viridescens." Am J Anat **151**(4): 539-55.

Reshkin, S. J., A. Bellizzi, V. Albarani, L. Guerra, M. Tommasino, A. Paradiso and V. Casavola (2000). "Phosphoinositide 3-kinase is involved in the tumor-specific activation of

human breast cancer cell Na(+)/H(+) exchange, motility, and invasion induced by serum deprivation." J Biol Chem **275**(8): 5361-9.

Robinson, D. R., Y. M. Wu and S. F. Lin (2000). "The protein tyrosine kinase family of the human genome." Oncogene **19**(49): 5548-57.

Rudenko, G., E. Hohenester and Y. A. Muller (2001). "LG/LNS domains: multiple functions -- one business end?" Trends Biochem Sci **26**(6): 363-8.

Sasaki, T., P. G. Knyazev, Y. Cheburkin, W. Gohring, D. Tisi, A. Ullrich, R. Timpl and E. Hohenester (2002). "Crystal structure of a C-terminal fragment of growth arrest-specific protein Gas6. Receptor tyrosine kinase activation by laminin G-like domains." J Biol Chem **277**(46): 44164-70.

Sato, M., N. Yasui, T. Nakase, H. Kawahata, M. Sugimoto, S. Hirota, Y. Kitamura, S. Nomura and T. Ochi (1998). "Expression of bone matrix proteins mRNA during distraction osteogenesis." J Bone Miner Res **13**(8): 1221-31.

Saxena, S. P., E. D. Israels and L. G. Israels (2001). "Novel vitamin K-dependent pathways regulating cell survival." Apoptosis **6**(1-2): 57-68.

Scadding, S. R. (1981). "Limb regeneration in adult amphibia." Can J Zool **59**: 34-46.

Scadding, S. R. (1984). "Forelimbs of the Newt Notophthalmus viridescens Continuously Denervated for up to 6 Weeks Prior to Amputation Do Not Regenerate." Journal of Experimental Zoology **229**(1): 155-161.

Schneider, C., R. M. King and L. Philipson (1988). "Genes specifically expressed at growth arrest of mammalian cells." Cell **54**(6): 787-93.

Schrag, J. A. and J. A. Cameron (1983). "Regeneration of adult newt skeletal muscle tissue in vitro." J Embryol Exp Morphol **77**: 255-71.

Scott, R. S., E. J. McMahon, S. M. Pop, E. A. Reap, R. Caricchio, P. L. Cohen, H. S. Earp and G. K. Matsushima (2001). "Phagocytosis and clearance of apoptotic cells is mediated by MER." Nature **411**(6834): 207-11.

Shanahan, C. M., D. Proudfoot, A. Farzaneh-Far and P. L. Weissberg (1998). "The role of Gla proteins in vascular calcification." Crit Rev Eukaryot Gene Expr **8**(3-4): 357-75.

Shankar, S. L., K. O'Guin, M. Cammer, F. A. McMorris, T. N. Stitt, R. S. Basch, B. Varnum and B. Shafit-Zagardo (2003). "The growth arrest-specific gene product Gas6 promotes the survival of human oligodendrocytes via a phosphatidylinositol 3-kinase-dependent pathway." J Neurosci **23**(10): 4208-18.

Shugart, E. C., A. S. Levenson, C. M. Constance and R. M. Umek (1995). "Differential expression of gas and gadd genes at distinct growth arrest points during adipocyte development." Cell Growth Differ **6**(12): 1541-7.

Simon, H. G., C. Nelson, D. Goff, E. Laufer, B. A. Morgan and C. Tabin (1995). "Differential expression of myogenic regulatory genes and Msx-1 during dedifferentiation and redifferentiation of regenerating amphibian limbs." Dev Dyn **202**(1): 1-12.

Steen, T. P. (1968). "Stability of chondrocyte differentiation and contribution of muscle to cartilage during limb regeneration in the axolotl (Siredon mexicanum)." J Exp Zool **167**(1): 49-78.

Stenflo, J., Y. Stenberg and A. Muranyi (2000). "Calcium-binding EGF-like modules in coagulation proteinases: function of the calcium ion in module interactions." Biochim Biophys Acta **1477**(1-2): 51-63.

Stitt, T. N., G. Conn, M. Gore, C. Lai, J. Bruno, C. Radziejewski, K. Mattsson, J. Fisher, D. R. Gies, P. F. Jones and et al. (1995). "The anticoagulation factor protein S and its relative, Gas6, are ligands for the Tyro 3/Axl family of receptor tyrosine kinases." Cell **80**(4): 661-70.

Stock, S. R., D. Blackburn, M. Gradassi and H. G. Simon (2003). "Bone formation during forelimb regeneration: A microtomography (microCT) analysis." Dev Dyn **226**(2): 410-7.

Stocum, D. L. and G. E. Dearlove (1972). "Epidermal-mesodermal interaction during morphogenesis of the limb regeneration blastema in larval salamanders." J Exp Zool **181**: 149-62.

Tanabe, K., K. Nagata, K. Ohashi, T. Nakano, H. Arita and K. Mizuno (1997). "Roles of gamma-carboxylation and a sex hormone-binding globulin-like domain in receptor-binding and in biological activities of Gas6." FEBS Lett **408**(3): 306-10.

Tanaka, E. M. and J. P. Brockes (1998). "A target of thrombin activation promotes cell cycle re-entry by urodele muscle cells." Wound Repair Regen **6**(4): 371-81.

Tanaka, E. M., D. N. Drechsel and J. P. Brockes (1999). "Thrombin regulates S-phase re-entry by cultured newt myotubes." Curr Biol **9**(15): 792-9.

Tanaka, E. M., A. A. Gann, P. B. Gates and J. P. Brockes (1997). "Newt myotubes reenter the cell cycle by phosphorylation of the retinoblastoma protein." J Cell Biol **136**(1): 155-65.

Tanaka, K., Y. Nagayama, T. Nakano, N. Takamura, H. Namba, S. Fukada, K. Kuma, S. Yamashita and M. Niwa (1998). "Expression profile of receptor-type protein tyrosine kinase genes in the human thyroid." Endocrinology **139**(3): 852-8.

Tassava, R. A. and D. J. Garling (1979). "Regenerative responses in larval axolotl limbs with skin grafts over the amputation surface." J Exp Zool **208**(1): 97-110.

Tassava, R. A., D. P. Treece and C. L. Olsen (1983). "Effects of partial denervation on the newt blastema cell cycle." Prog Clin Biol Res **110 Pt A**: 537-45.

Taylor, I. C., S. Roy and H. E. Varmus (1995). "Overexpression of the Sky receptor tyrosine kinase at the cell surface or in the cytoplasm results in ligand-independent activation." Oncogene **11**(12): 2619-26.

Thornton, C. S. (1960). "Influence of an eccentric epidermal cap on limb regeneration in *Amblystoma* larvae." Dev Biol **2**: 551-569.

Timpl, R., D. Tisi, J. F. Talts, Z. Andac, T. Sasaki and E. Hohenester (2000). "Structure and function of laminin LG modules." Matrix Biol **19**(4): 309-17.

Varnum, B. C., C. Young, G. Elliott, A. Garcia, T. D. Bartley, Y. W. Fridell, R. W. Hunt, G. Trail, C. Clogston, R. J. Toso and et al. (1995). "Axl receptor tyrosine kinase stimulated by the vitamin K-dependent protein encoded by growth-arrest-specific gene 6." Nature **373**(6515): 623-6.

Vollrath, D., W. Feng, J. L. Duncan, D. Yasumura, P. M. D'Cruz, A. Chappelow, M. T. Matthes, M. A. Kay and M. M. LaVail (2001). "Correction of the retinal dystrophy phenotype of the RCS rat by viral gene transfer of Mertk." Proc Natl Acad Sci U S A **98**(22): 12584-9.

Wallace, H. (1981). Vertebrate limb regeneration. Toronto, John Wiley & Sons.

Wang, C. P., K. Yagi, P. J. Lin, D. Y. Jin, K. W. Makabe and D. W. Stafford (2003). "Identification of a gene encoding a typical gamma-carboxyglutamic acid domain in the tunicate Halocynthia roretzi." J Thromb Haemost **1**(1): 118-23.

Wimmel, A., D. Glitz, A. Kraus, J. Roeder and M. Schuermann (2001). "Axl receptor tyrosine kinase expression in human lung cancer cell lines correlates with cellular adhesion." Eur J Cancer **37**(17): 2264-74.

Wimmel, A., I. Rohner, A. Ramaswamy, H. H. Heidtmann, R. Seitz, M. Kraus and M. Schuermann (1999). "Synthesis and secretion of the anticoagulant protein S and coexpression of the Tyro3 receptor in human lung carcinoma cells." Cancer **86**(1): 43-9.

Wu, C. W., A. F. Li, C. W. Chi, C. H. Lai, C. L. Huang, S. S. Lo, W. Y. Lui and W. C. Lin (2002). "Clinical significance of AXL kinase family in gastric cancer." Anticancer Res **22**(2B): 1071-8.

Xia, X. (1996). "Maximizing Transcription Efficiency Causes Codon Usage Bias." Genetics **144**(3): 1309-1320.

Yagami, T., K. Ueda, K. Asakura, T. Sakaeda, H. Nakazato, T. Kuroda, S. Hata, G. Sakaguchi, N. Itoh, T. Nakano, Y. Kambayashi and H. Tsuzuki (2002). "Gas6 rescues cortical neurons from amyloid beta protein-induced apoptosis." Neuropharmacology **43**(8): 1289-96.

Yanagita, M., H. Arai, T. Nakano, K. Ohashi, K. Mizuno, A. Fukatsu, T. Doi and T. Kita (2001). "Gas6 induces mesangial cell proliferation via latent transcription factor STAT3." J Biol Chem **276**(45): 42364-9.

Yin, J., C. McLachlan, X. Chaufour, M. A. McGuire, G. White, V. Turner, N. J. King and B. D. Hambly (2000). "Growth arrest-specific gene 6 expression in proliferating rabbit vascular smooth muscle cells in vitro and in vivo." Electrophoresis **21**(17): 3851-6.

APPENDIX I – CLONING AND CHARACTERIZING OF *NvGAPDH*

A. Introduction

A key aspect of any quantitative technique is the presence of a suitable normalizing factor to which expression levels in the gene of interest can be compared. An ideal normalization factor is a ubiquitous gene with stable expression over a wide variety of samples, treatments, conditions, and stages that is necessary for cell cycle progression, maintenance or survival. The most commonly used internal controls are β-actin, GAPDH, ribosomal RNA (rRNA), histone H3 and cyclophilin (Bustin 2000; Bustin 2002). Recently, the newt homologue of β-actin (Nvβ-actin) was cloned and validated for semi-quantitative RT-PCR studies involving B1H1 cell cultures, limb and lens regeneration (S. Vascotto, unpublished results). However, several recent studies have demonstrated that a single normalizing gene is inappropriate for real-time qPCR (Thellin et al. 1999; Tricarico et al. 2002; Vandesompele et al. 2002). To overcome this limitation the purpose of this side project was to isolate another normalization gene for accurate real-time qPCR profiling.

Housekeeping genes are commonly used because these factors are involved in cell survival, and their expression levels should not dramatically alter between conditions or states. GAPDH is an essential glycolytic enzyme that results in phosphorylation of glyceraldehyde-3-phosphate into 1,3-diphosphoglycerate with reduction of NADP+ to NADPH. *GAPDH* is one of the most common genes used as an internal standard because its expression has been presumed or demonstrated to be stable in a wide variety of tissues, experimental conditions and states. Recently, the GAPDH homologue for the axolotl (*Ambystoma mexicanum*) and *Pluerodeles waltl* was cloned and used for semiquantitative RT-PCR expression studies (Christensen et al. 2001; Ferretti et al. 2001). Although the above authors did not specify that *GAPDH* levels were constant and consistent, the apparent stable expression lends credibility for isolating the newt GAPDH homologue (NvGAPDH)

as another normalization factor for real-time qPCR analysis. GAPDH is commonly used due to its relatively low copy number, few number of pseudogenes and high enough homology to clone from a rare or highly derived species (Sturzenbaum and Kille 2001). Despite its wide usage, GAPDH is considered to be a poor normalizing factor because GAPDH is involved in other cellular activities (Sirover 1996; Sirover 1997; Tatton et al. 2000; Mazzola and Sirover 2002). Most studies that invalidate *GAPDH* as an internal standard focused on single cell masses, such as tumours, individual structures such as developing collateral arteries, microdissected tissues that most likely has contaminating cells, or individual cells such as erythrocytes (Thellin et al. 1999; Bustin 2000; Schmittgen and Zakrajsek 2000; Goidin et al. 2001; Hamalainen et al. 2001; Bustin 2002; Deindl et al. 2002; Tricarico et al. 2002). Despite this, NvGAPDH may be an appropriate candidate to pursue because the overall expression levels may not significantly vary during regeneration *in vivo* or in heterogeneous B1H1 cell line.

As the utilization of a single internal standard is apparently inappropriate for most cases, the purpose of this section of my thesis is to validate both *Nvβ-actin* and *NvGAPDH* as internal standards for real-time RT-qPCR. *Nvβ-actin* has been demonstrated to have stable expression levels in regenerating limbs up to 21 days post amputation, with increased expression at the palette stage and beyond (S. Vascotto unpublished results). As well, *Nvβ-actin* expression is consistent in different B1H1 cell conditions (S. Vascotto unpublished results). However, *Nvβ-actin* expression is not ubiquitous in limb regeneration and conflicts with B1H1 cell culture expression analysis; there was weak expression in muscle tissues, but strong expression in cultured myotubes (S. Vascotto unpublished results). The strategy outlined below describes the process of validating *NvGAPDH* along with *Nvβ-actin* as internal standards for real-time RT-qPCR.

B. Cloning of *NvGAPDH*

Degenerate GAPDH-specific oligonucleotides were designed by aligning nucleotide sequences of various species of GAPDH including *Bos taurus* (U85042), *Columba livia* (AF036934), *Gallus gallus* (AF047874), *Homo sapiens* (NM_002046), *Mus musculus* (AK002273), *Oryctolagus cuniculus* (L23961), *Oncorhynchus mykiss* (AF027130), *P. waltl* (AF343978), *Sus scrofa* (AF017079) and *Xenopus laevis* (U41753). The resulting NvGap3 and NvGap4 primers (Table A1) yield an expected amplicon of ~510 bp that corresponds to the *gapC* fragment (Mounaji et al. 2002).

Total RNA was isolated from newt liver using the Trizol reagent (Invitrogen) as described in Appendix II, Section A. After the absorbance at 260 nm was recorded, total RNA was analyzed by 1.2% agarose gel electrophoresis to ascertain integrity and to verify quantification. First strand synthesis was then performed as per Appendix II, Section B1. More specifically, 2 μg of liver total RNA was heat denatured with 50 ng NvGap4 at 65°C for 8 min, and a 30 μL first strand reaction was generated at 42°C. PCR was performed using a 1:25 dilution of the first strand in a 25 μL reaction containing 1X PCR buffer, 1.5 mM $MgCl_2$, 200 μM dNTP, 100 ng each primer and 1.25 U *Taq* DNA Polymerase (Invitrogen). The PCR procedure involved an initial denaturation of 95°C for 2 min, followed by 30 cycles of 94°C for 1 min, 49°C for 1 min and 72°C for 50 sec, and 72°C for 10 min on an Eppendorf Mastercycler Gradient Thermocycler. The PCR products were electrophoresed on a 1.3% ethidium bromide-stained agarose gel, and showed a single amplicon of approximately 500 bp (Figure A1). The amplicon was A-tailed in a 10 μL reaction with 8 μL PCR product, 5 U *Taq* Polymerase (Invitrogen) and 200 μM dATP, by incubating for 30 min at 70°C and placed on ice. The A-tailed product was ligated overnight at 4°C into either the pGEM-T or pGEM-T Easy Vector (Promega) according to the manufacturer's instructions. The ligated products were heat shocked, transformed into

TABLE A1. Primers used in this appendix and their respective sequences, length and melting temperature (T_m). T_m was determined from http://oligos.qiagen.com/oligos/toolkit.php.

Primer Sequence	**Sequence (5′ → 3′)**	**Length**	**T_m**
NvGap3	GCHTCBTGYACYACHAACTG	20	61.1
NvGap4	CCSCAYTCRTTRTCRTACCA	20	60.4
M13F	GTAAAACGACGGCCAGT	17	57.2
M13R	CAGGAAACAGCTATGAC	17	54.8
NvGAPDH_F	TGTGGCGTGACGGCAGAGGTG	21	68.4
NvGAPDH_R	TCCAAGCGGCAGGTCAGGTCAAC	23	68.1
Nvβ-Actin_For	CCACTGCTGCTTCTTCATCCTCTC	24	66.3
Nvβ-Actin_Rev	GGGCACCTGAACCGCTCATTG	21	66.5

Figure A1. Result of an RT-PCR using degenerate primers specific for GAPDH. An amplicon is observed in the ~500 bp region.

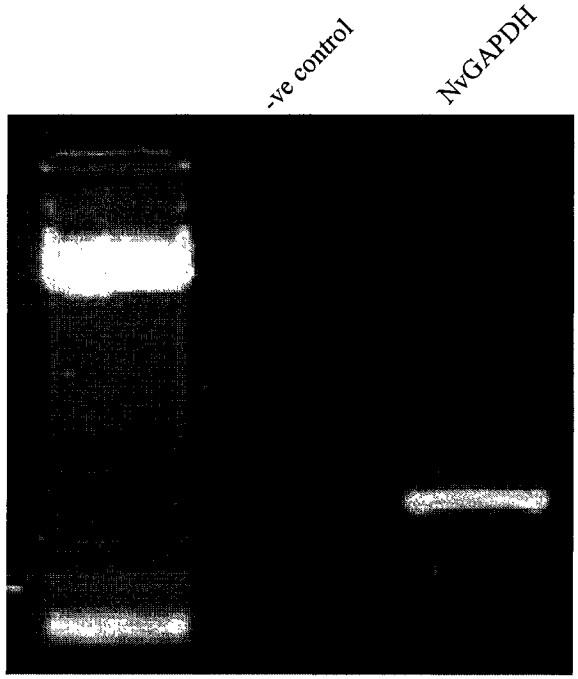
-ve control
NvGAPDH
- 500 bp

Figure A2. Multiple alignment of NvGAPDH nucleotide sequence with other GAPDH fragments. There is a high level of nucleotide conservation among all GAPDH sequences. Note that the mismatch the 5′ end correspond to degenerate primer sites utilised in cloning NvGAPDH. Yellow shaded areas represent nucleotide consensi. Analysis was performed with the CLUSTALV algorithm with the MegAlign (DNAStar) software. Species represented are axolotl (*A. mexicanum*, AF360983), red-spotted newt (*N. viridescens*, NvGAPDH), Iberian ribbed newt (*P. waltl*, AF343978), marsh frog (*R. ridibunda*, AY072703), African clawed frog (*X. laevis*, U41753), chicken (*G. gallus*, AF047874) and human (*H. sapiens*, NM_002046).


1 GCCTCCTGCACCACCAACTGCTTAGCACCCCTGGCCAAGGTCATCCATGACAACTTTGGTATCGTGGAAGGACT H. sapiens.SEQ
1 GCATCGTGCACCACCAACTGCCTGGCACCCTTGGCCAAGGTCATCCATGACAACTTTGGCATTGTGGAGGGTCT G. gallus.SEQ
1 GCATCCTGCACAACAAACTGTCTGGCTCCTCTTGCAAAGGTCATAAACGACAACTTTGGCATTGTTGAGGGACT X. laevis.SEQ
1 GCCTCCTGTACCACCAACTGCCTGGCTCCTCTTGCAAAGGTCATCAATGACAAATTTGGCATTGTGGAGGCGTT R. ridibunda.SEQ
1 GCCTCCTGCACTACAAACTGTCTGGCTCCTCTGGCTAAGGTCATCCACGACAACTTTCACATCGTCGAGGGTTT P. waltl.SEQ
1 GCHTCCTGTACTACCAACTGTCTGGCTCCTCTGGCTAAGGTCATCAATGACAACTTCCACATCGTCGAGGGTTT N. viridescens.SEQ
1 GCCTCCTGCACCACCAACTGCCTGGCTCCCTTGGCCAAAGTCATCAACGACAGCTTCCACATTGTGGAGGGTCT A. mexicanum.SEQ
75 CATGACCACAGTCCATGCCATCACTGCCACCCAGAAGACTGTGGATGGCCCCTCCGGGAAACTGTGGCGTGATG H. sapiens.SEQ
75 TATGACCACTGTCCATGCCATCACAGCCACACAGAAGACGGTGGATGGCCCCTCTGGGAAGCTGTGGAGAGATG G. gallus.SEQ
75 GATGACAACTGTCCATGCTTACACTGCCACCCAGAAGACAGTGGATGGCCCATCAGGGAAGCTGTGGAGAGATG X. laevis.SEQ
75 GATGACCACTGTCCATGCTTTCACCGCTACACAGAAGTGTGTGGACGGACCATCTGGCAAACTTTGGCGTGATG R. ridibunda.SEQ
75 GATGACCACTGTACATGCTGTGACAGCTACACAAAAGACTGTGGACGGTCCTTCTGGGAAACTGTGGCGTGACG P. waltl.SEQ
75 GATGACTACTGTCCATGCTGTGACTGCTACACAAAAGACTGTGGACGGTCCTTCTGGGAAACTGTGGCGTGACG N. viridescens.SEQ
75 CATGACGACGGTTCATGCTGTGACAGCCACCCAGAAGACTGTGGATGGTCCCTCTGGCAAACTGTGGCGCGATG A. mexicanum.SEQ
149 GCCGCGGGGCTCTCCAGAACATCATCCCTGCCTCTACTGGCGCTGCCAAGGCT-GTGGGCAAG-GTCATCCCTG H. sapiens.SEQ
149 GCAGAGGTGCTGCCCAGAACATCATCCCAGCGTCCACTGGGGCTGCTAAGGCT-GTGGGGAAA-GTCATCCCTG G. gallus.SEQ
149 GAAGAGGTGCCGGTCAGAACATCATCCCCGCCTCAACTGGTGCAGCAAAGGCT-GTCGGAAAA-GTTATCCCTG X. laevis.SEQ
149 GCAGAGGTGCTTCACAGAACATCATCCCAGCATC-ACTGGTGCTGCCAAGGCCCGTTGGCAAAAGTCATCCCTG R. ridibunda.SEQ
149 GCAGAGGTGCCAATCAGAATATCATTCCAGCCTCTACCGGGGCAGCCAAGGCC-GTGGGCAAA-GTTATTCCTG P. waltl.SEQ
149 GCAGAGGTGCCAATCAGAATATCATTCCAGCCTCCACTGGGGCAGCCAAGGCT-GTGGGCAAA-GTCATCCCTG N. viridescens.SEQ
149 GCAGAGGTGCCAACCAGAACATCATTCCAGCCTCCACTGGAGCTGCCAAAGCT-GTCGGCAAG-GTCATCCCAG A. mexicanum.SEQ
221 AGCTGAACGGGAAGCTCACTGGCATGGCCTTCCGTGTCCCCACTGCCAACGTGTCAGTGGTGGACCTGACCTGC H. sapiens.SEQ
221 AGCTGAATGGGAAGCTTACTGGAATGGCTTTCCGTGTGCCAACCCCCAATGTCTCTGTTGTTGACCTGACCTGC G. gallus.SEQ
221 AGCTGAACGGCAAACTCACAGGAATGGCTTTCCGTGTCCCCCGTTCCAAATGTGTCCGTTGTGGATCTGACCTGC X. laevis.SEQ
222 CTCTGAACGGAAAACT-ACTGGCATGGCCTTCAGAGTCCCCACTGCCAACGTATCTGTGGTTGACCTGACCTGC R. ridibunda.SEQ
221 AACTCAATGGGAAACTCACAGGCATGGCCTTCCGTGTACCTGTCCCCAATGTGTCTGTGGTTGACCTGACCTGC P. waltl.SEQ
221 AACTCAATGGGAAACTCACAGGCATGGCCTTCCGGGTACCTGTCGCCAATGTGTCTGTGGTTGACCTGACCTGC N. viridescens.SEQ
221 AGCTCAATGGGAAACTCACTGGAATGGCTTTCCG------TGTCCCCA A. mexicanum.SEQ
295 CGTCTAGAAAAACCTGCCAAATATGATGACATCAAGAAGGTGGTGAAGCAGGCGTCGGAGGGCCCCCTCAAGGG H. sapiens.SEQ
295 CGTCTGGAGAAACCAGCCAAGTATGATGATATCAAGAGGGTAGTGAAGCCTGCTGCTGATGGGCCCCTGAAGGG G. gallus.SEQ
295 CGCCTGAAGAAGCCTGCAAAGTATGATGATATCAAGGCTGCAGTTAAAGCTGCTGCAGAGGGACCAATGAAAGG X. laevis.SEQ
295 CGCCTGGAAAAGGCTGCCAAATATGATGACATCAAAGCTGCAGTGAAGGCCGCATCTGAGGGACCACTGAAGGG R. ridibunda.SEQ
295 CGCTTGGAGAAGGCTGCCTCATATGACGACATTAAGAAGGTGGTAAAGGCAGCAGCTGATGGGCCAATGAAAGG P. waltl.SEQ
295 CGCTTGGAGAAGGGTGCCTCTTATGACGACATTAAGAAGGTGGTAAAGGCAGCTGCTGATGGACCAATGAAAGG N. viridescens.SEQ
262 A. mexicanum.SEQ
369 CATCCTGGGCTACACTGAGCACCAGGTGGTCTCCTCTGACTTCAACAGCGACACCCACTCCTCCACCTTTGACG H. sapiens.SEQ
369 CATCCTAGGATACACAGAGGACCAGGTTGTCTCCTGTGACTTCAATGGTGACAGCCATTCCTCCACCTTTGATG G. gallus.SEQ
369 AATCCTGCAATACACACAAGACCAGGTTGTCTCCACTGACTTCAATGGCTGCACTTATTCCTCCATCTTTGATG X. laevis.SEQ
369 AATTCTGGGATACACAGAGGATCAGGTTGTCTCCAGTGACTTCAACGGTGACACCCATTCCTCCATCTTTGATG R. ridibunda.SEQ
369 AATTTTGGGATACACCGAGGAACAGGTGGTGTCCTCCGACTTCAACGGTGACGATCACTCATCAATCTTTGATG P. waltl.SEQ
369 AATTTTGGGATACACCGATGAACAGGTGGTGTCCTCTGACTTCAACGGTGACGATCACTCCTCCATCTTTGATG N. viridescens.SEQ
262 A. mexicanum.SEQ
443 CTGGGGCTGGCATTGCCCTCAACGACCACTTTGTCAAGCTCATTTCCTGGTATGACAACGAATTTGG H. sapiens.SEQ
443 CGGGTGCTGGCATTGCACTGAATGACCATTTCGTCAAGCTTGTTTCCTGGTATGACAATGAGTTTGG G. gallus.SEQ
443 CCGATGCTGGAATTGCATTGAATGAACACTTTGTGAAGCTGGTTTCCTGGTATGATAATGAATGCGG X. laevis.SEQ
443 CTGGCGCTGGCATTCAACTAAATGATCACTTCGTTAAACTAATTACTTGGTATGACAATGAATTCGG R. ridibunda.SEQ
443 CTGGTGCCGGTATTGCACTCAACGACCACTTTGTGAAACTGGTTTCTTGGTATGACAACGAATGGGG P. waltl.SEQ
443 CTGGTGCCGGTATTGCACTCAACGACCACTTTGTGAAACTGGTTTCTTGGTATGACAACGAGTGGGG N. viridescens.SEQ
262 A. mexicanum.SEQ

Figure A3. Multiple alignment of NvGAPDH amino acid sequence with other GAPDH sequences. Note that there is an extremely high level of evolutionary conservation throughout the whole sequence. Yellow shaded areas represent amino acid identity. Analysis was performed with the CLUSTALV algorithm with the MegAlign (DNAStar) software. Species represented are axolotl (*A. mexicanum*, AAL16956), red-spotted newt (*N. viridescens*, NvGAPDH), Iberian ribbed newt (*P. waltl*, AAO13359), marsh frog (*R. ridibunda*, AAL62488), African clawed frog (*X. laevis*, P51469), chicken (*G. gallus*, P00356), human (*H. sapiens*, NP_002037), Norway rat (*R. rattus*, CAA26150), mouse, (*M. musculus*, NP_032110), and enteric bacteria *Escherichia coli* (BAA15038).

```
1   A S C T T N C L A P L A K V I N D S F H I V E G L M T T V H A V T A A. mexicanum.PRO
1   A S C T T N C L A P L A K V I N D N F H I V E G L M T T V H A V T A N. viridescens.PRO
1   A S C T T N C L A P L A K V I H D N F H I V E G L M T T V H A V T A P. waltl.PRO
1   A S C T T N C L A P L A K V I N D N F G I V E G L M T T V H A F T A X. laevis.PRO
1   A S C T T N C L A P L A K V I N D K F G I V E A L M T T V H A F T A R. ridibunda.PRO
1   A S C T T N C L A P L A K V I H D N F G I V E G L M T T V H A I T A G. gallus.PRO
1   A S C T T N C L A P L A K V I H D H F G I V E G L M T T V H A I T A H. sapiens.PRO
1   A S C T T N C L A P L A K V I H D N F G I V E G L M T T V H A I T A R. rattus.PRO
1   A S C T T N C L A P L A K V I H D N F G I V E G L M T T V H A I T A M. musculus.PRO
1   A S C T T N C L A P L A K V I N D N F G I I E G L M T T V H A T T A E. coli.PRO

35  T Q K T V D G P S G K L W R D G R G A N Q N I I P A S T G A A K A V A. mexicanum.PRO
35  T Q K T V D G P S G K L W R D G R G A N Q N I I P A S T G A A K A V N. viridescens.PRO
35  T Q K T V D G P S G K L W R D G R G A N Q N I I P A S T G A A K A V P. waltl.PRO
35  T Q K T V D G P S G K L W R D G R G A G Q N I I P A S T G A A K A V X. laevis.PRO
35  T Q K C V D G P S G K L W R D G R G A S Q N I I P A S L V L P R P V R. ridibunda.PRO
35  T Q K T V D G P S G K L W R D G R G A A Q N I I P A S T G A A K A V G. gallus.PRO
35  T Q K T V D S P S G K L W R G G R G A A Q N L I P A S T G A A K A V H. sapiens.PRO
35  T Q K T V D G P S G K L W R D G R G A A Q N I I P A S T G A A K A V R. rattus.PRO
35  T Q K T V D G P S G K L W R D G R G A A Q N I I P A S T G A A K A V M. musculus.PRO
35  T Q K T V D G P S H K D W R G G R G A S Q N I I P S S T G A A K A V E. coli.PRO

69  G K V I P E L N G K L T G M A F R V P                               A. mexicanum.PRO
69  G K V I P E L N G K L T G M A F R V P V A N V S V V D L T C R L E K N. viridescens.PRO
69  G K V I P E L N G K L T G M A F R V P V P N V S V V D L T C R L E K P. waltl.PRO
69  G K V I P E L N G K I T G M A F R V P T P N V S V V D L T C R L Q K X. laevis.PRO
69  G K S H P C S E R K T T G M A F R V P T A N V S V V D L T C R L E K R. ridibunda.PRO
69  G K V I P E L N G K L T G M A F R V P T P N V S V V D L T C R L E K G. gallus.PRO
69  G K V I P E L D G K L T G M A F R V P T A N V S V L D L T C R L E K H. sapiens.PRO
69  G K V I P E L N G K L T G M A F R V P T P N V S V V D L T C R L E K R. rattus.PRO
69  G K V I P E L N G K L T G M A F R V P T P N V S V V D L T C R L E K M. musculus.PRO
69  G K V L P E L N G K L T G M A F R V P T P N V S V V D L T V R L E K E. coli.PRO

87                                                                  A. mexicanum.PRO
103 G A S Y D D I K K V V K A A A D G P M K G I L G Y T D E Q V V S S D N. viridescens.PRO
103 A A S Y D D I K K V V K A A A D G P M K G I L G Y T E E Q V V S S D P. waltl.PRO
103 P A K Y D D I K A A I K T A S E G P M K G I L G Y T Q D Q V V S T D X. laevis.PRO
103 A A K Y D D I K A A V K A A S E G P L K G I L G Y T E D Q V V S S D R. ridibunda.PRO
103 P A K Y D D I K R V V K A A A D G P L K G I L G Y T E D Q V V S C D G. gallus.PRO
103 P A K Y D D I K K V V K E A S E G P L K G I L G Y T E D E V V S D D H. sapiens.PRO
103 P A K Y D D I K K V V K Q A A E G P L K G I L G Y T E D Q V V S C D R. rattus.PRO
103 P A K Y D D I K K V V K Q A S E G P L K G I L G Y T E D Q V V S C D M. musculus.PRO
103 A A T Y E Q I K A A V K A A A E G E M K G V L G Y T E D D V V S T D E. coli.PRO

87                                                                  A. mexicanum.PRO
137 F N G D D H S S I F D A G A G I A L N D H F V K L V S W Y D N E W N. viridescens.PRO
137 F N G D D H S S I F D A G A G I A L N D H F V K L V S W Y D N E W P. waltl.PRO
137 F N G D T H S S I F D A D A G I A L N E N F V K L V S W Y D N E C X. laevis.PRO
137 F N G D T H S S I F D A G A G I Q L N D H F V K L I T W Y D N E F R. ridibunda.PRO
137 F N G D S H S S T F D A G A G I A L N D H F V K L V S W Y D N E F G. gallus.PRO
137 F N G S N H S S I F D A G A G I E L N D T F V K L V S W Y D N E F H. sapiens.PRO
137 F N S N S H S S T F D A G A G I A L N D N F V K L I S W Y D N E Y R. rattus.PRO
137 F N S N S H S S T F D A G A G I A L N D N F V K L I S W Y D N E Y M. musculus.PRO
137 F N G E V C T S V F D A K A G I A L N D N F V K L V S W Y D N E T E. coli.PRO
```

competent DH5α *E. coli* cells, streaked onto LB-ampicillin plates and incubated overnight at 37°C. Individual colonies were replica plated and screened by PCR with M13F and M13R sequencing primers under the following conditions: initial denaturation period at - 95°C for 2 min, followed by 31 cycles of 94°C for 1 min, 62°C for 90 sec and 72°C for 90 sec, with a final extension of 72°C for 10 min on an Eppendorf Mastercycler Gradient Thermocycler. The PCR products were run on a 1.3% agarose gel. A colony containing an approximately 700 bp band (500 bp insert plus ~100 bp vector sequence on either side) was inoculated in LB media under ampicillin selection at 37°C overnight with shaking, and the plasmid purified by the QIAprep Spin Miniprep Kit (Qiagen). The plasmid was submitted for sequencing to either CMRSInc or University of Ottawa Biotechnology Research Institute using the M13 sequencing primers. The above steps were independently repeated at least two more times using different first strand templates to generate a consensus sequence.

The 509 bp sequence isolated was irrefutably verified as the *gapdh_C* fragment by BLAST searches. The fragment shows 96% nucleotide level and 97% amino acid identity to *P. waltl* GAPDH as revealed by BLASTN and BLASTX, respectively. As well, the NvGAPDH fragment has high similarity to axolotl *GAPDH* (85%), and *O. mykiss* (90%) and *G. gallus* (90%) polypeptides. Overall, GAPDH is a significantly conserved gene, with high conservation at both the nucleotide and amino acid level (Figure A2 and A3). The nucleotide mismatches at the 5' end result from the degenerate primers, as the mismatches correspond to the degenerate areas of the oligonucleotides. Nevertheless, the resulting codon specifies for the same amino acid.

C. Temporal Expression Analysis

A valid normalization gene possesses several criteria: expression is constant among cell types, states or experimental conditions, is abundant and is essential for cell survival.

Since ribosomal RNA (rRNA) composes ~85-90% of total RNA and synthesis of rRNA is unlikely to widely fluctuate, fixed amount of starting total RNA is typically the most reliable measurement of ascertaining equal amounts of starting material for RNA techniques (Bustin 2000; Bustin 2002). As such, using a fixed amount of RNA to validate both *NvGAPDH* and *Nvβ-actin* as normalization genes was undertaken in this thesis to demonstrate similar expression profiles.

C.i Primer Design and Validation

Primers specific for real-time qPCR were designed using PrimerSelect (DNASTAR) with the following conditions: amplicon size between 75 and 175, and Tm around 65°C. NvGAPDH_F and NvGAPDH_R correspond to 137..157 nt and 250..302 nt of the NvGAPDH fragment respectively, and Nvβ-Actin_For and Nvβ-Actin_Rev correspond to 325..348 nt nucleotide and 395..415 nt of the Nvβ-actin fragment, respectively (Table A1).

A preliminary RT-PCR was performed using these primers to ascertain the absence of primer-dimer formation, the presence of a single amplicon and investigate the possibility that the primers span at least one intron. B1H1 cells were maintained as per Chapter 2.2. First strand cDNA was generated from 2 μg confluent B1H1 total RNA using NvGAPDH_R and Nvβ-Actin_Rev reverse primers. The 25 μL PCR conditions were as above with the following exceptions: final primer concentration was 400 nM,, and the template consisted of 250 ng genomic NvDNA (prepared as in Appendix II, Section E) and 1:100 of Nvβ-actin and 1:60 of NvGAPDH final dilution of first strand. The PCR parameters were as follows: initial denaturation at 95°C for 120 sec, 33 cycles of 94°C for 60 sec and 66°C for 120 sec with a final extension of 72°C for 10 min. The PCR products were examined on a 1.3% ethidium bromide-stained agarose gel.

To demonstrate that the relative PCR efficiencies of both *NvGAPDH* and *Nvβ-actin* are approximately equal and thus, comparison of the C_T between the two genes is permitted,

a relative PCR efficiency plot of *NvGAPDH* and *Nvβ-actin* is necessary. First strand was generated from 2 μg of DNaseI-treated total RNA from confluent B1H1 cells primed with 500 ng each of oligo(dT) and random hexamers in a 30 μL reaction (Appendix II, Section B2), and 33.33, 6.67, 3.33, 0.66, 0.33, 0.067 and 0.033 ng first strand was used for real-time RT-qPCR. The 25 μL PCR reaction involved 1X PCR Buffer, 2 mM $MgCl_2$, 200 μM each dNTP, 200 nM each primer, 0.9 U *Taq* DNA polymerase, 3:125,000X SYBR Green I Dye (Molecular Probes) and 8 nM calibration dye (Bio-Rad). qPCR was performed on an iCycler iQ real-time thermocycler (Bio-Rad) with the following parameters: an initial denaturation step of 3 min at 95°C, 40 cycles of 94°C and 63°C of 25 sec each, and 83°C for 25 sec. This was followed by a 10 min extension at 72°C with a dissociation-curve analysis of a 60 sec denaturation step at 95°C, annealing step for 60 sec at 55°C, and 80 cycles of 0.5°C increments every 10 sec. Each reaction condition was performed in triplicate to obtain average values with standard deviation units. Each representative reaction condition was subjected to 2.5% agarose gel electrophoresis to ascertain specific PCR amplification. ΔC_T and standard deviation values were calculated as described in Appendix II, Section D, and statistical analysis was performed using the computer program RT (Manly 1997).

Both *NvGAPDH* and *Nvβ-actin* primers are ideal for real-time RT-qPCR, and for use as a basis of comparison. The primers amplify a single product, result in no primer-dimer formation and *NvGAPDH* spans an intron (Figure A4). However, the absence of an intron-spanning region for *Nvβ-actin* warrants DNaseI treatment of the total RNA population, as the Trizol RNA extraction procedure may have minute amounts of genomic DNA contamination. The PCR efficiencies are above 90%, with *NvGAPDH* and *Nvβ-actin* at 91.8% ($R^2 = 0.996$) and 95.5% ($R^2 = 0.992$), respectively (Figure A5a). Although increasing *NvGAPDH* efficiency by designing new primers (a new combination or

Figure A4. A primer pair PCR analysis of both *NvGAPDH* and *Nvβ-actin* genes. Using genomic DNA as template, the NvGAPDH spans at least one intron; however *Nvβ-actin* does not. Noticeable in this picture are the absence of primer-dimer pairs and non-specific amplification, and the presence of a single amplicon using cDNA as a template.

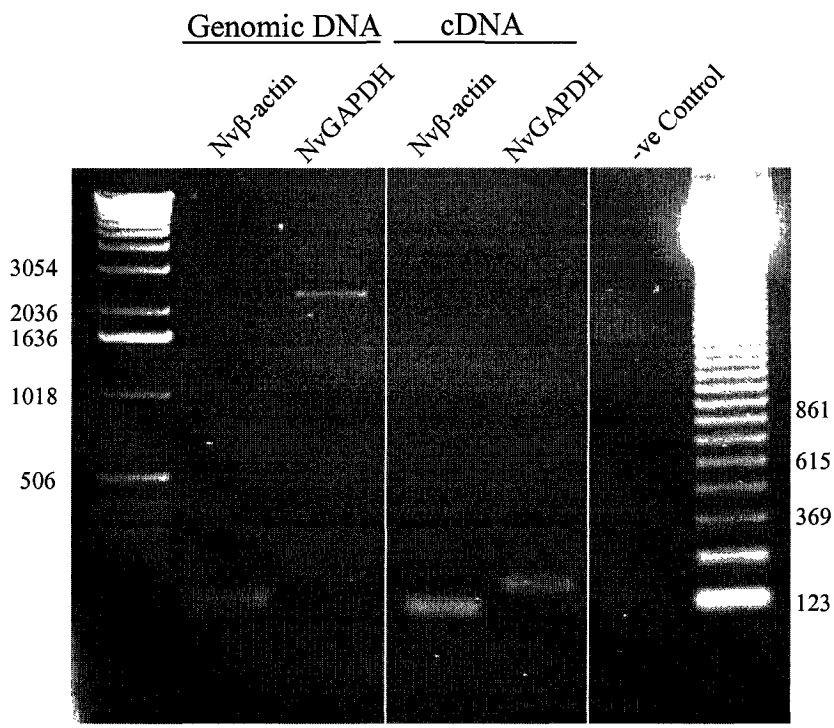
Genomic DNA
cDNA
Nvβ-actin
NvGAPDH
Nvβ-actin
NvGAPDH
-ve Control
3054
2036
1636
1018
506
861
615
369
123

Figure A5. Analysis of *NvGAPDH* and *Nvβ-actin* primer pairs for real time qPCR analysis. a) A real-time RT-qPCR analysis of the primer efficiency of both *NvGAPDH* and *Nvβ-actin* genes. An efficiency plot of both genes over a 500-fold concentration difference in B1H1 cDNA demonstrates that the efficiency is over 90%. c) A relative efficiency plot of both *NvGAPDH* and *Nvβ-actin* reveals that the slope approaches zero, and thus, comparisons between the two genes by the $\Delta\Delta C_T$ method is permissible. As such, the primers appear ideal candidates for real-time qPCR. The dotted line denotes the mean.

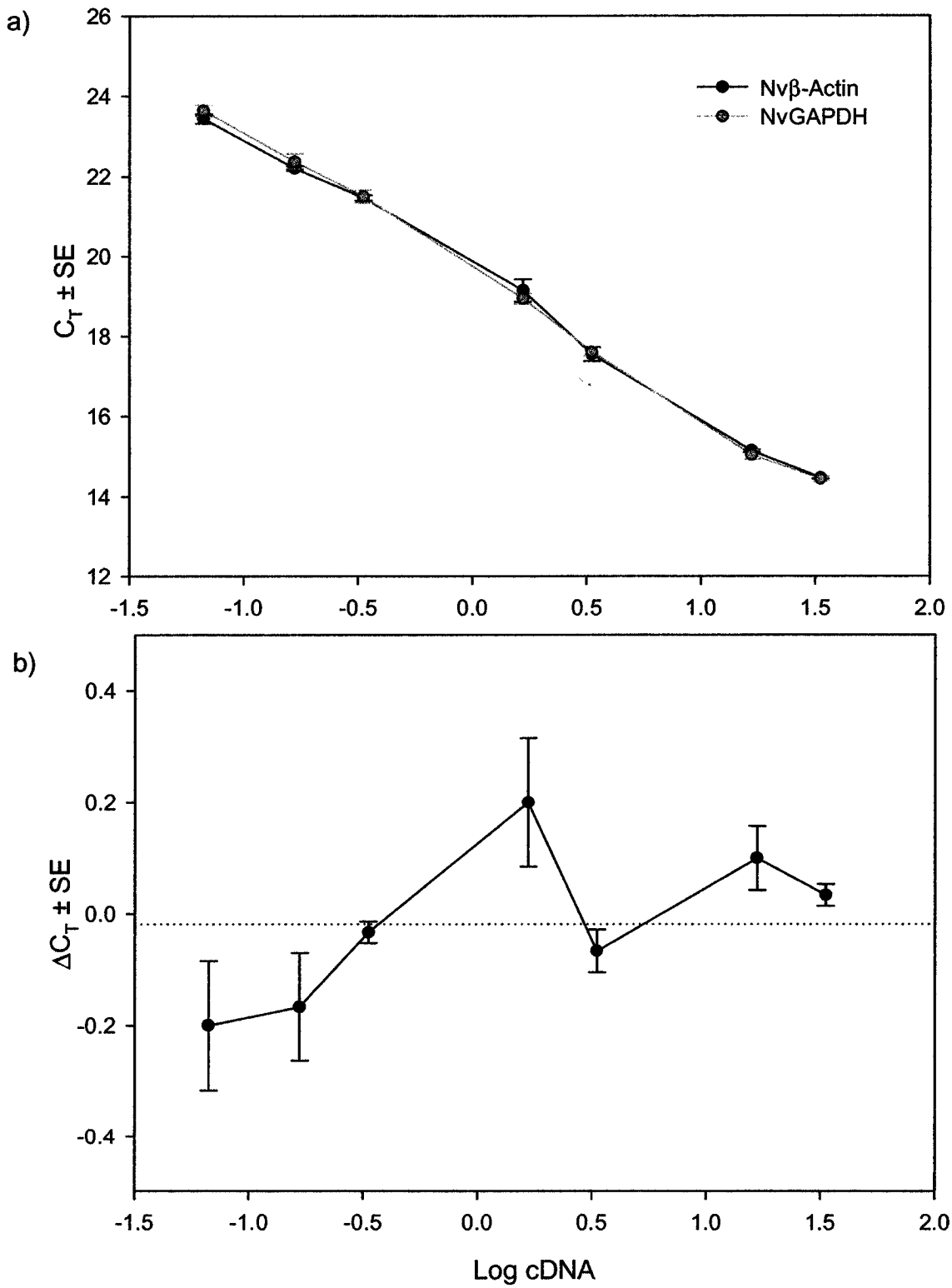
a)
Nvβ-Actin
NvGAPDH
$C_T \pm SE$
26
24
22
20
18
16
14
12
-1.5
-1.0
-0.5
0.0
0.5
1.0
1.5
2.0
b)
$\Delta C_T \pm SE$
0.4
0.2
0.0
-0.2
-0.4
Log cDNA

Figure A6. *NvGAPDH* and *Nvβ-actin* B1H1 expression under different culture conditions. a) *NvGAPDH* appears to be stably expressed as analysed by real-time RT-qPCR. However, *Nvβ-actin* expression increases during myogenesis. b) A plot of C_T values between *NvGAPDH* and *Nvβ-actin* demonstrates that *NvGAPDH* and *Nvβ-actin* expression are stable during cell proliferation, but *Nvβ-actin* increases during myogenesis and cell cycle reentry relative to *NvGAPDH*. Therefore, *Nvβ-actin* is not an ideal candidate to be utilised as a normalising factor.

a)

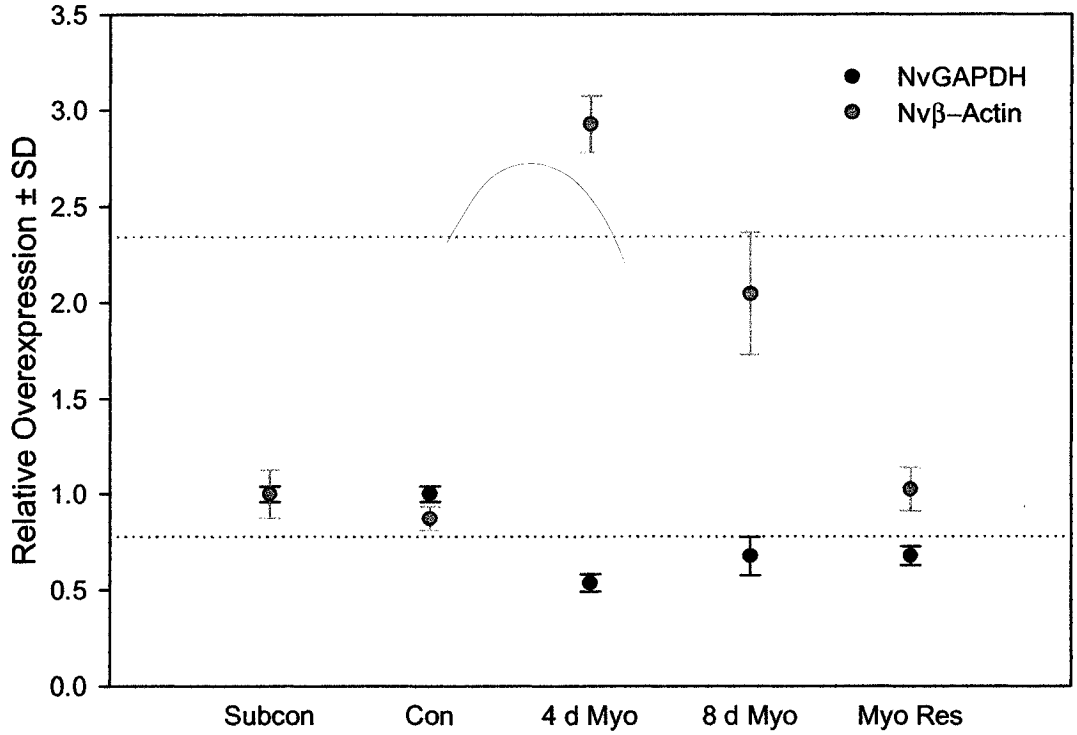
NvGAPDH
Nvβ–Actin
Relative Overexpression ± SD
3.5
3.0
2.5
2.0
1.5
1.0
0.5
0.0
Subcon
Con
4 d Myo
8 d Myo
Myo Res

b)

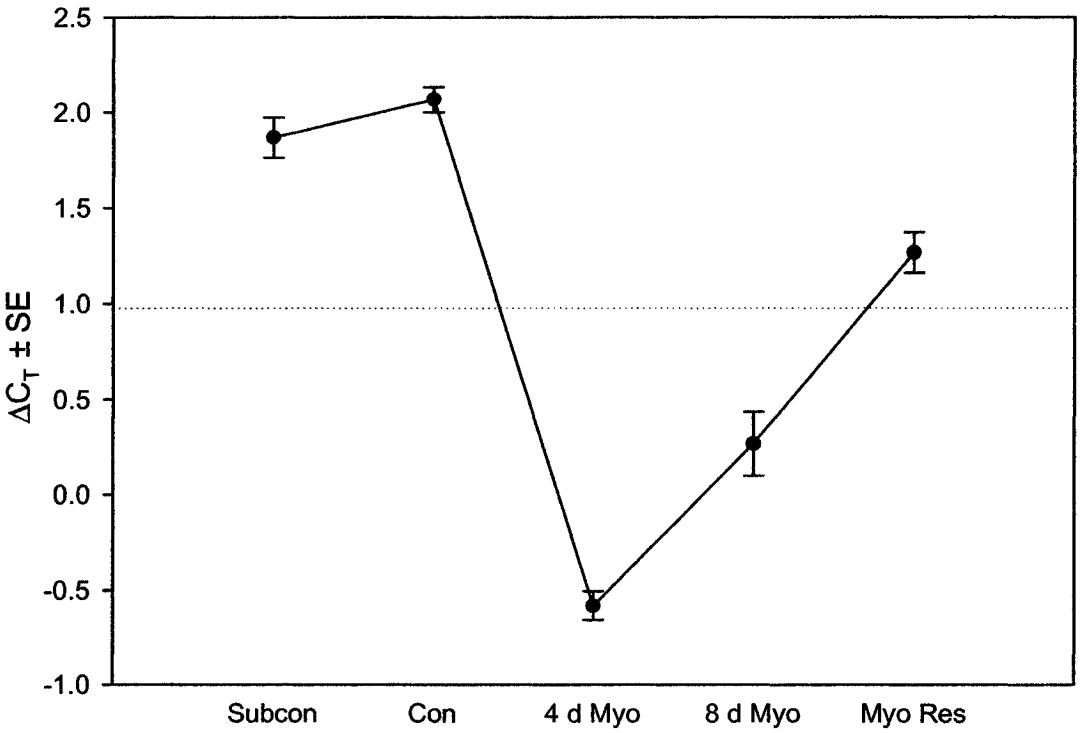
ΔC_T ± SE
2.5
2.0
1.5
1.0
0.5
0.0
-0.5
-1.0
Subcon
Con
4 d Myo
8 d Myo
Myo Res

Figure A7. Limb regeneration profile of both *NvGAPDH* and *Nvβ-actin* genes as assayed by real-time RT-qPCR during limb regeneration. a) Both *Nvβ-actin* and *NvGAPDH* appears to be stably expressed. The large difference between 24hr and other sample points is likely due to pipetting errors. b) A subtraction plot demonstrates that both *NvGAPDH* and *Nvβ-actin* are stably expressed up to 21 days postamputation, at which point *Nvβ-actin* expression increases at the palette stage. These results indicate that both candidates are sufficient as normalising factors in the initial regenerative phases but *Nvβ-actin* may not be an ideal normalising candidate during the differentiation stages. Dotted lines denote averages.

a)

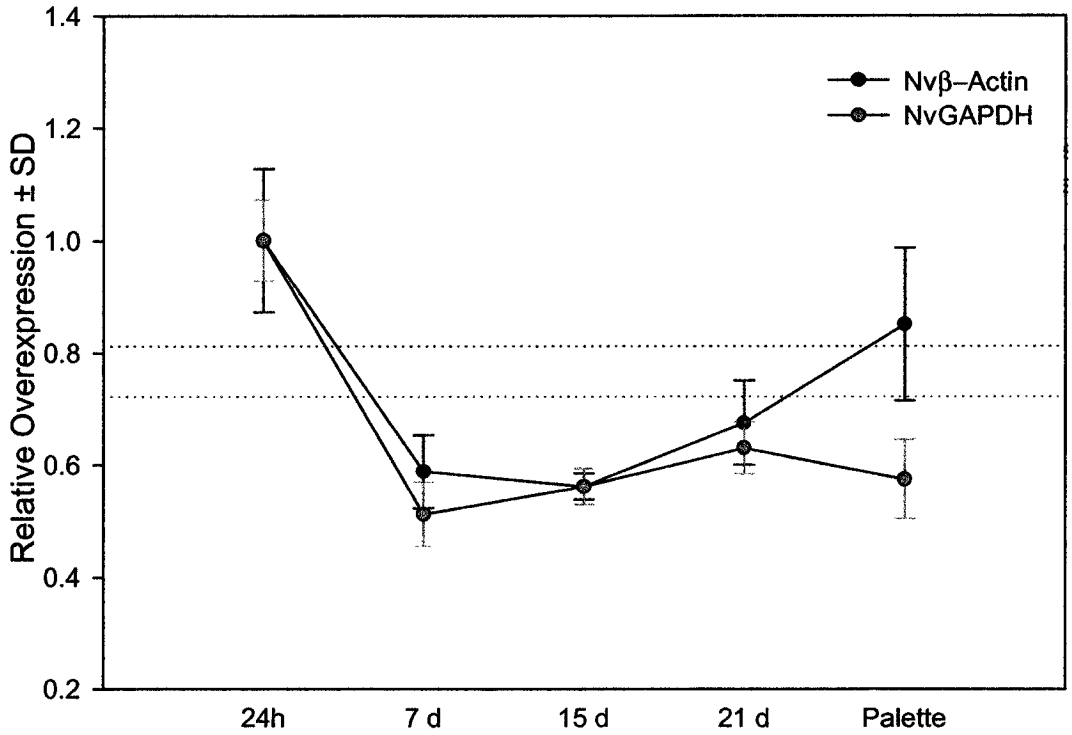
Nvβ–Actin
NvGAPDH
Relative Overexpression ± SD
1.4
1.2
1.0
0.8
0.6
0.4
0.2
24h
7 d
15 d
21 d
Palette

b)

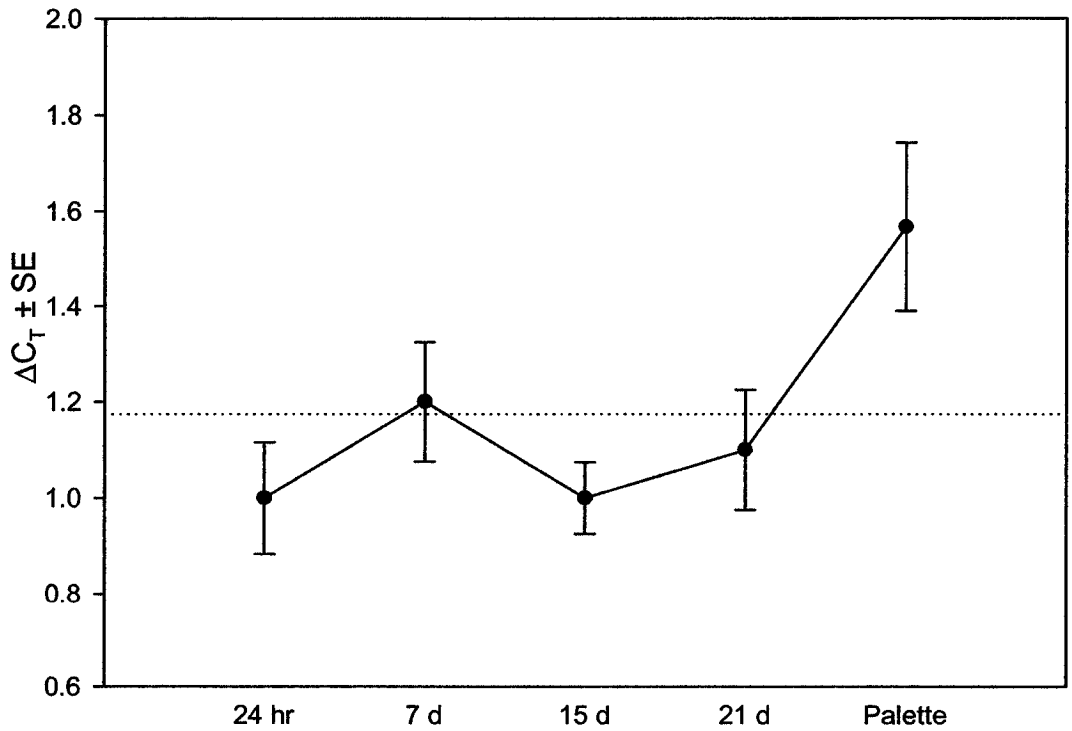
ΔC_T ± SE
2.0
1.8
1.6
1.4
1.2
1.0
0.8
0.6
24 hr
7 d
15 d
21 d
Palette

generation of a shorter amplicon) or altering the PCR parameters was possible, it was felt that a primer pair that demonstrates over 90% efficiency is valid for normalization purposes. As well, comparisons between both normalizing genes is validated, as the absolute slope of ΔC_T is 0.094 ($F = 1.73$, $df = 1$, $p_r = 0.162$, $R^2 = 0.102$), below an arbitrary cut-off value of 0.1 (Figure A5b)

C.ii. B1H1 Real-Time RT- qPCR Profile

B1H1 conditions and total RNA extractions were as previously described (Chapter 2.2). RNA was extracted from subconfluent cells, confluent cells, 4 day myotubes, 8 day myotubes and myotubes resupplemented. Total RNA concentration was measured at 260 nm, and analysed on a 1.2% agarose gel to verify quantification and integrity.

First strand cDNA was generated on DNaseI-treated total RNA samples from 2 μg of each B1H1 cell sample (Appendix II, Section B2) and RT-qPCR was as described above with triplicates of each condition. The PCR products were analyzed on a 2.5% agarose gel to confirm the presence of a single amplicon with no primer-dimer formation as indicated on a melting curve analysis. The above steps were repeated at least 2 more times with independent first strand cDNA syntheses.

NvGAPDH had uniform expression levels throughout the B1H1 cell culture conditions, but *Nvβ-Actin* had elevated expression levels during myogenesis (Figure A6a). Compared to subconfluent B1H1 cells, both *NvGAPDH* and *Nvβ-Actin* were significantly different between subconfluent and 4 day myotube cultures (t-test = 9, p = 0.012 and t-test = -31, p = 0.0045, respectively, while only *Nvβ-Actin* was significantly between subconfluent and 8 day myotubes (*Nvβ-Actin*, t-test = -31, p = 0.001; *NvGAPDH*, t-test = 3.96, p = 0.06). This was repeated at least 3 times and the results were consistent. However, in the case of *NvGAPDH*, these differences were probably due to extremely low variations between replicates. In order to determine whether these profiles were affected by minute variations

of starting material or pipetting errors, the difference in C_T were evaluated between *NvGAPDH* and *Nvβ-Actin*. These differences should not be significant if the expression levels of the genes did not vary since both samples are amplified from the same master mix. This figure shows large variations in ΔC_T between *NvGAPDH* and *Nvβ-Actin*, suggesting that *Nvβ-Actin* levels are dramatically changing between different culture conditions (Figure A6b). These results indicated that *NvGAPDH* is a suitable candidate for normalizing purposes and *Nvβ-Actin* is not.

C.iii. Limb Regeneration Real-Time RT-qPCR Profile

The same approach was undertaken with limb regenerates to analyze the real-time qPCR profiles. Briefly, newts were anaesthetized in MS222, amputated and subsequently amputated 1, 7, 15, 21 days PA and at the palette stage as per Chapter 2.1. Total RNA was extracted as per Appendix II, and Section A, and verified for integrity and quantification as mentioned above. Generation of the first strand from 2 μg limb regenerate total RNA, RT-qPCR and analysis was as described above.

Both *NvGAPDH* and *Nvβ-Actin* exhibited similar expression profiles, except for the palette stage of regeneration (Figure A7a). Although the expression levels were not statistically uniform (*NvGAPDH*, $F = 11.53$, $df = 4,10$, $p_r = 0.027$; *Nvβ-Actin*, $F = 21.67$, $df = 4,10$, $p_r = 0.022$), comparison of the ΔC_T values revealed that expression values for both normalizing factors was similar up to 21 d PA, at which point *Nvβ-Actin* levels significantly increased (t-test = -4.44, $df = 2$, $p = 0.047$; Figure A7b). Repetition with different RNA sources yielded similar values. Taken together, it appears that both normalizing genes are stably expressed up to the palette stage, whereby *Nvβ-Actin* is not recommended as a normalizing factor. Nevertheless, both normalizing factors were used in this thesis.

D. Spatial Expression Analysis

A key aspect of a normalizing factor is ubiquitous, unaltered expression under different conditions. To analyze if *NvGAPDH* is expressed in all tissues at roughly the same expression level, *NvGAPDH* expression was examined at the regenerative stages commonly studied.

The method listed below is based on the protocol kindly provided by V. Wallace (OHRI, Ottawa, Canada) and is detailed in Appendix II, Section H. To generate the antisense and sense probe, pGEM-T-NvGAPDH was digested with SpeI and NcoI, respectively, and DIG-labelling of the RNA probe was as per the manufacturer's instructions (Roche). The probe was visualized on a 1.2% agarose gel and stored at -70°C until used.

Regenerate samples were harvested as previously described. Tissues were fixed in 4% paraformaldehyde O/N at 4°C, placed in 30% sucrose/1X PBS at 4°C O/N, equilibrated with a 50:50 mixture of 30% sucrose/1X PBS and tissue embedding medium (OCT) for one hr with rocking, oriented and frozen in the above mixture. Blocks were stored at -70°C until sectioned on a Shandon cryostat. Samples were sectioned at 16 μm, dried at RT for 1 hour and stored desiccated at -70°C.

Slides were hybridized in a solution of 1X salt, 50% deionised formamide, 10% dextran sulfate, 1 mg/mL yeast tRNA and 1X Denhardt's at 65°C O/N. The slides were washed in 50% formamide, 1X SSC and 0.1% Tween-20 three times at 65°C. The slides were transferred to 1X MABT twice for 30 min at RT, blocked with 20% sheep serum, 2% blocking reagent (Roche) and 1X MABT for 2 hr, and stained with anti-DIG antibody diluted 1:1500 in the above solution for 9 hours at 4°C.

The slides were washed 4 times for 20 min each with 1X MABT at RT with agitation, equilibrated twice with 100 mM NaCl, 100 mM Tris-Cl pH 9.3, 50 mM $MgCl_2$,

0.1% Tween-20 and 10% PVA with agitation at RT. The colorimetric reaction proceeded with the above solution with 0.45 mg/mL NBT (4-nitroblue tetrazolium chloride) and 0.175 mg/mL BCIP (x-phosphate/5-bromo-4-chloro-3-indolyl-phosphate) for approximately 18 hours in the dark. The reaction was stopped by washing with 1X PBS, and sections were counterstained with Eosin-Y and mounted with Permount.

NvGAPDH is almost ubiquitously expressed, although the expression pattern is not homogenous throughout different tissues (Figure A8). In the 5 day regenerate, extensive staining is observed in the muscle, connective tissues, epidermal cells and distal mesenchymal cells. Noted are occasional staining of the small subcutaneous glands, with little staining of the stratum spongiosum and stratum compactum layers, and no staining at the stratum serosa layer. There were similar staining patterns in the 7 day and 15 day regenerates, except that there was more staining of dedifferentiated and blastemal cells. The 21d regenerate had more heavy and uniform expression within the blastemal cells, with a notable decrease of expression in dedifferentiated cells at the base of the regenerate. At the palette stage, extensive staining was apparent at the condensing chondrocytes and differentiating myotubes, but with uniform expression of the distal mesenchymal cells.

E. Discussion and Conclusions

NvGAPDH is highly conserved in a wide variety of species, from bacteria to eukaryotes, clearly showing the importance of this gene in metabolism. Since NvGAPDH has a high degree of similarity to *P. waltl* GAPDH, one can speculate that a *GAPDH* primer pair can be synthesized for most salamander species, since *N. viridescens* and *P. waltl* share a common ancestor somewhere between the Upper Cretaceous and Palaeocene (55-144 million years ago, Griffiths 1996). Also of notable interest is the high similarity to the axolotl, which is classified in a different family and last shares a common ancestor before the Palaeocene (Titus and Larson 1995; Griffiths 1996)

Figure A8. *NvGAPDH in situ* hybridization analysis during forelimb regeneration. Staining in the (a) 5-day, (b) 7-day, (c) 15-day, (d) 21-day and (e) palette regenerates. (f) Sense control of 7 day regenerate. (g) Expression in intact muscle (M) from 7-day regenerate. (h) Staining within the dermal layer from the 21-day regenerate. (i) Staining in the epidermis and dermal glands in the 7-day regenerate. Closed arrow represents staining at a dermal gland. Open arrow represents staining in epithelium. (j) Expression in dedifferentiating cells in the 15 day regenerate. (k) Blastemal cell expression in the 21 day regenerate. (l) Staining in the condensing cartilage (C) and differentiating muscle (M) from the palette regenerate. Dotted lines represent approximate amputation planes.

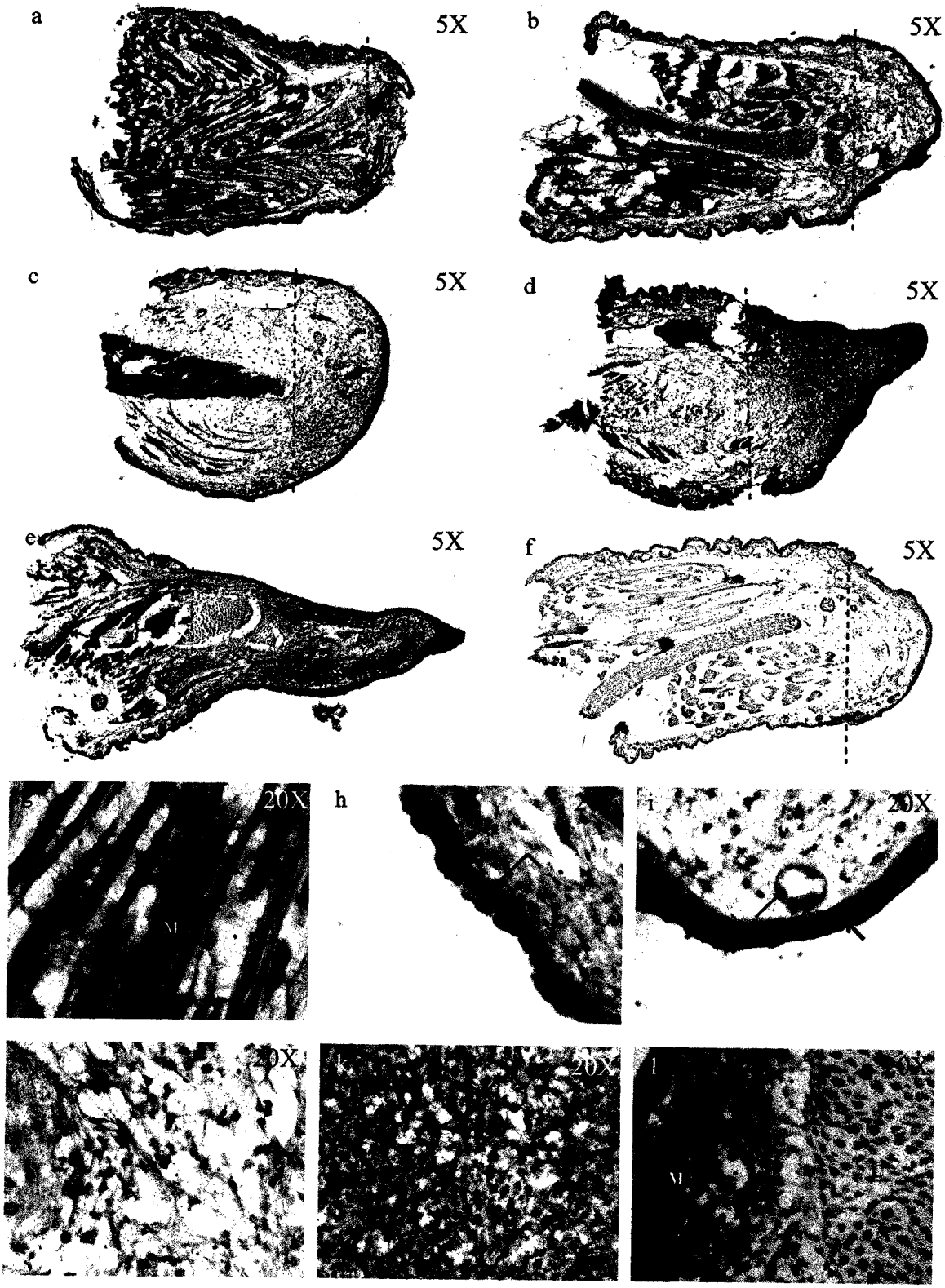
a
5X
b
5X
c
5X
d
5X
e
5X
f
5X
20X
h
i
20X
20X
20X
l
M

A surprising result from B1H1 culture under conditions of proliferation, myogenesis and cell cycle reentry is that only *NvGAPDH* had uniform expression levels. This is in contradiction to S. Vascotto's unpublished results, in which, *Nvβ-Actin* cell culture *in situ* experiments resulted in an apparent even staining in all cell morphologies. There are a couple reasons for this discrepancy. Namely, the real-time qPCR approach is several fold times more sensitive, and thus, more accurate than the semiquantitative technique by gel densitometric analysis. Quantifying band intensities by gel densitometry is accomplished by quantifying the number of pixels per square area in a logarithmic scale. On the other hand, real-time qPCR with SYBR Green I intercalating dye is highly sensitive since there is a proportional increase of emitted fluorescence with double stranded DNA. Secondly, the *in situ* hybridization technique may not be sensitive enough to detect subtle expression differences. Moreover, consistent with S. Vascotto's unpublished results is the downregulation of *Nvβ-Actin* with further differentiation in B1H1 myotubes. *Nvβ-Actin* is not expressed in mature muscles *in vivo*, but in differentiating myotubes. In other studies, *β-Actin* expression has been shown to increase during keratinocyte differentiation (Steele et al. 2002), and has been found to vary during experimental conditions in certain cell lines (e.g., Zhong and Simons 1999; Schmittgen and Zakrajsek 2000). This lends credence to the fact that *Nvβ-Actin* is not an appropriate normalizing candidate in B1H1 cells. Although expression increases during myogenesis, *Nvβ-Actin* can be used as a normalizing factor during proliferative states since expression was stable and consistent with *NvGAPDH*.

NvGAPDH appears to be stably expressed in B1H1 culture under different conditions. As with β-Actin studies, GAPDH has been demonstrated to fluctuate during differentiation (e.g., Steele et al. 2002) and experimental treatments (e.g., Zhong and Simons 1999; Schmittgen and Zakrajsek 2000). As well, elevated transcript levels have been found in some cancer cells and lines (Gong et al. 1996; Kim et al. 1998; Wu and Rees

2000). However, these differences have been found to be cell-specific and not all studies have invalidated GAPDH as a normalizing factor (e.g., Gorzelniak et al. 2001). In the polyclonal B1H1 cell line *NvGAPDH* does not appear to fluctuate under different conditions, even though GAPDH has been implicated in nonglycolytic activities such as membrane transport and fusion, microtubule assembly, nuclear RNA export, translational control, phosphotransferase/kinase reactions, and DNA replication and repair (Sirover 1999).

Although *NvGAPDH* is apparently an ideal candidate for normalizing under different B1H1 culture conditions, several issues must be kept in mind. Further validation of this normalizing candidate is necessary for other experimental manipulations such as retinoic acid treatment, hypoxia or induction of differentiation into different lineages. Another aspect that must be resolved is demonstration of relative equal expression in the different cell types within this polyclonal cell line. A cell culture *in situ* hybridization will resolve this issue. Another factor to bear in mind is the methodology of cell collection. For example, trypsinization influences gene expression (Aggeler et al. 1984), which can alter housekeeping gene expression. Finally, since rRNA comprise more than 90% of the total RNA population in most cells, and can vary with cell type, functional state and cell cycle stage (Varesio et al. 1992), differences between total and messenger RNA can confound or skew the results. There are differences between B1H1 cell states in terms of cell number and type (S. Vascotto, unpublished results), suggesting that this may affect the total RNA levels and composition. A simple experiment to calculate the total RNA levels throughout the culture conditions will partially resolve this issue.

NvGAPDH and Nvβ-Actin are sufficient as normalizing factors up to 21 days PA, at which point *Nvβ-Actin* expression increases while *NvGAPDH* expression is constant. This is surprising since *NvGAPDH* does not appear to be equally expressed in all cell types

throughout regeneration. Some cell types express *NvGAPDH* at a higher rate than others. The most striking example is within muscle tissue, which is in agreement with its elevated metabolic rates. Since RT-qPCR suggests that expression is consistent within the regenerative stages, it may be proposed that the variations between tissues balance each other out such that the overall expression when all tissue types are combined is balanced (i.e., the proportion of high- and low-expressing cells may be consistent throughout regeneration). Moreover, the fact that *Nvβ-Actin* expression increases at the palette stage confirms the unpublished observations by S. Vascotto. This is in agreement with Sturzenbaum and Kille (2001), who assert that β-actin should not be used when connective tissue physiology is under states of active flux.

Several points must be factored in when normalizing expression profiles to both normalizing candidates through the regenerative stages. Regeneration is not a stable, linear process, but rather a complex, heterogeneous mechanism. It should be noted that the samples used to generate the *NvGAPDH* and *Nvβ-Actin* profiles also contained nonregenerating stump tissue. The level of amputation and the inclusion or exclusion of stump tissues may affect the expression profiles. Using more than one normalizing factor for quantification studies is thus recommended. Vandesompele et al. (2002) and Tricarico et al. (2002) recommend using more than 2 reference genes in a given study, as normalizing to one factor is inappropriate in most systems. As well, there are no perfect single normalizing factors since there is always variable gene expression (Vandesompele et al. 2002). This study only examined the efficiency of 2 candidates, and although both are adequate for regeneration up to 21 days PA, only *NvGAPDH* is sufficient for the B1H1 cell culture conditions examined. In this case, rRNA levels can be used as another level of control, assuming that both the quantity and quality levels are the same. Despite the inadequacy of using *Nvβ-Actin* beyond 21d PA, it was felt that using this normalizing factor past the late

bud stage should provide similar expression profiles as those normalized to *NvGAPDH* if there are large differences in fold overexpression levels.

The above results are critical to my thesis and for the urodelean regeneration community. This validates that use of *NvGAPDH* in both *in vitro* and *in vivo* models, while *Nvβ-Actin* is only sufficient for up to 21 day regenerates.

F. References

Aggeler, J., S. M. Frisch and Z. Werb (1984). "Changes in cell shape correlate with collagenase gene expression in rabbit synovial fibroblasts." J Cell Biol **98**(5): 1662-71.

Bustin, S. A. (2000). "Absolute quantification of mRNA using real-time reverse transcription polymerase chain reaction assays." J Mol Endocrinol **25**(2): 169-93.

Bustin, S. A. (2002). "Quantification of mRNA using real-time reverse transcription PCR (RT-PCR): trends and problems." J Mol Endocrinol **29**(1): 23-39.

Christensen, R. N., M. Weinstein and R. A. Tassava (2001). "Fibroblast growth factors in regenerating limbs of Ambystoma: cloning and semi-quantitative RT-PCR expression studies." J Exp Zool **290**(5): 529-40.

Deindl, E., K. Boengler, N. van Royen and W. Schaper (2002). "Differential expression of GAPDH and beta3-actin in growing collateral arteries." Mol Cell Biochem **236**(1-2): 139-46.

Ferretti, P., F. Zhang, L. Santos-Ruiz and J. D. W. Clarke (2001). "FGF signalling and blastema growth during amphibian tail regeneration." International Journal of Developmental Biology **45**: S127-S128.

Goidin, D., A. Mamessier, M. J. Staquet, D. Schmitt and O. Berthier-Vergnes (2001). "Ribosomal 18S RNA prevails over glyceraldehyde-3-phosphate dehydrogenase and beta-actin genes as internal standard for quantitative comparison of mRNA levels in invasive and noninvasive human melanoma cell subpopulations." Anal Biochem **295**(1): 17-21.

Gong, Y., L. Cui and G. Y. Minuk (1996). "Comparison of glyceraldehyde-3-phosphate dehydrogenase and 28s-ribosomal RNA gene expression in human hepatocellular carcinoma." Hepatology **23**(4): 734-7.

Gorzelniak, K., J. Janke, S. Engeli and A. M. Sharma (2001). "Validation of endogenous controls for gene expression studies in human adipocytes and preadipocytes." Horm Metab Res **33**(10): 625-7.

Griffiths, R. A. (1996). Biogeography and evolution. Newts and salamanders of Europe. San Diego, Academic Press: 33-47.

Hamalainen, H. K., J. C. Tubman, S. Vikman, T. Kyrola, E. Ylikoski, J. A. Warrington and R. Lahesmaa (2001). "Identification and validation of endogenous reference genes for expression profiling of T helper cell differentiation by quantitative real-time RT-PCR." Anal Biochem **299**(1): 63-70.

Kim, J. W., S. J. Kim, S. M. Han, S. Y. Paik, S. Y. Hur, Y. W. Kim, J. M. Lee and S. E. Namkoong (1998). "Increased glyceraldehyde-3-phosphate dehydrogenase gene expression in human cervical cancers." Gynecol Oncol **71**(2): 266-9.

Manly, B. F. J. (1997). RT Program Manual. Cheyenne, Wyoming, USA.

Mazzola, J. L. and M. A. Sirover (2002). "Alteration of intracellular structure and function of glyceraldehyde-3-phosphate dehydrogenase: a common phenotype of neurodegenerative disorders?" Neurotoxicology **23**(4-5): 603-9.

Mounaji, K., N. E. Erraiss, A. Iddar, M. Wegnez, A. Serrano and A. Soukri (2002). "Glyceraldehyde-3-phosphate dehydrogenase from the newt Pleurodeles waltl. Protein purification and characterization of a GapC gene." Comp Biochem Physiol B Biochem Mol Biol **131**(3): 411-21.

Schmittgen, T. D. and B. A. Zakrajsek (2000). "Effect of experimental treatment on housekeeping gene expression: validation by real-time, quantitative RT-PCR." J Biochem Biophys Methods **46**(1-2): 69-81.

Sirover, M. A. (1996). "Minireview. Emerging new functions of the glycolytic protein, glyceraldehyde-3-phosphate dehydrogenase, in mammalian cells." Life Sci **58**(25): 2271-7.

Sirover, M. A. (1997). "Role of the glycolytic protein, glyceraldehyde-3-phosphate dehydrogenase, in normal cell function and in cell pathology." J Cell Biochem **66**(2): 133-40.

Sirover, M. A. (1999). "New insights into an old protein: the functional diversity of mammalian glyceraldehyde-3-phosphate dehydrogenase." Biochim Biophys Acta **1432**(2): 159-84.

Steele, B. K., C. Meyers and M. A. Ozbun (2002). "Variable expression of some "housekeeping" genes during human keratinocyte differentiation." Anal Biochem **307**(2): 341-7.

Sturzenbaum, S. R. and P. Kille (2001). "Control genes in quantitative molecular biological techniques: the variability of invariance." Comp Biochem Physiol B Biochem Mol Biol **130**(3): 281-9.

Tatton, W. G., R. M. Chalmers-Redman, M. Elstner, W. Leesch, F. B. Jagodzinski, D. P. Stupak, M. M. Sugrue and N. A. Tatton (2000). "Glyceraldehyde-3-phosphate dehydrogenase in neurodegeneration and apoptosis signaling." J Neural Transm Suppl(60): 77-100.

Thellin, O., W. Zorzi, B. Lakaye, B. De Borman, B. Coumans, G. Hennen, T. Grisar, A. Igout and E. Heinen (1999). "Housekeeping genes as internal standards: use and limits." J Biotechnol **75**(2-3): 291-5.

Titus, T. A. and A. Larson (1995). "A molecular phyolgenetic perspective on the evolutionary radiation of the salamander family, Salamandridae." Syst. Biol. **44**: 125-151.

Tricarico, C., P. Pinzani, S. Bianchi, M. Paglierani, V. Distante, M. Pazzagli, S. A. Bustin and C. Orlando (2002). "Quantitative real-time reverse transcription polymerase chain reaction: normalization to rRNA or single housekeeping genes is inappropriate for human tissue biopsies." Anal Biochem **309**(2): 293-300.

Vandesompele, J., K. De Preter, F. Pattyn, B. Poppe, N. Van Roy, A. De Paepe and F. Speleman (2002). "Accurate normalization of real-time quantitative RT-PCR data by geometric averaging of multiple internal control genes." Genome Biol **3**(7): RESEARCH0034.

Varesio, L., D. Radzioch, B. Bottazzi and G. L. Gusella (1992). "Ribosomal RNA metabolism in macrophages." Curr Top Microbiol Immunol **181**: 209-37.

Wu, Y. Y. and J. L. Rees (2000). "Variation in epidermal housekeeping gene expression in different pathological states." Acta Derm Venereol **80**(1): 2-3.

Zhong, H. and J. W. Simons (1999). "Direct comparison of GAPDH, beta-actin, cyclophilin, and 28S rRNA as internal standards for quantifying RNA levels under hypoxia." Biochem Biophys Res Commun **259**(3): 523-6.

APPENDIX II – DETAILED PROCEDURE AND SOLUTION SHEETS

A. Total RNA Extraction

This method is based on the Trizol (Gibco # 15596) protocol, using 50-100 mg tissue.

1. Sample Preparation
    a. Tissues
        - homogenize tissues in 1 mL Trizol
        - incubate at RT for 5 min
        - centrifuge 13,000 rpm (16,600 x g), 10 min at 4°C
        - transfer supernate to new tube
    b. Monolayer cells
        - resuspend cell pellet in 1 mL Trizol
        - incubate at RT for 5 min
        - centrifuge 10 min at 4°C
        - transfer supernate to new tube
2. Phase Separation
    a. Add 0.2 mL chloroform and shake vigorously for 15 sec.
    b. Incubate at RT for 2-3 min.
    c. Centrifuge at for 15 min at 4°C.
3. RNA Precipitation
    a. Transfer top phase to a fresh eppendorf.
    b. Add 0.5 mL isopropanol and mix by inversion.
    c. Incubate for 10 min at RT.
    d. Centrifuge at for 10 min at 4°C.
4. RNA Wash
    a. Decant supernate.
    b. Wash pellet with 1 mL 75% EtOH.
    c. Centrifuge for 5 min at 4°C.
5. Redissolving the RNA and Storage
    a. Decant supernate.
    b. Air dry RNA pellet.
    c. Resuspend in DEPC-treated H_2O.
    d. Store at -70°C.

B. First Strand Synthesis Protocol

1. A. Antisense Reverse Primer 50 ng
RNA 2 µg
DEPC H_2O up to 7 µL
Incubate at 65°C for 5-10 min and place on ice.

B. 5X Reverse Transcriptase Buffer 6 µL
0.1 M DTT 3 µL
2.5 mM each dNTP 12 µL
RNAguard (Amersham) 1 µL
M-MLV RT (Invitrogen; 200 U/µL) 1 µL
Part A Solution 7 uL
Total Volume 30 µL
a. Incubate at 37 or 42°C for 1 hour.
b. Incubate at 65°C for 15 min and place on ice.

2. A. RNA 2 µg
10X DNase Buffer 1 µL
DNase I (1 U/µL) 1 µL
DEPC H_2O up to 10 µL
a. Incubate at RT for 15 min.
b. Add 1µL stop solution
c. Heat at 65°C for 10 min and chill on ice.

B. 500 ng/µL Random Primers 1 µL
500 ng/µL Oligo d(T) 1 µL
DEPC H_2O 1 µL
Heat at 65°C for 10 min and chill on ice.

C. 5X Reverse Transcriptase Buffer 6 µL
0.1 M DTT 3 µL
6 mM each dNTP 5 µL
RNAguard (Amersham) 1 µL
M-MLV (Invitrogen; 200 U/µL) 1 µL
Part A Solution 14 uL
Part B Solution 3 µL
Total Volume 30 µL
a. Incubate at RT for 10 min then place at 37°C for 1 hour.
b. Incubate at 65°C for 15 min and place on ice.

C. Poly(A) Isolation

This protocol is based on several assumptions and extrapolations: 50 μL equals 1 mg beads which binds maximum 3.48 μg poly(A) RNA. Assuming that 1.5% of total RNA is mRNA, 100 μg total RNA yields 1.5 μg poly(A) RNA. It is advisable to keep total RNA volume as low as possible to facilitate poly(A) RNA binding. Prior DNase treatment is recommended to eliminate genomic DNA.

Notes: Centrifuge speed and time is 13,500 rpm (17,000 x g) and 20 sec.
Keep RNA on ice between steps.
All solutions are made in DEPC-treated H_2O.

1. Isolate total RNA, and verify quantity and integrity.
2. a) Wash 0.5 g oligo(dT) beads (Amersham 27-5543-03) with 12.5 mL DEPC H_2O.
   b) Pellet and resuspend in 25 mL Buffer 0.5.
   c) Store at 4°C.
3. a) Add 50 μL bead slurry to a 1.5 mL eppendorf tube.
   b) Centrifuge and pipette off supernate.
4. DNase treatment (z = 0.1 volumes of y)

Total RNA	≥100 μg
10X Reaction buffer	z μL
DEPC H_2O	x = (y) – (2*z) μL
DNase I	z μL
Total Volume	y μL

   - incubate for 15 min at RT.
   - add z μL stop solution.
   - incubate at 65°C for 10 min.

5. a) Transfer DNaseI-treated RNA into a new tube.
   b) Add 0.5 volumes of 2X Loading Buffer (prewarmed to 65°C).
   c) Heat at 65°C for 3-5 min.
   d) Add denatured RNA to pelletted beads.
   e) Mix at RT for 5 min by inversion.
6. Centrifuge and pipette out supernate.
7. a) Resuspend by washing pellet 5 times with 250 μL Buffer 0.1.
   b) Spin after each wash. *(For last wash, use a P200 tip to remove supernate).*
8. Elute poly(A) from beads with 250 μL Elution Buffer by inverting for 5 min at RT.
9. a) Spin and transfer eluant to a new 1.5 mL eppendorf tube.
   b) Precipitate RNA by adding 0.1 volumes 3M NaOAc (pH 5.2) and 2.5 volumes cold 100% EtOH.
   c) Incubate at -70°C for at least 1 hour.
10. a) Spin for 15 min at 4°C at max speed (18000 rpm = 31800 x g).
    b) Wash with cold 70% EtOH.
    c) Spin for 5 min at max speed, 4°C.
11. a) Decant and pipette supernate.
    b) Air dry poly(A) RNA.
    c) Resuspend in DEPC H_2O.

12. Solutions

Buffer 0.5
20 mM Tris-HCl, pH 7.6
0.5 M NaCl
1 mM EDTA
0.1% SDS
-Autoclave before SDS addition. Keep at 4°C.

Loading Buffer
40 mM Tris-HCl, pH 7.6
1 M NaCl
2 mM EDTA
0.2% SDS
-Autoclave before SDS addition. Keep at RT.

Buffer 0.1
20 mM Tris-HCl, pH 7.6
0.1 M NaCl
1 mM EDTA
0.1 % SDS
-Autoclave before SDS addition. Keep at RT.

Elution Buffer
10 mM Tris-HCl pH 7.6
1 mM EDTA
0.1% SDS
-Autoclave before SDS addition. Keep at RT.

D. Real-Time RT-qPCR Analysis Strategy

Before utilizing the $\Delta\Delta C_T$ method for quantification, the PCR efficiencies between a target and reference gene must be demonstrated to be approximately equal. ΔC_T is the difference in threshold cycle (C_T) between the gene of interest and the normalizing gene under a specific condition. Plotting the ΔC_T values per log total RNA yields a relative efficiency plot whereby the slope is calculated, representing the difference in PCR efficiencies between 2 genes. If the slope approaches zero, then the $\Delta\Delta C_T$ calculation is valid. The ΔC_T formula is below:

$$\Delta C_T = C_{T,X} - C_{T,R}$$

where $C_{T,X}$ is the threshold cycle of the target gene and $C_{T,X}$ is the threshold cycle of the reference gene. Also taking into account with replicates is the overall standard deviation, s:

$$s = (s_1^2 + s_2^2)^{1/2}$$

where s_1 and s_2 are standard deviations of the gene of interest and reference gene.

The overall $\Delta\Delta C_T$ formula used in this thesis is based on Livak and Schmittgen (2001):

$$2^{\Delta\Delta C_T} = 2^{-(\Delta C_{T,q} - \Delta C_{T,cb})}$$

which represents the level of fold-expression of a target that is normalized to a reference gene and is relative to a calibrator. In order to calculate the fold-overexpression of a gene from condition A to condition B, the normalizing gene's C_T value is subtracted from the gene of interest's C_T value for each condition, and the relative change in ΔC_T from one condition to another is calculated by subtracting one ΔC_T from another (i.e., $\Delta\Delta C_T = \Delta C_{TA} - \Delta C_{TB}$). Fold-overexpression is 2 raised to the $-\Delta\Delta C_T$ power.

E. Genomic DNA Isolation

This protocol is adapted from a DNA tail prep method.

1. Add 200 μL lysis buffer, 300 μL ABI lysis buffer, 30 μL 20 mg/mL proteinase and 2 μL 5 mg/mL RNaseA to tissues.
2. Incubate at 50-55°C O/N.
3. Centrifuge 13,000 rpm (15,800 x g) for 60 sec and transfer supernatant to a fresh tube.
4. PCI (phenol-chloroform-isoamyl alcohol) Extraction
    a. Add equal volume PCI (25:24:1).
    b. Vortex 2-3 sec and centrifuge at 13,000 rpm (16,600 x g) for 3 min at 4°C.
    c. Remove top phase, and repeat steps a and b.
    d. Reextract with equal volume chloroform-isoamyl alcohol (24:1).
    e. Spin and transfer top phase to a new tube.
5. Add 0.1 volume 3 M NaOAc (pH 5.2) and 2 volumes 100% EtOH.
6. Leave at -20°C for 30 min.
7. Centrifuge 13,000 rpm at 4°C for 15 min.
8. Wash with 70% EtOH.
9. Centrifuge at 13,000 rpm at 4°C for 10 min.
10. Air dry and resuspend in TE buffer. To facilitate dissolving, heat at 50°C for 5-10 min.
11. Allow samples to cool to RT before storage at 4°C.

12. Solutions

Lysis Buffer
100 mM NaCl
10 mM Tris-HCl, pH 8.0
25 mM EDTA
0.5% SDS
Filter sterilize and store at 4°C.

TE Buffer
10 mM Tris (pH 8.0)
1 mM EDTA
Autoclave and store at RT.

F. Southern Blot and Hybridization

This protocol is based on Current Protocols in Molecular Biology (Ausubel et al. 1998) and the manual from S&S Nytran Supercharge (Schleicher & Schuell #01E052), and serves to identify potential single clone transcripts to be utilized for hybridization assays.

1. Digest approximately 1 μg plasmid overnight with 5 U restriction endonuclease(s).
2. Load digested products into an agarose gel. Run at 70V until bromophenol blue dye has migrated at least halfway.
3. Wash gel with ddH_2O.
4. Soak gel in denaturation buffer for 30 min at RT with shaking.
5. Wash gel with transfer buffer with shaking for at least 15 in at RT. Minimum time is until bromophenol blue dye turns yellow.
6. Membrane preparation
    a. Measure and cut a S&S Nytran® Supercharge membrane to exact dimensions of gel.
    b. Completely soak membrane in ddH_2O.
    c. Soak membrane in transfer buffer until use.
7. Capillary transfer (as per Ausubel et al. 1998)
    a. Place gel tray upside down in a plastic container and fill with transfer buffer.
    b. Cut 1 piece of blotting paper (VWR 28303-102), soak with transfer buffer and place on top of tray with 2 ends touching transfer buffer.
    c. Cut 3 pieces of blotting paper to same dimensions of gel, soak and place on top of tray.
    d. Lay gel on blotting paper.
    e. Place saran wrap over edges of gel.
    f. Gently place wetted membrane on top of gel. Flood surface with transfer buffer
    g. Lay 3 pieces of prewetted blotting paper cut to same dimensions as membrane and place on top of membrane.
    h. Place paper towels on top of membrane (minimum 10 cm).
    i. Place a 500 gm weigth on top and leave overnight.
    j. Place membrane in 0.2 M sodium phosphate (pH 8.6) for 3 min and store dry at 4°C.
8. Hybridization and Development
    a. Prewet membrane with 6X SSC.
    b. Incubate membrane in prehybridization solution in a heat-sealed plastic bag (1 mL prehyb per 10 cm^2 membrane) at 68°C for at least 15 min with shaking.
    c. Dilute 50 ng genomic DNA in 45 μL TE and boil for 10 min at 95-100°C. Place on ice for 5 min.
    d. Add DNA to Rediprime II (Amersham RPN1633) reaction tube.
    e. Add 5 μL ^{32}P-dCTP and pipette 12 times.
    f. Incubate at 37°C for at least 10 min.
    g. Stop reaction by adding 5 μL 0.2 M EDTA and 40 μL 10 mM Tris (pH 8.0).
    h. Prepare a Microspin 3S-400 HR Column (Amersham 27-5140-01) by vortexing column, losen cap 1/4th, snap off bottom closure and centrifuge in a 1.5 mL eppendorf for 1 min at 735 x g.
    i. Place column in new eppendorf, discard cap and apply probe into centre of resin.
    j. Centrifuge at 735 x g for 2 min.
    k. Biol probe at 95-100°C for 5-10 min. Place on ice for 5 min.
    l. Reserve 5 μL of probe for liquid scintillation counting.

m. Replace prehybridization solution with equivolume hybridization solution prewarmed to 68°C. Add probe to hybridization solution.
n. Shake at 68°C overnight.
o. Drain hybridization solution and wash 2 times with 2X SSC/0.1% SDS for 5 min each at RT.
p. Wash 2 times with 0.2 X SSC/0.1% SDS for 5 min each at RT.
q. Wash 2 times with 0.2X SSC/0.1% SDS (prewarmed to 42°C) for 15 min each at 42°C.
r. Rinse in 2X SSC, blot excess liquid, wrap in saran wrap and expose to Kodak Biomax MS film.

9. Solutions

Denaturation Buffer
3 M NaCl
0.4 M NaOH
Store at RT.

Transfer Buffer
3 M NaCl
0.8 M NaOH
Store at RT.

20X SSC
3 M NaCl
0.3 M Sodium Citrate
a. Adjust pH to 7.0 with 1 M HCl.
b. Autoclave and store at RT.

100X Denhardt's
2% (w/v) Bovine Serum Albumin (Heat inactivated for 30 min at 56°C)
2% (w/v) Ficoll 400™
2% (w/v) Polyvinyl pyrolidone
Filter sterilize and store at -20°C.

10 mg/mL Sheared Salmon Sperm (10 mL)

Salmon Sperm (Sigma; Type III)	100 mg
ddH_2O	10 mL

a. Pass salmon sperm through a 18-G needle at least 30 times. Repeat with a 25-G needle.
b. Boil at 95-100°C for 10 min and cool on ice for 5 min.
c. Use immediately or aliquot into 1 mL portions and store at -20°C.

Prehybridization/Hybridization Solutions
5X SSC
5X Denhardts
1% SDS
0.1 mg/mL Sheared Salmon Sperm
a. Biol salmon sperm and cool on ice just before use.
b. Warm to 68°C before addition.

G. Mini-Prep Protocol

Note: Chill Solution III, 100% and 70% ethanol (EtOH) on ice at start of protocol.

1. Grow cultures overnight in 5 mL LB broth under antibiotic selection.
2. Pipette culture into a 1.5 mL eppendorf and spin at 14,000 rpm (18,300 x g) for 2 min at RT. Decant supernatant and repeat until whole culture is pelleted.
3. Resuspend with 300 µL Solution I with 100 ng/µL RNaseA. Incubate at RT for 5-15 min.
4. Add 300 µL Solution II. Mix by inversion (4-6 times) and incubate at RT for 2-5 min.
5. Add 300 µL Solution III. Mix by inversion (4-6 times) and incubate on ice for 15 min.
6. Centrifuge for 10 min at 13,500 rpm (17,000 x g) at RT. Transfer supernatant to a new tube.
7. Add equal amount of phenol-choloform-isoamyl alcohol (PCI; 25:24:1). Shake vigorously for 15 seconds.
8. Centrifuge 1 min. Transfer top layer to a new tube. Repeat if necessary.
9. Reextract with chloroform-isoamyl alcohol (24:1). Shake and spin for 2 min.
10. Add equal amount isoproponal, mix and incubate at RT/-70°C for 30 min.
11. Spin at 18,000 rpm (31,800 x g) at 4°C for 15 min.
12. Wash with 70% EtOH and centrifuge at 13,000 rpm (16,600 x g) for 5 min at 4°C.
13. Air dry and resuspend in 5 mM Tris-HCl buffer.

14. Solutions

Solution I
- 50 mM Glucose
- 25 mM Tris-HCl (pH 8.0)
- 10 mM EDTA

Solution II
- 0.2 N NaOH
- 1% SDS

Solution III (100 mL)

5 M KAc	60 mL
Glacial Acetic Acid	11.5 mL
ddH_2O	28.5 mL

H. Sectioned *In situ* Hybridization

This method is adapted from the detailed protocol kindly provided by V. Wallace (OHRI, Ottawa, Canada). All solutions, otherwise indicated are made in DEPC-treated H_2O.

1. Tissue Fixation and Sectioning
    a. Place amputated limbs into 4% paraformaldehyde/1X PBS precooled to 4°C. Store at 4°C O/N.
    b. Rinse 3 times in 1X PBS.
    c. Add 30% sucrose/1X PBS. Store at 4°C O/N.
    e. Aspirate 30% sucrose/1X PBS and add embedding medium.
    f. Rock at RT for at least 1 hour.
    g. Freeze limbs in embedding medium either on liquid N_2 or at -70°C.
    h. Store blocks at –70°C until use.
    i. Section on a cryostat and transfer sections to Superfrost slides (VWR 48311-703) and air dry for at least 1 hour.
    j. Store slides dessicated at -20°C. Warm slides at RT for at least 30 min before opening box.
2. DIG-Labelled Antisense and Sense Probes
    a. Linearize ~10 ug DNA with restriction enzyme that generate 5′ overhangs.
    b. DNA Extraction
        i. Add equal volume PCI (phenol-choloroform-isoamyl alcohol; 25:24:1).
        ii. Shake vigorously for 15 sec.
        iii. Centrifuge max speed (15,000 rpm = 21,000 x g) 30 sec at RT.
        iv. Transfer top phase into a new eppendorf. Repeat steps i-iv if necessary.
        v. Add equal volume chloroform-isoamyl alcohol (24:1).
        vi. Shake for 15 sec.
        vii. Centrifuge 14,000 rpm (18,300 x g) for 2 min at RT.
        viii. Transfer top phase to a new eppendorf.
        ix. Add 0.1 volumes 3 M NaOAc, pH 5.2 and 2 volumes cold 100% EtOH.
        x. Place at -70°C for at least 30 min.
        xi. Spin at maximum speed (18,000 rpm = 31,800 x g) for 15 min, 4°C.
        xii. Wash with cold 70% EtOH.
        xiii. Spin 13500 rpm (17,900 x g) for 5 min, 4°C.
        xiv. Air dry and resuspend pellet in ~25 µL DEPC H_2O (want final [DNA] = 0.2-0.4 g/L).
    c. *In vitro* Transcription

5X Transcription Buffer	5 µL
RNAguard	1 µL
10X DIG-UTP (Roche # 1277073)	2.5 µL
RNA Polymerase (SP6, T3, T7)	1 µL
Linearized DNA	1 µg
DEPC H_2O	up to 25 µL

        i. Incubate at 37°C for 1 hour.
        ii. Add another 1 µL and incubate for 1 hour.
        iii. EtOH precipitate as above and resuspend in 100 µL DEPC H_2O.
        iv. Verify integrity by agarose gel electrophoresis (3 µL).
        v. Store probe at -70°C.
3. Hybridization and Antibody Staining
    a. Warm slides to RT for at least 30 min.

b. Dilute probe in hybridization solution, vortex.
c. Denature at 65°C for at least 10 min and vortex.
d. Pipette 150 µL onto slides and place a coverslip on the slide.
e. Place slides in a slide moat prewarmed to 65°C. Place 50% Formamide/1X Salt on slide moat grooves.
f. Incubate O/N at 65°C.
g. Wash with wash buffer (prewarmed to 65°C) at 65°C for 15 min with rocking.
h. Repeat twice for 30 min each.
i. Transfer slides into 1X MABT and incubate at RT at least 30 min with rocking.
j. Line bottom of a hydrated chamber with blotting paper (VWR 28303-102) saturated with 1X PBS.
k. Dry slides around edges and trace an outline with a hydrophobic pen (DAKO S2002).
l. Add blocking solution to slides and incubate at RT for at least 1 hour in hydrated chamber.
m. Aspirate blocking solution and add 200 µL of anti-DIG antibody (Roche 1093274) diluted 1:1500 in blocking solution.
n. Incubate in hydrated chamber O/N at 4°C.
o. Wash slides with 1X MABT 4-5 times for 20 min each.

4. Colour Reaction
a. Equilibrate sections in staining buffer (lacking NBT and BCIP) twice for 10 min each with rocking at RT.
b. Add ~30 mL staining buffer with NBT and BCIP to tall coplin jars, and place slides in jar.
c. Incubate at RT in the dark.
d. Stop reaction by rinsing 3 times in 1X PBS.

5A. Mount with 1:1 glycerol/1X PBS and seal with nail polish and store slides at 4°C.

5B. Eosin Y Counterstain:
a. Soak in 1X PBS for 10 min.
b. Transfer to dH_2O for 10 min.
c. Transfer to tap H_2O for 5 min.
d. Counterstain in Eosin Y solution for ~1 min.
e. Dip slides 3-5 times in 50% EtOH.
f. Repeat in 75% EtOH.
g. Repeat in 95% EtOH.
h. Dip 5 times in 100% EtOH.
i. Soak in fresh 100% EtOH twice for 1 min each.
j. Soak in xylene for 1 min.
k. Place in fresh xylene for 2 min.
l. Repeat in fresh xylene for 2 min (slides can remain in xylene indefinetly).
m. Mount in Permount and store at RT.

6. Solutions

10X PBS (1 L)

NaCl	80 g
KCl	2 g
Na_2HPO_4-$7H_2O$	26.8 g
KH_2PO_4	2.4 g
DEPC H_2O	up to 1 L

a. Adjust to pH 7.4.
b. Autoclave and store at RT.

Embedding Medium
50% 30% Sucrose/1X PBS
50% Frozen Section Medium (OCT)
a. Place in 65°C H_2O bath at least 30 min with periodic inversion.
b. Store at RT.

10X Salt (1 L)

NaCl	114 g
Tris HCl (pH 7.5)	14.04 g
Tris Base	1.34 g
NaH_2PO_4-$2H_2O$	7.8 g
Na_2HPO_4	7.1 g
0.5 M EDTA	100 mL
DEPC H_2O	up to 1 L

Autoclave and store at RT.

Deionized Formamide (100 mL)

Bio-Rad AG 501-X8 Resin Beads	5 g
Formamide	100 mL

a. Stir in dark for 1 hour.
b. Filter sterilize and store at 4°C in the dark.

10 mg/mL Yeast tRNA

Yeast tRNA (BM)	125 mg
DEPC H_2O	10 mL

a. Incubate at 65°C with periodic mixing to dissolve. Don't worry if some does not go into solution.
b. Centrifuge for 5 min at 11,000 rpm (16,700 x g) at 4°C.
c. Transfer supernate to a new tube.
d. Extract tRNA with equal volume PCI (phenol-chloroform-isoamyl alcohol; 25:24:1).
e. Spin for 2 min at 4°C.
f. Transfer top phase to a new tube, and repeat Steps d and e.
g. Re-extract with an equal amount of choloform-isoamyl alcohol.
h. Spin for 2 min and transfer top phase to a new tube.
i. Add 0.1 volume 3 M sodium acetate (pH 5.2) and 2.5 volumes cold 100% EtOH.
j. Store at -70°C for at least 30 min.
k. Centrifuge at max speed (16,000 rpm = 35,300 x g) for 15 min at 4°C.
l. Wash pellet with 70% EtOH.
m. Centrifuge at max speed for 5 min at 4°C.
n. Redissolve in DECP H_2O.
o. Measure absorbance at 260 nm and adjust concentration to 10 mg/mL.
p. Store at -20°C.

100X Denhardt's
- 2% (w/v) Bovine Serum Albumin (Heat inactivated for 30 min at 56°C)
- 2% (w/v) Ficoll 400™
- 2% (w/v) Polyvinyl pyrolidone

Filter sterilize and store at -20°C.

Hybridization Buffer
- 1X Salt
- 50% Deionized Formamide
- 10% Dextran Sulfate
- 1 mg/mL Yeast tRNA
- 1X Denhardt's

a. Aliquot and store at -20°C.
b. Prewarm to 65°C before adding probe.

20X SSC
- 3 M NaCl
- 0.3 M Sodium Citrate

a. Adjust pH to 7.0 with 1 M HCl.
b. Autoclave and store at RT.

Wash Buffer
- 1X SSC
- 50% Formamide
- 0.1% Tween-20

a. Use ddH_2O.
b. Make fresh and prewarm to 65°C before use.

5X MABT
- 0.5 M Maleic Acid
- 0.75 M NaCl
- 0.5% Tween-20

a. Dissolve maleic acid first then add NaOH (~32 g) to pH 7.5.
b. Add NaCl and autoclave.
c. Add Tween-20 and store at RT.

10% Blocking Reagent (10 mL)

Blocking Reagent (BM #1096176)	1 g
5X MABT	2 mL
ddH_2O	8 mL

a. May need to heat to dissolve.
b. Store at -20°C.

Blocking Solution (10 mL)
- 20% Sheep Serum
- 2% Blocking Reagent
- 1X MABT

a. Make in ddH_2O.
b. Heat inactivate sheep serum at 56°C for 30 min.

Staining Buffer

100 mM NaCl
100 mM Tris-Cl pH 9-9.5
50 mM $MgCl_2$
0.1% Tween-20

a. Make in ddH_2O.
b. Add polyvinyl alcohol to 10% to a solution of NaCl, Tris-HCl and ddH_2O.
c. Heat to 80°C to dissolve with constant stirring.
d. Remove from heat source and add $MgCl_2$ and Tween-20. Continue stirring.
e. Add NBT (4-nitroblue tetrazolium chloride; BM 1383213; [final] = 0.45 mg/mL) and BCIP (x-phosphate/5-bromo-4-chloro-3-indolyl-phosphate; BM 1383221; [final] = 0.175 mg/mL). Keep dark.

Eosin Y Solution (1 L)

Eosin Y	5 g
dH_20 or Tap H_20	1 L

Note: Add 0.5 mL glacial acetic acid per 100 mL solution before use. Solution is stable for at least one week.

I. General Solutions

MS222 (1 L)

Sodium Hydrogen Carbonate	0.6 g
3-Aminobenzoic Acid Ethyl Ester	0.5 g

a. Use dechlorinated tap H_2O.
b. Adjust to pH 7.0
c. Store at 4°C up to 1 month.

0.75 % Gelatin (100 mL)

Gelatin	0.75 g
Sterile ddH_2O	100 mL

a. Dissolve at 65°C with gentle mixing.
b. Filter sterilize and store at 4°C.
c. Warm up to 37°C prior to addition to plates and aspirate excess gelatin.

Insulin (50 mL)

a. Add 50 mg insulin (bovine pancreas) to 5 mL 0.1 M HCl
   - 5 mL 0.1 M HCl = 42.5 µL 36% HCl or 77.7 µL 20% HCl diluted with sterile ddH_2O
b. Dilute slowly by adding 45 mL A.PBS with gentle shaking.
c. Filter sterilize and store at -20°C.

A.MEM (100 mL)	10%	0.5%
MEM with Earl's Salts	63 mL	63mL
Sterile ddH_2O	24 mL	33.5 mL
Fetal Bovine Serum (FBS)	10 mL	0.5 mL
100X L-Glutamine	1 mL	1 mL
Insulin	1 mL	1 mL
Penicillin/Streptomycin	1 mL	1 mL

Heat inactivate FBS at 56°C for 30 min.
Store at 4°C.

A.PBS (1 L)

10X Dulbeco's PBS without Ca^{2+} and Mg^{2+}	80 mL
Sterile ddH_2O	920 mL

Store at 4°C.